Electromagnetic-Theoretic Analysis and Design of MIMO Antenna Systems

by

Mehrbod Mohajer Jasebi

A thesis
presented to the University of Waterloo
in fulfillment of the
thesis requirement for the degree of
Doctor of Philosophy
in
Electrical and Computer Engineering

Waterloo, Ontario, Canada, 2011

AUTHOR'S DECLARATION

I hereby declare that I am the sole author of this thesis. This is a true copy of the thesis, including any required final revisions, as accepted by my examiners.

I understand that my thesis may be made electronically available to the public.

Abstract

Multiple-Input Multiple-Output (MIMO) systems are a pivotal solution for the significant enhancement of the band-limited wireless channels' communication capacity. MIMO system is essentially a wireless system with multiple antennas at both the transmitter and receiver ends. Compared to the conventional wireless systems, the main advantages of the MIMO systems are the higher system capacity, more bit rates, more link reliability, and wider coverage area. All of these features are currently considered as crucial performance requirements in wireless communications. Additionally, the emerging new services in wireless applications have created a great motivation to utilize the MIMO systems to fulfil the demands these applications create. The MIMO systems can be combined with other intelligent techniques to achieve these benefits by employing a higher spectral efficiency.

The MIMO system design is a multifaceted problem which needs both antenna considerations and baseband signal processing. The performance of the MIMO systems depends on the cross-correlation coefficients between the transmitted/received signals by different antenna elements. Therefore, the Electromagnetic (EM) characteristics of the antenna elements and wireless environment can significantly affect the MIMO system performance. Hence, it is important to include the EM properties of the antenna elements and the physical environment in the MIMO system design and optimizations.

In this research, the MIMO system model and system performance are introduced, and the optimum MIMO antenna system is investigated and developed by considering the electromagnetic aspects within three inter-related topics:

1) Fast Numerical Analysis and Optimization of the MIMO Antenna Structures:

An efficient and fast optimization method is proposed based on the reciprocity theorem along with the method of moment analysis to minimize the correlation among the received/transmitted signals in MIMO systems. In this method, the effects of the radio package (enclosure) on the MIMO system performance are also included. The proposed optimization method is used in a few practical examples to find the optimal positions and orientations of the antenna elements on the system enclosure in order to minimize the cross-correlation coefficients, leading to an efficient MIMO operation.

2) Analytical Electromagnetic-Theoretic Model for the MIMO Antenna Design:

The first requirement for the MIMO antennas is to obtain orthogonal radiation modes in order to achieve uncorrelated signals. Since the Spherical Vector Waves (SVW) form a complete set of orthogonal Eigen-vector functions for the radiated electromagnetic fields, an analytical method based on the SVW approach is developed to excite the orthogonal SVWs to be used as the various orthogonal modes of the MIMO antenna systems. The analytic SVW approach is used to design spherical antennas and to investigate the orthogonality of the radiation modes in the planar antenna structures.

3) Systematic SVW Methodology for the MIMO Antenna Design:

Based on the spherical vector waves, a generalized systematic method is proposed for the MIMO antenna design and analysis. The newly developed methodology not only leads to a systematic approach for designing MIMO antennas, but can also be used to determine the fundamental limits and degrees of freedom for designing the optimal antenna elements in terms of the given practical restrictions. The proposed method includes the EM aspects of the antenna elements and the physical environment in the MIMO antenna system, which will provide a general guideline for obtaining the optimal current sources to achieve the orthogonal MIMO modes. The proposed methodology can be employed for any arbitrary physical environment and multi-antenna structures. Without the loss of generality, the SVW approach is employed to design and analyze a few practical examples to show how effective it can be used for MIMO applications.

In conclusion, this research addresses the electromagnetic aspects of the antenna analysis, design, and optimization for MIMO applications in a rigorous and systematic manner. Developing such a design and analysis tool significantly contributes to the advancement of high-data-rate wireless communication and to the realistic evaluation of the MIMO antenna system performance by a robust scientifically-based design methodology.

Acknowledgements

I would like to express my sincere gratitude to my supervisors, Prof. Safieddin Safavi-Naeini and Prof. Sujeet K. Chaudhuri, for their invaluable direction, assistance, and guidance. Without their support and encouragement, it was impossible for me to progress in this research.

I am also thankful to the external examiner, Prof. Michael A. Jensen, and the University of Waterloo Examining Committee members, Prof. Liang-Liang Xie, Prof. Amir Hamed Majedi, Prof. Slim Boumaiza, Prof. Adrian Lupascu, and Prof. Frank Wilhelm, for their suggestions and comments in my PhD defense and comprehensive examination.

I express my thanks to all of my colleagues at *Intelligent Integrated Radio and Photonics Group* (IIRPG) who provided me with such a friendly and active environment during the course of this research.

I am very grateful to my school teachers and my university professors who opened the doors of knowledge to me and inspired me to follow this direction.

Last but not least, I would extend my heartfelt appreciations to my family for their everlasting love and patience.

Dedication

To my dear parents who taught me how to live, and

To my beloved wife who taught me how to love

Table of Contents

List of Figures

List of Tables

Chapter 1
Introduction

In wireless communications, the transmitted signals may be received through multiple propagation paths due to the environmental scatterers [1]. *Multipath propagation* may result in the destructive or constructive combinations of radio signals which can cause signal fluctuations. The resultant *multipath fading* can decrease the level of received signal to a level less than the required threshold, and therefore, can significantly affect the *system outage* and *reliability* [1, 2]. Conventionally, *Diversity* techniques are used to combat the multipath fading effects [1]. In various diversity schemes such as space, angle, polarization, and pattern diversities, multiple antennas are employed to transmit or receive the independent radio signals that contain identical information. By obtaining independent signals caused by the independent wireless channel effects, the probability of simultaneous fading for independent signals will decrease and the system reliability can be improved [1].

In recent years, the ever-increasing demand for high data rate wireless applications has required new wireless communication systems to have a higher *system capacity* for data transmission. The system capacity is defined as the maximum mutual information which can be transferred through the wireless channel [1-4]. Among various techniques to increase the system capacity, *Multiple-Input Multiple-Output* (MIMO) systems have recently attracted great attention in both the research community and the industry as a suitable solution for the significant enhancement of the band-limited wireless systems' communication capacity [2]. The MIMO system is essentially a wireless system with multiple antennas at both the transmitter and receiver ends as illustrated in Fig. 1.1. Compared to the *Single-Input Single-Output* (SISO) systems, the main advantages of the MIMO systems are the higher capacity, increased data rates, reduced multi-path fading effects, more link reliability, and wider coverage area.

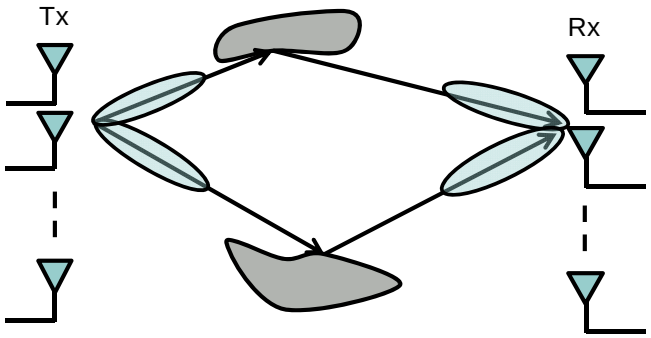

Figure 1.1: The MIMO system in a multipath propagation environment

As shown in Fig. 1.1, if different propagation paths can be resolved by multiple antennas, the independent data can be transferred through each propagation path, and therefore, the system capacity can be enhanced [3]. Since the independent data is transferred at the same frequency, MIMO systems can provide a higher spectral efficiency in comparison to SISO communications [4]. However, the capacity enhancement depends on the number of resolvable propagation paths which can be obtained through the wireless channel. For instance, if there is only one dominant propagation path in the wireless channel, the same information is extracted by multiple antennas and no capacity improvement can be obtained [5, 6]. Hence, it should be emphasized that MIMO systems are beneficial in rich multipath environments which contain multiple propagation paths resolvable by multiple antennas. Once the environment provides multipath propagations, the MIMO system can be employed to exploit the wireless channel's degrees of freedom.

In order to resolve various propagation paths and encode multiple independent data, *spatial multiplexing* has been proposed to obtain orthogonal communication *Eigen-channels* by using the *Singular Value Decomposition* (SVD) of the wireless channel [1-4]. In spatial multiplexing, the multiple data is weighted so that independent data is transferred through different Eigen-channels which can be physically interpreted as independent propagation paths. In rich multipath environments, spatial multiplexing yields a linear increase of the system capacity by the minimum number of Tx and Rx antennas [1, 4]. However, since the data streams occupy the same frequency and time, the accurate detection of received streams is sensitive to the noise and the quality of the channel [3, 4]. In order to increase the robustness to the wireless channel, the combination of space and time diversities, known as the *space-time diversity coding* [4], can be employed, in which the data streams are transmitted through different antenna elements over various time periods. For instance, in the simplest space-time diversity code, the *Alamouti scheme* [7], two different symbols, s_1 and s_2, are simultaneously transmitted by two different antenna elements, antenna#1 and antenna#2, over the first period of time. Then, the mathematically manipulated symbols, $-s_2^*$ and s_1^*, are sent through antenna#1 and antenna#2, respectively, over the following time period. The Alamouti signaling strategy improves the symbol error rate by transmitting each symbol twice, but a higher-rate temporal code is required in comparison to spatial multiplexing [3, 4]. The Alamouti diversity scheme can be extended to a more general case, known as *Orthogonal Space-Time Block Coding* (OSTBC), where arbitrary numbers of transmitter and receiver antennas are utilized [8].

Alternatively, the combination of diversity and multiplexing techniques, often called the *space-time coding*, can be employed for MIMO systems [1-4]. Of course, there is a fundamental tradeoff between the diversity and the multiplexing improvements. The signaling strategy would be determined depending on the performance tradeoffs (the spatial multiplexing gain versus the diversity gain), to transmit the data streams through multiple antennas over multiple time periods [9].

Independent of the chosen space-time code signaling, the MIMO system performance improvement depends on the correlation of the communication channel pipes between the transmitter and the receiver [10, 11]. If the communication channels obtained from the multipath environment are correlated, the same information is obtained through different channels, and therefore, there are no channel's degrees of freedom to be extracted by the MIMO systems through either diversity or multiplexing techniques [10]. Hence, the lower the correlation between the MIMO signals, the better performance the MIMO system can achieve. Typically, the MIMO system firstly estimates the wireless channel, and then uses orthogonalization procedures in the base-band signal processing to determine the uncorrelated channel pipes. In this procedure, it is assumed that the MIMO antenna elements are capable of governing independent signals from the wireless channels [2], and the orthogonalization procedure is performed before transmitting or after receiving the signals by the antenna elements. Hence, the Electromagnetic (EM) properties of the MIMO antenna elements are usually considered as part of the wireless channel, whereas the MIMO antenna structures can play a crucial role to make the MIMO signals uncorrelated instead. By embedding antennas in the wireless channel, an important design liberty is underscored to combat the dynamic variations of the wireless channel. Additionally, the electromagnetic effects of the MIMO antennas enforce fundamental limitations in the MIMO system performance. If the EM limitations and interactions of the antennas are ignored, the MIMO system performance may be underestimated or overestimated, and as a result imprecise evaluations of the MIMO systems may be obtained. Hence, the MIMO system design requires the EM antenna considerations in addition to the baseband signal processing.

1.1 MIMO Antenna Challenges and State of Arts

Considering the effect of the correlation between the communication channel pipes on the MIMO system performance, the design of the MIMO antennas leads to the minimizing of the correlation coefficients between antenna elements [12]. Conventionally, the correlation between the signals can be reduced by using large distances between the antenna elements [13]. However, because of practical considerations, compact multi-element radio/antenna systems with low correlation are in

high demand. In many applications, there is not enough space on the radio enclosure or package to place several antennas with the sufficient spacing. Thus, it is necessary to install multiple antennas in a limited space in such a way that the correlation coefficient between the antennas remains as small as possible. Many papers have been published to achieve a better system performance using the compact *co-located antennas* [14-21].

On the other hand, the number of elements and their interactions will affect the general pattern and the cross-correlation coefficients of the MIMO antennas. Hence, a general design procedure is required to not only provide the optimum compact MIMO antenna structure in order to achieve the uncorrelated signals, but also to determine how many degrees of freedom exist to design the antenna structure [22, 23]. As mentioned, the EM domain poses some limitations which restrict the design of the information theory domain [24]. Thus, it is important to know the maximum number of MIMO antenna elements or modes which can be employed to achieve the desirable system performance for the given physical limitations in the EM domain such as the bandwidth and the size of the antenna structure. Many papers have been devoted to finding the degrees of freedom determined by the electromagnetic domain [22-25].

The other important aspect of the MIMO antenna design is the fact that the physical environment providing a dynamic wireless channel will also impress the correlation between the MIMO signals. Thus, the ultimate design should adapt itself to the wireless channel in order to provide the uncorrelated signals in an arbitrary physical environment [26, 27]. This adaptation can be performed in both the signal processing and electromagnetic-antenna domains. In addition to performing the signal processing on the received signals to form a suitable radiation pattern, it is beneficial to design the intelligent antenna elements to properly reconfigure the antenna characteristics including the frequency of the operation, the radiation pattern, the polarization, and even the antenna locations. The adaptive elements are able to reconfigure themselves to the channel variations. Many papers have been published to present different reconfigurable antennas [26-34]. The majority of them are using the *Micro-Electro-Mechanical System* (MEMS) switches as a low-loss connection between various metal sections to either form different types of traditional antennas or a set the parasitic elements to change the antenna characteristics [26]. However, the feed-networks required to control the MEMS switches will make the antenna structure very bulky and inefficient. Alternatively, the PIN diodes and variable capacitors have also been employed to control the antenna features by changing the matching

stubs or reactive loads of parasitic antennas in which the loss and required biasing voltages are important issues [33, 34].

Although extensive research has been devoted to the MIMO antenna systems, considering both the electromagnetic and signal processing aspects of the MIMO antenna design, still poses several challenges:

1) The MIMO antenna utilizing the space, pattern, and polarization diversities must be able to provide uncorrelated communication paths with the maximum signal orthogonality in order to obtain the maximum performance in the MIMO system. This needs novel antenna structures that make the space-time signal processing less complex and easier to implement.

2) The physical wireless channel effects and the EM interactions of the scatterers in the vicinity of antenna structure should be included in the MIMO antenna designs to obtain the desired MIMO system performance in realistic and practical situations. Including the wireless channel effects, it is possible to design MIMO antennas adaptive to the channel variations.

3) In practical applications, fast and efficient methods are required to optimize the physical parameters of the MIMO antenna elements in terms of the given practical restrictions.

4) Accurate models are required to study the impact of the antenna structure on the performance of the MIMO systems. Considering the developed models and criteria, a systematic methodology is also needed to appropriately design and analyze the MIMO antenna systems.

5) Using several antennas in a small package such as a cell phone may not be feasible. The optimal MIMO antenna elements and the maximum number of co-located antennas should be explored in terms of the practical limitations such as limited space.

Most of the research accomplishments present an optimum design for a case study, and a general methodology can be rarely found to evaluate the possibility of employing MIMO antenna elements for practical limitations and also lead to an optimum MIMO antenna design that includes the wireless environment effects. The only comprehensive studies, which propose a general methodology for the MIMO antenna design, can be categorized as follow:

1) ***Characteristic Mode* (*CHM*) *Approach*:** The characteristic modes are the Eigen vectors of the impendence matrix in the *Method of Moments* (*MoM*), which leads to orthogonal current modes for a given geometry [35-37]. The Characteristic Modes radiate orthogonal characteristic radiation patterns which can be utilized to achieve orthogonal multi modes for the MIMO application [38-44]. The antenna design using the CHM strategy is advantageous in the sense that it establishes the orthogonal radiation patterns and also provides physical insight to the modal excitations of the antenna geometry. However, it is practically difficult to excite the characteristic modes on the antenna structures. Another drawback is the fact that CHM orthgonality is not necessarily held at the near field region [36]. Near field interactions of characteristic radiation patterns may cause poor isolations between the MIMO antenna elements, resulting in a higher correlation and lower radiation efficiency. Meanwhile, the physical environment and the channel variation model have not been taken into account and the degree of freedom for the MIMO antenna design is uninvestigated in the published papers. In general, it should be mentioned that the characteristic mode analysis is an efficient approach for scattering problems, but it faces several drawbacks for the antenna design problems [39, 41].

2) ***Spherical Vector Wave* (*SVW*) *Approach*:** The SVWs form a complete set of orthogonal Eigen-vector functions for the radiated electromagnetic fields rather than the current sources [45-48]. Since any radiated electromagnetic field can be expanded in terms of the SVWs, studying the behaviour and interactions of these vector waves in a specific propagation condition will fully characterize the wireless environment [49-55]. The SVW expansions of the field generated by each MIMO antenna element are all one needs to fully investigate the MIMO antenna system performance. Additionally, the SVWs are orthogonal everywhere outside a sphere surrounding the radiating antenna [46, 47]. Hence, by using the SVWs as the MIMO antenna elements, better isolation and less interaction between the radiated modes can be achieved. Thus, the SVWs can be used as an analytic tool to study complex MIMO antenna systems and to provide physical insight into the design and optimization of different MIMO antenna systems based on the minimization of the cross-correlation coefficient and the mutual coupling between the antenna elements.

In this thesis, the aim is to include the EM aspects of the MIMO antennas and the physical environments into the MIMO system performance evaluations and optimizations. Additionally, a

systematic methodology is developed to not only obtain the optimal MIMO antenna elements considering the EM effects, but to also determine the degrees of freedom and fundamental limitations in terms of given practical restrictions for implementing the MIMO antennas. For this purpose, the SVW approach is employed to:

1) Determine the maximum number of orthogonal communication channels generated by the MIMO antenna elements.

2) Generate optimal MIMO antenna radiations in order to minimize the correlation coefficient of the MIMO signals for an arbitrary set of antenna elements in a given wireless environment.

The SVWs are utilized in both the analytical and numerical analysis, and as well as the design of the MIMO antennas. The analytical derivations, which are convenient for spherical and planar geometries, have not been presented before, but the SVWs have been already used to numerically analyze the MIMO antennas and wireless channels [49-51]. However, the SVW formulation presented in this thesis is different from the available approaches in the literature, and provides a systematic method to analyze the MIMO wireless channel, as well as appropriately design the optimal MIMO antenna elements and the feed circuit for a given wireless environment. The presented formulation can be also used to determine the liberties of designing the MIMO antennas in terms of desired MIMO system performance and the given practical considerations.

1.2 Thesis Outline

The chapters of this thesis are organized as follows. Chapter 2 reviews the MIMO system models including the MIMO antenna elements and introduces the MIMO system performance. For MIMO antenna designs, a criterion is required to link the electromagnetic characteristics of the MIMO antennas to the required system performance. As a suitable connecting parameter, the correlation coefficient between the antenna elements will be minimized to enhance the MIMO system performance. However, the scattering parameters of the antenna system should also be taken into account to achieve an efficient MIMO antenna structure. Finally, the physical channel models are quickly reviewed for MIMO applications.

The objective of Chapter 3 is to develop a fast optimization method for synthesizing MIMO antennas with minimal correlation, which can deliver maximum capacity. For this purpose, a *reciprocity approach* along with numerical Method of Moments [56] is employed which is very efficient and fast to include the radio package and the enclosure effects in the correlation coefficient

calculations. Including the package effects, an optimization problem is defined and a few practical examples are solved to obtain an optimum low-correlation MIMO antenna.

In Chapter 4, the theory of *Vector Wave Functions* (VWF) is discussed, and the orthogonal properties of the spherical vector waves will be introduced for the MIMO antenna designs. The analytical SVW approach is presented to obtain the orthogonal current distributions for the spherical MIMO antennas. Additionally, the influences of the planar antenna geometries on the SVW excitations are considered and a few orthogonal properties of planar structures are explored for the MIMO antenna designs.

The general SVW formulation is proposed in Chapter 5 to obtain a systematic methodology for the MIMO antenna designs. The presented SVW formulation allows for the separate investigation of the physical channel effects, the MIMO antenna elements, and the feed circuit characteristics. The proposed formulation is employed for different practical cases in which the physical wireless channel is evaluated, and the optimal MIMO antennas and feed circuits are designed and analyzed.

Chapter 6 summarizes the accomplishments and achievements through this research and suggests possible directions for future works.

Chapter 2

MIMO System Model and Performance Parameters

In this chapter, the aim is to model a general MIMO system and introduce the MIMO system parameters as the required criteria for the MIMO antenna designs. Since the main advantage of the MIMO systems is the higher system capacity in comparison to the SISO systems, it is important to design the MIMO antennas so that the system capacity is maximized. It will be shown that the correlation coefficients between the MIMO antenna elements should be minimized to obtain the maximum system capacity. The correlation coefficient calculations will consider the MIMO wireless channel to include the physical environment in the MIMO antenna design. Hence, the physical MIMO channel models are also discussed in this chapter.

2.1 MIMO System Model

The general model of the MIMO antenna configuration is illustrated in Figure 2.1, showing N_T and N_R as the number of antenna elements in the transmitter and receiver sides, respectively, and H_{mn} represents the channel coefficient between the n^{th} transmitter and the m^{th} receiver.

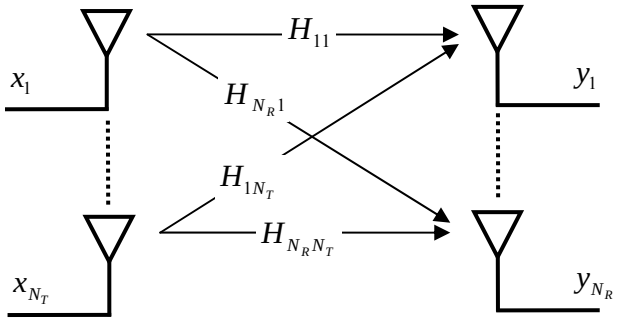

Figure 2.1: The general geometry of MIMO Antennas

Using the dyadic channel response function $\overline{\overline{G}}(\omega,\Omega_R,\Omega_T)$, which relates the received field distribution by the receiver, $\vec{P}_R(\omega,\Omega_R)$, to the radiated field pattern of the transmitter array, one can write [3, 10]:

$$\vec{P}_R(\omega,\Omega_R)=\int \overline{\overline{G}}(\omega,\Omega_R,\Omega_T).\vec{P}_T(\omega,\Omega_T)\,d\Omega_T \tag{2.1}$$

where Ω_R and Ω_T are the solid angles with respect to the receiver and transmitter coordinate systems, respectively. The radiated field pattern by the transmitter array can be written as follows [3, 10]:

$$\vec{P}_T(\omega,\Omega_T) = \sum_{n=1}^{N_T} x_n(\omega)\,\vec{F}_{T,n}(\omega,\Omega_T) \tag{2.2}$$

where x_n is the up-converted symbol fed to the n^{th} antenna element, and $\vec{F}_{T,n}$ is the vector field radiation pattern of the n^{th} transmitting antenna element in the presence of other antenna elements. Using the channel dyadic function, the received signal by the m^{th} receiving antenna element can be found as:

$$y_m(\omega) = \int_{\Omega_R} \vec{F}_{R,m}(\omega,\Omega_R).\vec{P}_R(\omega,\Omega_R)\,d\Omega_R \tag{2.3}$$

where $\vec{F}_{R,m}$ is the field radiation pattern of the m^{th} receiving antenna element in presence of other antenna elements. Using equations (2.1) to (2.3), the vector signal received by the receiving antenna elements, after adding the additive noise contribution, will be obtained as follows [10]:

$$\begin{aligned} &\mathbf{y}(\omega) = \mathbf{H}(\omega)\,\mathbf{x}(\omega) + \boldsymbol{\eta}(\omega) \\ &H_{mn}(\omega) = \int\int \vec{F}_{R,m}(\omega,\Omega_R).\overline{\overline{G}}(\omega,\Omega_R,\Omega_T).\vec{F}_{T,n}(\omega,\Omega_T)\,d\Omega_T d\Omega_R \end{aligned} \tag{2.4}$$

Considering the flat fading or non-selective frequency channels, the *channel transfer matrix*, the matrix $\mathbf{H}$, remains constant over the signal bandwidth. However, it still varies over the time. As it can be seen, the field radiation patterns of the receiver and transmitter antennas affect the channel transfer matrix. Since the channel dyadic function is determined by the environment and cannot be manipulated, the antenna field patterns should be effectively designed so that the desired MIMO system performance is achieved.

2.2 System Capacity and Correlation Coefficient

The main advantage of MIMO systems is the system capacity enhancement. The system capacity is defined as the maximum mutual information between the transmitters and the receivers [1]. Under the assumptions that the channel is unknown for the transmitter and known for the receiver, the MIMO system capacity can be obtained as follows [1, 2, 4, 57, and 58]:

$$C = \log_2\left[\det\left(\mathbf{I}_{N_R} + \frac{SNR}{N_T}\mathbf{H}\mathbf{H}^{\dagger}\right)\right] \tag{2.5}$$

where $\mathbf{I}_{N_R}$ is an identity matrix, *SNR* is the signal to noise ratio, and † denotes the complex conjugate transpose. The system capacity in (2.5) can be obtained via the Singular Value Decomposition (SVD) of the channel transfer matrix:

$$C = \sum_{i-1}^{N_{\min}} \log_2(1 + \frac{SNR}{N_T}\lambda_i^2) \tag{2.6}$$

where λ_i is the singular value of the matrix $\mathbf{H}$ (consequently, λ_i^2 is the Eigen values of the matrix $\mathbf{H}\mathbf{H}^{\dagger}$), and $N_{\min}$ is the minimum of N_T and N_R. Note that if the transmitter has the full knowledge of the *Channel State Information* (CSI), the *water-filling* method can be employed to optimally allocate the transmitting powers to various Eigen channels so that the system capacity is maximized [1, 2, 10]. In the case that the transmitter has no knowledge of the channel, the transmitted power is equally distributed between the transmitter antennas (SNR/N_T), and the relationship (2.6) is obtained.

The channel transfer matrix can be decomposed into Line-of-Sight (LOS) and Non-Line-of-Sight (NLOS) components [12]:

$$\mathbf{H} = \sqrt{\frac{K}{1+K}}\mathbf{H}_{LOS} + \sqrt{\frac{1}{1+K}}\mathbf{H}_{NLOS} \tag{2.7}$$

where *K* is the *Ricean K-factor* defined as the ratio of the LOS signal power to the power of the multi-path signals. The LOS component accounts for the non-fading contribution and depends on the AoD (Angle of Departure) and the AoA (Angle of Arrival) at the transmitter and receiver sides, respectively. The NLOS channel component, $\mathbf{H}_{NLOS}$, is the stochastic part representing the multi-path fading effects. In order to evaluate the MIMO system capacity, the NLOS component of the channel transfer matrix should be modeled. There are a variety of wireless MIMO channel models to characterize the channel transfer matrix by using either analytical formulas or the physical properties of the environment [59]. Most of the analytical models are based on the *Kronecker correlation-based channel model*. Based on the Kronecker model, the spatial receiver and transmitter correlations are separable as follows [12, 59]:

$$\mathbf{H}_{NLOS} = \mathbf{R}_R^{\frac{1}{2}} \, \mathbf{H}_G \, \mathbf{R}_T^{\frac{1}{2}} \tag{2.8}$$

where $\mathbf{R}_R$ and $\mathbf{R}_T$ are the spatial receiver and transmitter correlation matrices, respectively, and $\mathbf{H}_G$ is the zero-mean complex Gaussian matrix. This model is useful in the sense that it allows to optimize receiver and transmitter antenna arrays separately. The entries of the spatial correlation matrices can be obtained by calculating the correlation coefficient between the received signals by the MIMO antenna elements. Hence, elements of the correlation matrix can be obtained as [11, 60, and 61]:

$$\rho_{ij} = \frac{r_{ij}}{(r_{ii} r_{jj})^{1/2}} \qquad r_{ij} = E\left\{ y_i y_j^* \right\} \tag{2.9}$$

where $E\{\ \}$ represents the mathematical expectation operator. Replacing (2.3) into (2.9) and considering the statistical properties of the received field distributions, $\vec{P}_R(\omega, \Omega_R)$, one can obtain:

$$\begin{aligned} r_{ij} &= \iint_{4\pi} E\left\{ \vec{P}_R(\Omega_R) . \vec{P}_R^*(\Omega_R) \right\} \ \vec{F}_{R,i}(\Omega_R) . \vec{F}_{R,j}^{\,*}(\Omega_R) \, d\Omega_R \\ &= \iint_{4\pi} P(\Omega_R) \ \ \vec{F}_{R,i}(\Omega_R) . \vec{F}_{R,j}^{\,*}(\Omega_R) \, d\Omega_R \end{aligned} \tag{2.10}$$

where $P(\Omega)$ is the probability distribution of the *Power Angular Spectrum* (PAS) of incoming waves impinging on the MIMO antenna elements. Thus, the correlation coefficient of the received signals by the i^{th} and j^{th} antenna elements can be written in the following general form [11, 60]:

$$\rho_{ij} = \frac{< \vec{F}_i , \vec{F}_j >_P}{\left[< \vec{F}_i , \vec{F}_i >_P < \vec{F}_j , \vec{F}_j >_P \right]^{1/2}} \tag{2.11}$$

where

$$< \vec{A}, \vec{B} >_P = \iint_{4\pi} \vec{A} \cdot \vec{B}^* \ P(\Omega) \, d\Omega$$

Considering equation (2.5), the system capacity is maximized when the spatial correlation matrices are diagonal and the channel transfer matrix is a full rank matrix [1-4, 57]. In this case, the vector field radiation patterns can be thought of as *MIMO Eigen modes* or *MIMO modes* which establish parallel communication channels through a wireless multipath environment [10]. Hence, the Eigen

values of the matrix $\mathbf{HH}^{\dagger}$, which are proportional to the diagonal elements of the correlation matrices, determine the power gains of the communication channels associated with the MIMO Eigen modes. Therefore, when maximizing the system capacity, the cross-correlation coefficients should be minimized and the diagonal elements of the correlation matrices should be equalized to achieve identical power gains for the parallel communication channels [10].

For lossless antennas and uniform PAS ($P(\Omega) = 1$), the cross-correlation coefficient in (2.11) can be expressed in terms of scattering-parameters [62]:

$$\overline{\rho}_{ij} = \frac{\sum_{p=1}^{N} S_{pi}^{*} S_{pj}}{\left[(1 - \sum_{p=1}^{N} S_{pi}^{*} S_{pi})(1 - \sum_{p=1}^{N} S_{pj}^{*} S_{pj}) \right]^{1/2}} \tag{2.12}$$

where S_{pi} is the scattering parameter between the p^{th} and i^{th} ports of the N-port antenna structure. In many MIMO antenna designs, the equation (2.12) has been used as a criterion to provide uncorrelated signals for wireless communication systems. Since the correlation coefficient defined in (2.12) does not include the wireless channel effects in the correlation calculations, there is no guarantee that the MIMO antenna design can lead to orthogonal signals in different channel realizations, whereas equation (2.11) allows for the evaluation of the statistical performance parameters of the designed MIMO antenna architecture in different environments modeled by existing stochastic MIMO channel models. Hence, equation (2.11), which contains the wireless channel information in addition to the vector field radiation pattern of the MIMO antenna modes, will be a suitable criterion for designing the MIMO antenna system. At the same time, the scattering parameters of the MIMO antenna structure should also be evaluated to investigate the isolation between the antenna elements and radiation efficiency of MIMO modes.

2.3 Physical MIMO Channel Model

In order to design MIMO antennas through equation (2.11), it is required to separate the influences of the channel and the antenna arrays on the matrix $\mathbf{H}$, and model the power angular spectrum of the incoming waves through the MIMO wireless channel. There are varieties of channel models for MIMO wireless communications. Note that the expression (2.11) is general, and accordingly, any arbitrary PAS model can be used for designing the MIMO antenna system. For site specific

environments, deterministic channel models such as the ray-tracing model can be used to rigorously obtain the PAS of incoming rays to the MIMO antennas [59]. To include the dynamic effects of the wireless environment, a geometry-based stochastic channel can be used as an alternative model in which the scatterer locations are changed in a random fashion, and for each random location, the propagation path between the Tx and the Rx is obtained by using a simplified ray-tracing model [59]. Unlike the geometry-based channel models, the non-geometrical stochastic channel models describe the propagation paths by random parameters rather than the physical geometry of scatterers. Most of the non-geometrical stochastic models consider the multi-path rays impinging the MIMO antennas as clusters (Figure 2.2) and randomly change the cluster characteristics according to certain Probability Density Functions (PDF). The cluster model was firstly proposed by Saleh and Valenzuela [63], and then extended and verified by many other researchers [59].

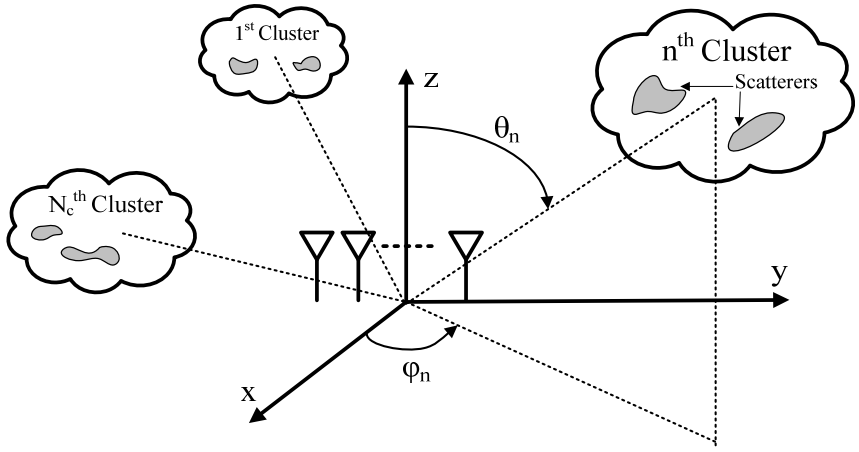

Figure 2.2: The cluster channel model for the MIMO antenna system

Laplacian distribution has been widely used as the probability density function of PAS, and verified for various wireless channel environments. The IEEE 802.11/n standard has also approved of the Laplacian channel model and has developed the TGn channel model to characterize the random parameters for different classes of wireless environments [64, 65]. Assuming N_C is the number of clusters in a wireless environment, the Laplacian PAS model is represented as [53, 61, 64, 66]:

$$P(\Omega) = \sum_{n=1}^{N_C} Q_n \exp\left[-\frac{\sqrt{2}|\varphi - \varphi_n|}{\sigma_{\phi n}}\right] \exp\left[-\frac{\sqrt{2}|\theta - \theta_n|}{\sigma_{\theta n}}\right] \tag{2.13}$$

where Q_n is the normalized power coefficient of the n^{th} cluster, φ_n and θ_n are the center of the azimuth and elevation angle of arrival, and $\sigma_{\phi n}$ and $\sigma_{\theta n}$ are the azimuth and elevation angular spread of each cluster, respectively. According to the TGn channel model, the number of clusters varies from 1 to 7 for different environments, and the mean angles of arrival of each cluster are uniformly distributed. It has been experimentally shown that the elevation angular spread is much smaller than the azimuth angular spread. That is the reason why the Laplacian distribution has been considered for only azimuth directions in many publications. Since in wireless applications such as mobile communications, the MIMO antenna structure is randomly rotated in different directions, the randomness of the elevation angle of arrival, θ_n, should be included in the Laplacian PAS distribution, as presented in (2.13).

2.4 Conclusion

To maximize the MIMO system capacity, the cross-correlation coefficient between the MIMO antenna elements should be minimized. Although the S-parameter based formula is not an appropriate criterion for the correlation coefficient calculation, the scattering parameters of the antenna structure should be studied to achieve an efficient MIMO design. To include the physical environment variations in the MIMO system performance, equation (2.11) is a suitable criterion for the correlation coefficient calculations. The definition of (2.11) is general and can be used for any arbitrary physical channel model. Without the loss of generality, the Laplacian channel model is used for the MIMO antenna design and analysis in this research.

Chapter 3
MIMO Antenna Optimizations

In the previous chapter, the correlation coefficient in (2.11), which was introduced as a criterion for maximizing the MIMO system capacity, considers the PAS to include the wireless channel effects in the MIMO system performance. The PAS only represents the incoming waves due to the sources and scattering objects in the far field, whereas in many practical cases, the other parasitic elements are located in the vicinity of the MIMO antennas. The scattering objects in the near field region will affect the field radiation patterns of the MIMO antenna elements, and consequently, the orthogonality of the received signals can significantly deteriorate. Also, the interactions of the scatterers and the antenna elements in near field region may cause a strong coupling between the MIMO antenna elements, and reduce the system capacity [21]. Hence, in addition to PAS modeling the far-field effects, it is vital to include the near field effects of the scatterers on the field radiation patterns to have a more realistic analysis of the physical environment effects.

In some practical cases, the type of antenna and consequently the current sources are known, and it is required to optimize the antenna parameters such as the antenna position, the orientation, and the input current excitations in order to obtain uncorrelated signals. In such a scenario, it is crucial to include the radio package influence on the field radiation pattern of each MIMO antenna element in the correlation coefficient calculations. For optimizing the MIMO antenna parameters, it is necessary to change the antenna parameters and then evaluate the system performance until an optimum parameter set is obtained. Hence, optimizing the antenna parameters is very challenging in the sense that a full-wave problem should be solved in each iteration. Using commercial software such as the *High Frequency Structure Simulator* (HFSS) for the required analysis at each optimization step would be time wasting and inefficient. Therefore, an efficient and fast method is required to save time in the optimization process.

In this chapter, a very fast and efficient optimization method, based on the reciprocity theorem along with the Method of Moment analysis, is proposed to minimize the correlation between the received signals in the MIMO antenna systems. In this method, the effect of the radio package (enclosure) on the MIMO system performance is also included. The proposed optimization method is used to find the optimal positions and orientations of the antenna elements on the system package to minimize the cross-correlation coefficients.

3.1 Packaging Effects on MIMO Antenna Radiation Patterns

In most practical cases, a fixture package is used to maintain the MIMO antenna elements. These days, the largest class of integrated antenna elements mounted on portable radio packages are in the form of planar or quasi-planar elements of various shapes. These elements in general, can be modeled either by a very short electric current element perpendicular to the body of the package, or by an equivalent magnetic current. For instance, let us assume *N* is the number of antenna elements that are supposed to be located on a given *Perfect Electric Conductor* (PEC) enclosure as depicted in Figure 3.1. For the sake of the simplicity of the description, a general magnetic current source is used as a general model of the antenna over the package or box, which is chosen to be made of PEC.

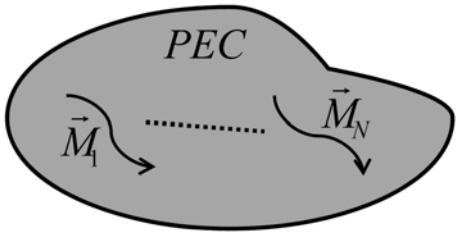

Figure 3.1: The magnetic current sources on PEC enclosure

Note that, since the electric current along the surface of a PEC enclosure would not radiate, only magnetic currents are considered here. However, these assumptions on the geometry and the material of the box will not reduce the generality of the method to be discussed here.

To find the radiated fields from a magnetic current mounted on a PEC fixture, the *Reciprocity theorem* [48, 67] is employed. To this end, a second "b" problem reciprocal to the first (original) "a" problem is constructed. In the second (reciprocal) problem, the magnetic current sources are removed, and an infinitesimal dipole, which is directed along either $\hat{\theta}$ or $\hat{\varphi}$ at a particular θ and φ, at a far distance from the PEC, radiates towards the PEC enclosure, as shown in Figure 3.2 for a cubic fixture.

The radiated fields from the magnetic current in presence of the PEC are obtained by: 1) solving for the scattered field from the PEC fixture due to the infinitesimal dipole radiation at the far field region (problem (b)), and 2) using the reciprocity relationship below to find the radiated fields in the original problem (a):

$$\hat{p}\cdot\vec{E}^{a} = -\iiint \vec{H}^{b}.\vec{M}^{a}dv = \iint (\hat{n}\times\vec{J}^{b}).\vec{M}^{a}ds, \quad \hat{p}=\hat{\theta}\ \mathbf{or}\ \hat{\varphi} \tag{3.1}$$

where $\vec{E}^a$ is the electric field due to the magnetic current density, $\vec{M}^a$ (the antenna model) on the PEC fixture, and $\vec{H}^b$ and $\vec{J}^b$ are respectively the magnetic field and induced electric current density on the PEC due to the infinitesimal dipole located at the observation point specified by θ and φ.

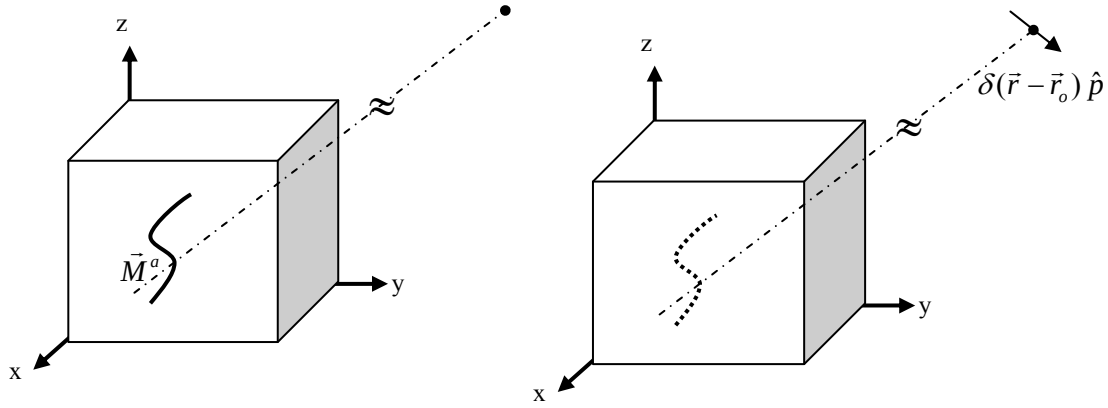

Problem (a) Problem (b)

Figure 3.2: The reciprocity problems

Therefore, the problem of the radiated field due to the magnetic current on the PEC fixture is simply converted to the scattering problem by the PEC. Once the induced electric current (problem (b)) is found at the place of the magnetic current, equation (3.1) simply gives the radiated field due to the magnetic current density (original problem (a)) in the presence of the PEC. The advantage of the reciprocity approach is that the scattering field from the object and the induced electric current can be obtained independent from the magnetic current source in the original problem. Therefore, the scattering problem can be solved once, and simply be used for calculating the equation (3.1) for any arbitrary magnetic source. Hence, using the reciprocity approach is very efficient for the optimization problem. However, note that equation (3.1) calculates the radiated electric field at a certain observation point at which the infinitesimal dipole is located. To obtain the electric field in all directions, the scattering problem, defined as problem (b) should be solved for infinitesimal dipoles located at all desired directions specified by various θs and φs. Hence, the numerical method, required for solving the scattering problems, should be chosen appropriately. The Method of Moments is an efficient numerical method to calculate the induced current on the PEC object due to the infinitesimal dipole located at any arbitrary direction. In the Method of Moments, the interactions between the meshes are numerically calculated to form the impedance matrix (Z-matrix) which is

independent of the electromagnetic excitations [56]. Once the impedance matrix is calculated, the induced current on the PEC object is obtained by multiplying the inverse of the Z-matrix (admittance matrix) and exciting electromagnetic field due to the infinitesimal dipole at a particular direction. Hence, the Z-matrix calculation has to be performed only once for an arbitrary PEC object, and therefore, the MoM is a very efficient numerical method for MIMO antenna optimization purposes.

To find the induced current $\vec{J}_S$ due to an infinitesimal dipole, the Method of Moments has been implemented in MATLAB (see the Appendix A). To obtain $\vec{E}_S$ from equation (3.1) at all directions, it is required to achieve a bank of induced currents attributed to different directions. Having saved the bank of induced currents, the physical parameters of the MIMO antenna elements can be changed during each optimization iteration and the field radiation patterns associated with the given parameters are calculated through equation (3.1) in a very fast manner. Considering the influence of the PEC object on the field radiation patterns, an optimization problem is defined to minimize the correlation coefficient between the MIMO antenna elements:

$$Min\left|\rho_{nm}\right| = Min\left|\frac{\iint_{4\pi}\vec{F}_n(\vec{r}_n',\vec{r},\beta_n,I_n,AT_n,Object)\cdot\vec{F}_m^{*}(\vec{r}_m',\vec{r},\beta_m,I_m,AT_m,Object)\,d\Omega}{\left[\iint_{4\pi}\vec{F}_n\cdot\vec{F}_n^{*}\,d\Omega\ \iint_{4\pi}\vec{F}_m\cdot\vec{F}_m^{*}\,d\Omega\right]^{\frac{1}{2}}}\right| \qquad (3.2)$$

$$Const.:\vec{r}_n' \text{ and } \vec{r}_m' \in Object,\ AT_n \text{ and } AT_m \text{ are know},\ I_n \text{ and } I_m \text{ are fixed}$$

where $\vec{r}_n'$ and $\vec{r}_m'$ are the position vectors of the n^{th} and m^{th} antenna elements confined to the locations on the PEC enclosure, $\vec{r}$ is the position vector pointing at the observation point, β_n and β_m are the antenna orientations, I_n and I_m are the excitation currents of each antenna element, AT_n and AT_m are the antenna element types, and finally $Object$ determines the shape of enclosure or chassis. Note that the channel power angular spectrum function is assumed to be uniform. However, the formulation can be used for other channel models including the Laplacian cluster model or the ray-tracing channel model.

In the next section, two different applications of the reciprocity approach along with the MoM formulation will be discussed to investigate how the proposed method can be applied for MIMO antenna optimizations in practical cases.

3.2 Practical Examples of MIMO Antenna Optimizations

As two examples of the MIMO antenna systems, consider two patch antennas operating at 2.45GHz in two different configurations: 1) a PEC cube with the side length of λ, and 2) a rectangular PEC ground plane with the side of λ and a thickness of 0.02λ, as depicted in Figure 3.3. The problem is to optimize antennas' locations and orientations in such a way that the two patch antennas (or, in general, any other number of this type of antenna) mounted on the PEC object produce orthogonal patterns and uncorrelated signals for the MIMO system.

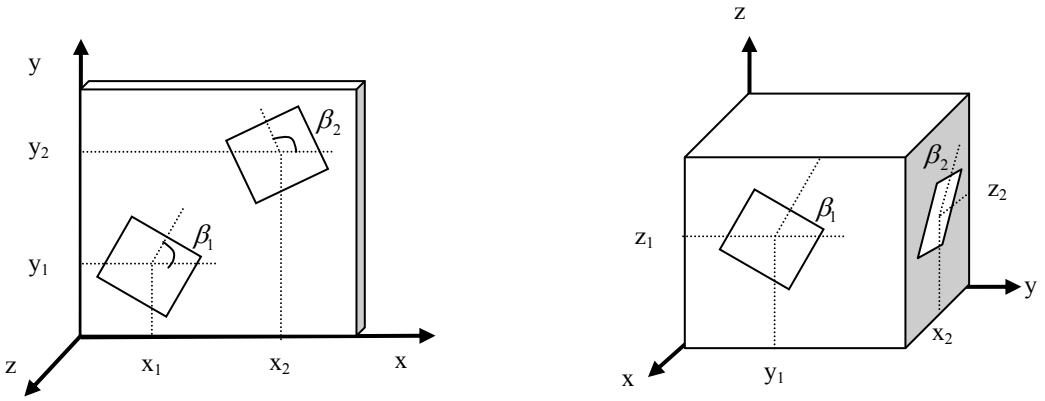

(a) (b)

Figure 3.3: Two patch antennas located on
a) a ground plane, b) two faces of a PEC cube [67]

The patch antenna can be modeled by two magnetic currents extracted from the well-known cavity model [68]. In order to find the radiation field produced by the patch antenna on the PEC box, the MoM approach along with the reciprocity theory discussed in the previous section is used. The induced electric current is derived and can be used in equation (3.1) for any arbitrary magnetic source $\vec{M}$ located on the PEC object. Therefore, $\vec{F}_1$ and $\vec{F}_2$ can be obtained as a function of $\vec{r}_1'$ and $\vec{r}_2'$ which are positions of the two patch antennas. It is preferable to fix the complex exciting currents to avoid any complexity in the feed network.

Using the proposed approach, $\vec{F}_1$ and $\vec{F}_2$ can be found for each parameter sets of (x_1, y_1, β_1, x_2, y_2, β_2) and (y_1, z_1, β_1, x_2, z_2, β_2). Performing the optimization problem given in equation (3.2)

with respect to these six parameters, it is found that ($x_1 = 0.42\lambda$, $y_1 = 0.44\lambda$, $\beta_1 = 164^\circ$, $x_2 = 0.81\lambda$, $y_2 = 0.32\lambda$, $\beta_2 = 33^\circ$) and ($y_1 = \lambda/2$, $z_1 = \lambda/2$, $\beta_1 = 225^\circ$, $x_2 = \lambda/2$, $z_2 = 3\lambda/4$, $\beta_2 = 90^\circ$) provide the minimum correlation coefficients which are approximately 9.02×10^{-5} and 2.18×10^{-5}, respectively [67]. Therefore, the low-correlation coefficient MIMO antenna systems have been obtained using the proposed optimization procedure, which maximizes the system capacity.

In the absence of PEC objects, it would be expected that the 90 degrees difference in the rotation angles of the patch antennas would give the orthogonal radiation patterns because the polarizations would be orthogonal. As it can be observed, when the PEC effects are included, the 90 degrees difference is not necessarily required to achieve the best orthogonality. This shows that the packaging effects play an important role in the MIMO antenna design. The radiation patterns of the two patch antennas in presence of the PEC box are shown in Figure 3.4 for the optimal antenna parameters in Figure 3.3.b. As expected, the radiation patterns are different from one single patch antenna in absence of the PEC box.

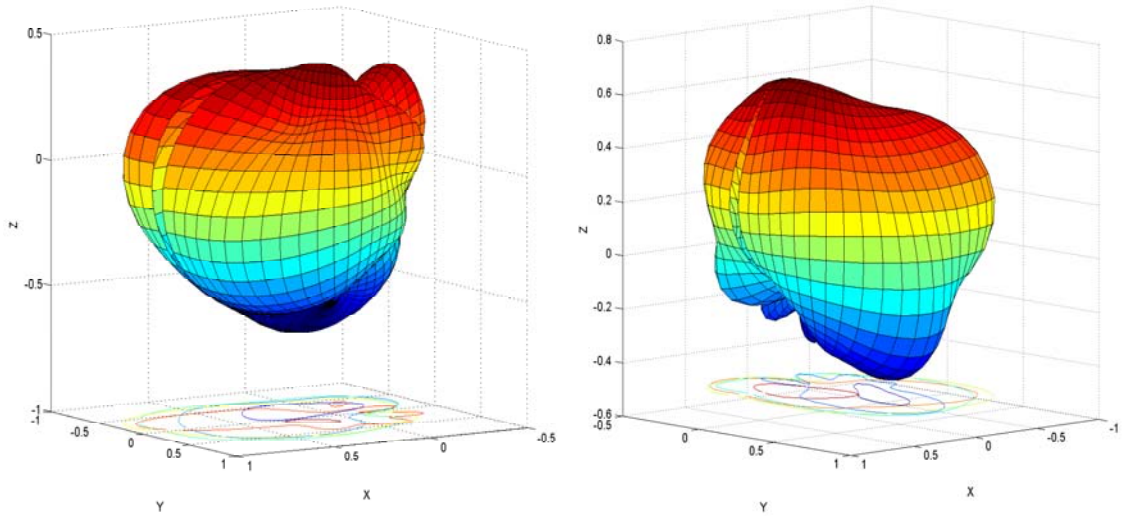

(a) (b)

Figure 3.4: The radiation patterns for MIMO antenna elements shown in Figure 3.3.b

Another interesting case would be the MIMO antenna implementation for mobile applications. Assume that two antenna elements are supposed to be located on the handset's ground plane with the size of 100mm×45mm×2mm to achieve a MIMO mobile system with a low cross-correlation coefficient, as illustrated in Figure 3.5.

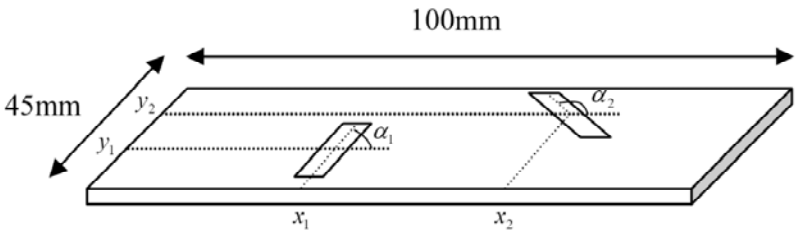

Figure 3.5: MIMO antenna elements on the practical handset's ground plane [69]

It has been shown that the strong coupling between the MIMO antenna elements occurs through the handset's ground plane, and it is difficult to isolate the multiple antennas placed on the handset PCB [21]. To include the effect of the ground plane in the correlation coefficient calculation, the proposed approach can be employed to optimize the position and the orientation of the MIMO antenna elements on the ground plane. The single element antenna has been designed to be used as the MIMO antenna element in the mobile communication. The antenna structure and its return loss (S_{11}) are illustrated in Figure 3.6.

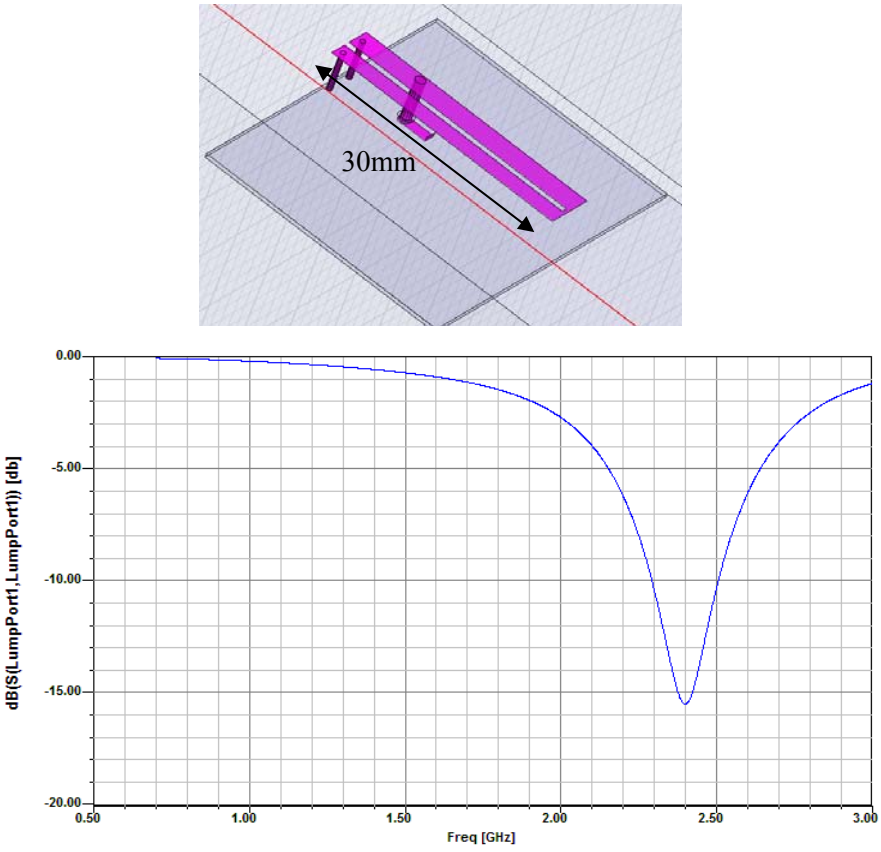

Figure 3.6: A single element antenna operating at 2.4GHz [69]

The single antenna element has been simulated and optimized in HFSS to operate at 2.4GHz efficiently. To use the proposed method, the antenna should be modeled by the magnetic currents to be used in equation (3.1). Since the antenna element contains a slot and is shortened at one end, it can be modeled by the following magnetic current distribution:

$$M = Sin(kl) \quad 0 < l < \lambda / 4 \tag{3.3}$$

where l is the distance of a point along the antenna structure from the grounded end, and k is the wave number. This model is also consistent with the electrical field distribution observed in the HFSS simulation. The closed form model (3.3) is used to optimize the antenna parameters. Performing an optimization on the cross-correlation coefficient using equation (3.2), one possible set of optimum parameters is found as $x_1 = 29.9mm$, $y_1 = 22.5mm$, $\alpha_1 = 0^\circ$, $x_2 = 84.7mm$, $y_2 = 22.5mm$, and $\alpha_2 = 102.85^\circ$ [69]. This way, when having a single antenna designed for a mobile handset, a fast and efficient design methodology can be achieved to obtain a low cross-correlation MIMO system for mobile applications.

3.3 Conclusion

In order to enhance the MIMO system capacity, the correlation coefficients between the MIMO antenna elements should be minimized. The far field channel effects can be modeled by the power angular spectrum used in equation (2.11), whereas the scattering objects in the near field region also affects the field radiation patterns of the MIMO antenna elements, and it is crucial to include the near field effects in the MIMO system performance evaluations. A reciprocity approach, which is a very suitable and efficient method for the MIMO antenna optimizations, is employed along with the MoM to calculate the radiation patterns in presence of scattering objects. The proposed methodology is a novel approach and one of the main contributions of this thesis in the MIMO antenna optimizations. The method was applied to find the optimal locations and orientations of two-antenna MIMO systems for various practical examples. The proposed method can be generalized as a design strategy for finding the optimum positions and orientations of arbitrary MIMO antenna elements in presence of an arbitrary object (package or enclosure). This method will be also used in Chapter 5 to include the effect of PEC fixture package.

Chapter 4
Analytical Spherical Vector Wave Approach

In this chapter, a systematic method is developed to analytically analyze and design the MIMO antenna elements which provide uncorrelated signals to achieve the maximum capacity. In order to maximize the capacity, the presented metric in (2.11) should be minimized for different antenna elements. In the ideal case, it is desired to achieve zero cross-correlation for the i^{th} and j^{th} field radiation patterns:

$$< \vec{F}_i \ , \ \vec{F}_j >\Big|_P = \iint_{4\pi} \vec{F}_i(\Omega) \cdot \vec{F}_j^{*}(\Omega) P(\Omega)\, d\Omega = 0 \tag{4.1}$$

If the antenna elements are chosen in such a way that each pair of field radiation patterns is orthogonal through the equation (4.1), the system capacity will increase. Since the spherical vector waves form a complete set of orthogonal Eigen-vector functions for the radiated electromagnetic fields in free space, the spherical vector wave functions satisfy equation (4.1) for the uniform PAS, $P(\theta,\varphi)=1$. The orthogonality properties of the spherical vector waves inspire a SVW approach as an analytical method to design various orthogonal radiation modes for the MIMO antenna systems.

In this chapter, the Vector Wave Functions are first reviewed in a general curvilinear coordinate system, and then the orthogonality of the VWFs is employed to design and analyze the spherical and planar antennas. It is also discussed how the SVWs can be used to investigate the degrees of freedom and mutual coupling of the designed antenna configurations.

4.1 Vector Wave Functions in Curvilinear Coordinates

Let us consider the curvilinear coordinates ξ_1, ξ_2, and ξ_3 with the unit vectors $\hat{a}_1$, $\hat{a}_2$, $\hat{a}_3$ and the scale factors h_1, h_2, h_3, respectively [45]. The field vectors $\vec{E}$, $\vec{H}$, $\vec{D}$, $\vec{B}$ and vector potentials, in a source free, homogeneous and isotropic medium obey the vector Helmholtz equation [45, 46]:

$$\begin{aligned} &\vec{\nabla}\vec{\nabla}\cdot\vec{F} - \vec{\nabla}\times\vec{\nabla}\times\vec{F} + k^2\vec{F} = 0 \\ &k^2 = \varepsilon\mu\omega^2 + j\sigma\mu\omega \end{aligned} \tag{4.2}$$

It has been shown that following independent Vector Wave Functions satisfy equation (4.2) [45, 46]:

$$\vec{L} = \vec{\nabla}\psi, \qquad \vec{M} = \vec{\nabla} \times (\hat{a}\psi), \qquad \vec{N} = \frac{1}{k}\vec{\nabla} \times \vec{M} \tag{4.3}$$

where $\hat{a}$ is any arbitrary constant unit vector, and the scalar function ψ is a solution of the scalar Helmholtz equation:

$$\nabla^2\psi + k^2\psi = 0 \tag{4.4}$$

The important properties of these three vectors are [45, 46]:

$$\begin{aligned} &\vec{\nabla} \times \vec{L} = 0, \qquad \vec{\nabla} \cdot \vec{L} = \nabla^2\psi = -k^2\psi, \\ &\vec{\nabla} \cdot \vec{M} = 0, \qquad \vec{\nabla} \cdot \vec{N} = 0 \end{aligned} \tag{4.5}$$

which means that the $\vec{L}$ vector is curl-less, and the $\vec{M}$ and $\vec{N}$ vector functions are divergence-less. It is advantageous to decompose the vector solution of equation (4.2) into longitudinal and transverse parts. Notice that the longitudinal and transverse vector functions are defined as zero-curl and zero-divergence vectors, respectively [45]. Hence, the electromagnetic fields can be represented as a linear combination of $\vec{L}$ (longitudinal part), $\vec{M}$, and $\vec{N}$ (transverse parts) which are the vector Eigen-functions of equation (4.2).

The representation (4.3) is based on the constant unit vector $\hat{a}$. This representation can be extended to the cases where the unit vector $\hat{a}$, which is perpendicular to a constant coordinate surface in a curvilinear coordinate system, is not fixed. If the unit vector is $\hat{a}_1$, then $\vec{M}$ and $\vec{N}$ should be redefined as follows [45]:

$$\vec{L} = \vec{\nabla}\psi, \qquad \vec{M} = \vec{\nabla} \times (\hat{a}_1\chi\psi), \qquad \vec{N} = \frac{1}{k}\vec{\nabla} \times \vec{M} \tag{4.6}$$

where $\hat{a}_1$ is the unit vector normal to the curved surface $\xi_1 = C$, and χ is a scalar function to be determined so that the $\vec{M}$ and $\vec{N}$ functions satisfy the vector Helmholtz equation. The choice of $\hat{a}_1$ leads $\vec{L}$ to be longitudinal, and the $\vec{M}$ and $\vec{N}$ vectors to be transverse with respect to $\hat{a}_1$. It is shown in [45] that $\vec{M}$ and $\vec{N}$ satisfy equation (4.2) if and only if:

1- $h_1 = 1$,

2- h_2 / h_3 is independent of ξ_1,

3- χ is either 1 or ξ_1, and

4- f_1 is either 1 or ξ_1^2, [f_n is defined by $h_1 h_2 h_3 / h_n^2 = f_n(\xi_n)\, g_n(\xi_i, \xi_j),\ \ i, j \neq n$].

Only six separable coordinate systems, Cartesian, three cylindrical ones, spherical and conical, out of the eleven well-known separable coordinate systems, satisfy all these conditions. For other coordinate systems, such as the spheroidal coordinate system, either a constant unit vector or position vector $\vec{r}$ is used to construct the VWFs. However, the constructed VWFs are not orthogonal [45].

4.2 Vector Green's Function

Since the free space can be thought of as a spherical waveguide, the radiated fields can be represented in the spherical coordinate system. The solution of the homogeneous scalar Helmholtz equation in the spherical coordinate system is as follows [46, 47]:

$$\psi_{\substack{e\\o}mn}^{(i)} = z_n^{(i)}(kr)\ P_n^m(\cos\theta) \begin{matrix}\cos\\ \sin\end{matrix}(m\phi) \tag{4.7}$$

where e and o stand for the even and odd modes, $P_n^m(\cos\theta)$ is the associated Legendre Polynomial, and $z_n^{(i)}(kr)$ is an appropriate spherical function namely $j_n(kr)$, $n_n(kr)$, $h_n^{(1)}(kr)$, or $h_n^{(2)}(kr)$ for i=1, 2, 3, and 4, respectively. Based on the representation (4.6), the SVWs establish the orthogonal basis functions for the field expansion (see Appendix B):

$$\vec{L}_{\substack{e\\o}mn}^{(i)} = \vec{\nabla}\psi_{\substack{e\\o}mn}^{(i)}, \qquad \vec{M}_{\substack{e\\o}mn}^{(i)} = \vec{\nabla}\times(r\,\hat{r}\,\psi_{\substack{e\\o}mn}^{(i)}), \qquad \vec{N}_{\substack{e\\o}mn}^{(i)} = \frac{1}{k}\vec{\nabla}\times\vec{M}_{\substack{e\\o}mn}^{(i)} \tag{4.8}$$

The free space *Dyadic Green's Function* is expanded in terms of the SVWs [47]:

$$\overline{\overline{G}}_0(\vec{r}/\vec{r}\,') = \frac{jk}{4\pi}\sum_{n=1}^{\infty}\sum_{m=0}^{n}(2-\delta_0)\frac{2n+1}{n(n+1)}\frac{(n-m)!}{(n+m)!}\begin{cases}\vec{M}_{\substack{e\\o}mn}^{(4)}(\vec{r})\vec{M}_{\substack{e\\o}mn}^{(1)}(\vec{r}\,') + \vec{N}_{\substack{e\\o}mn}^{(4)}(\vec{r})\vec{N}_{\substack{e\\o}mn}^{(1)}(\vec{r}\,'), & r > r' \\ \vec{M}_{\substack{e\\o}mn}^{(1)}(\vec{r})\vec{M}_{\substack{e\\o}mn}^{(4)}(\vec{r}\,') + \vec{N}_{\substack{e\\o}mn}^{(1)}(\vec{r})\vec{N}_{\substack{e\\o}mn}^{(4)}(\vec{r}\,'), & r < r'\end{cases} \tag{4.9}$$

$$\delta_0 = \begin{cases}1, & m = 0\\ 0, & m \neq 0\end{cases}$$

Using the dyadic Green's function, the electric field radiated by an electric current source $\vec{J}(\vec{r}')$ enclosed by a sphere with a radius of r_0 can be represented in terms of SVWs as [45-47]:

$$\vec{E}(r,\theta,\phi)=\sum_{n=1}^{\infty}\sum_{m=0}^{n}\left[a_{\substack{e\\o}mn}\vec{M}^{(4)}_{\substack{e\\o}mn}(r,\theta,\phi)+b_{\substack{e\\o}mn}\vec{N}^{(4)}_{\substack{e\\o}mn}(r,\theta,\phi)\right] \quad for \;\; r_0<r \tag{4.10}$$

where

$$\begin{bmatrix}a_{\substack{e\\o}mn}\\ b_{\substack{e\\o}mn}\end{bmatrix}=\alpha\beta_{mn}\int_{V'}\begin{bmatrix}\vec{M}^{(1)}_{\substack{e\\o}mn}(r',\theta',\phi')\\ \vec{N}^{(1)}_{\substack{e\\o}mn}(r',\theta',\phi')\end{bmatrix}\cdot\vec{J}(\vec{r}')\,dv'$$
$$\alpha=-\frac{\omega\mu\,k}{4\pi},\quad \beta_{mn}=(2-\delta_0)\frac{2n+1}{n(n+1)}\frac{(n-m)!}{(n+m)!} \tag{4.11}$$

Equations (4.10) and (4.11) are well-known solutions to the forward problem, in which the radiated fields are determined for a given current source. As $k\,r\to\infty$, the far field can be approximated by replacing $h_n^{(2)}(k\,r)$ with $j^{n+1}\exp(-jk\,r)/(k\,r)$ in equation (4.10). Hence, the coefficients calculated by (4.11) are identical for far fields as well. This way, the far field can be back-propagated to the near field region, and a similar equation can be written for the coefficients obtained from the far field spherical harmonics [45].

4.3 SVWs for MIMO Antenna Radiations

The orthogonal properties of the SVWs, presented in Appendix B, can be employed to obtain the orthogonal radiations for the MIMO antennas. The complete orthogonality of the SVWs is spoiled because the inner products of the *L* and *N* vector wave functions with the same orders do not vanish over the spherical surface. Although the completeness can be obtained by integrating over all space and wave numbers, such integrations are unnecessary, because the radiating electromagnetic fields in the source free region are divergence less and there is no need to include the *L* vector wave functions in the field expansions. Hence, as shown in (4.10), the *M* and *N* vector wave functions are enough to establish a complete orthogonal set for representing any EM field in the source free regions.

For the special case of the uniform PAS, the orthogonality condition (4.1) is satisfied by the SVWs. Hence, any two current sources, which excite the SVWs with different orders of *m* and *n*, can be used

as the MIMO antenna elements. Thus, for instance, the design and optimization criterion for the MIMO antenna elements can be set as a condition preventing the excitation of the same SVW by two different MIMO antenna elements. To clarify the criterion, assume the current $\vec{J}_i(\vec{r}')$ is used as one MIMO antenna element and has generated *a* and *b* coefficients in (4.10) with orders which are members of the integer sets, A_m, A_n, B_m, and B_n, respectively. The design or optimization criterion for the other current source $\vec{J}_j(\vec{r}')$ can be expressed as:

$$\alpha\beta_{mn}\int_{V'}\begin{bmatrix}\vec{M}_{e_{o}^{m'n'}}^{(1)}(\vec{r}')\\ \vec{N}_{e_{o}^{mn}}^{(1)}(\vec{r}')\end{bmatrix}\cdot\vec{J}_j(\vec{r}')\,dv'=0 \qquad (4.12)$$

$$for\ any\quad m'\in A_m,\quad n'\in A_n,\quad m\in B_m,\ and\quad n\in B_n$$

Note that the criterion defined in (4.12) is over-constrained in the sense that the individual SVW components excited by i^{th} and j^{th} current sources are forced to be orthogonal, whereas in general, the weighting coefficients of SVWs can be chosen in such a way that the orthogonal vector field radiation patterns are achieved through (4.1). The general SVW formulation, in which the orthogonal radiating fields are obtained through the weighting coefficient adjustments, will be discussed in Chapter 5.

4.3.1 Degrees of Freedom

As a typical set of MIMO antenna design constraints, one may consider a specific shape, the given size, and the bandwidth. The MIMO antenna elements should be designed to provide uncorrelated signals to achieve the maximum capacity and sufficient degrees of freedom for the given constraints. In this context, the *degrees of freedom* refer to possible number of feasible configurations produced by the MIMO antenna elements in the given volume to enhance the system capacity. Since the vector radiation pattern of each MIMO antenna element can be expanded in terms of the SVWs, the degrees of freedom for the MIMO antenna design can be determined by studying the excited SVWs which satisfy equation (4.1) for the given PAS.

In addition to investigating whether the structure is capable of exciting particular SVWs, it is required to know which ones can be propagated. *Chu's theorem* can answer this question [46, 70]. Accordingly, for a given Quality factor, or equivalently a specific bandwidth, an upper bound can be determined for the gain of an antenna structure fitted within a sphere with a radius of r_0, and it is not

possible to get any higher [70]. This limit can be attributed to the number of SVWs which are able to be propagated through the free space.

If the free space is considered as a spherical waveguide then only a finite number of spherical waves, having a *cutoff radius* rather than a *cutoff wavelength* in this waveguide, can propagate in the space [48]. To illustrate the cutoff radius concept, the wave impedances related to the Hankel functions can be defined for both TE and TM modes in free space. Chu used a recurrence formula to represent the wave impedances as a partial fraction expansion, and illustrated the wave impedances as a ladder network that included series capacitances and shunt inductances [68]. Based on the *Filter Theory*, it can be shown that for a fixed radius of r_0, the power of the lower mode number n can only be transmitted to the end of the ladder network. Basically, the input impedance of the free space for various TE and TM spherical modes are in such a way that only a finite number of SVWs can be transmitted and higher order modes will be reactively stored around the source region. It can be shown that the wave impedances are dominantly reactive for those modes that are of the order $n>N=kr_0$ and dominantly resistive for the modes of the order $n<N=kr_0$ where n is the order of the Hankel function. The order of the Legendre functions (m) does not deal with cutoff radius [48, 70].

Therefore, one can conclude that for a given antenna enclosed by a sphere with a radius of r_0 and a bandwidth (or equivalently Q factor), only the first $n<N=kr_0$ modes with any arbitrary m will appear at the vector field radiation pattern. Consequently, those SVWs, whose order n is less than N, can be used as the vector field radiation pattern of a MIMO antenna element to satisfy equation (4.1) in the given PAS. This determines an upper limit for the number of possible MIMO antenna elements for a given size and bandwidth.

4.3.2 Mutual Coupling

To illustrate how the mutual coupling can be related to the SVWs, Figure 4.1 shows an N port antenna structure in two problem scenarios. In each problem, only one antenna port (either port# i or j) is excited by a point current source, and all other ports are left open circuit. I_i^b and I_j^a denote the point current sources at port# i in problem (b) and port# j in problem (a), respectively. V_i^a, and V_j^b also represent the induced voltages across the port# i in problem (a) and port# j in problem (b), respectively. The surface s is the smallest sphere with the volume of v enclosing all antenna structures, and the rest of the free space is denoted by volume v'.

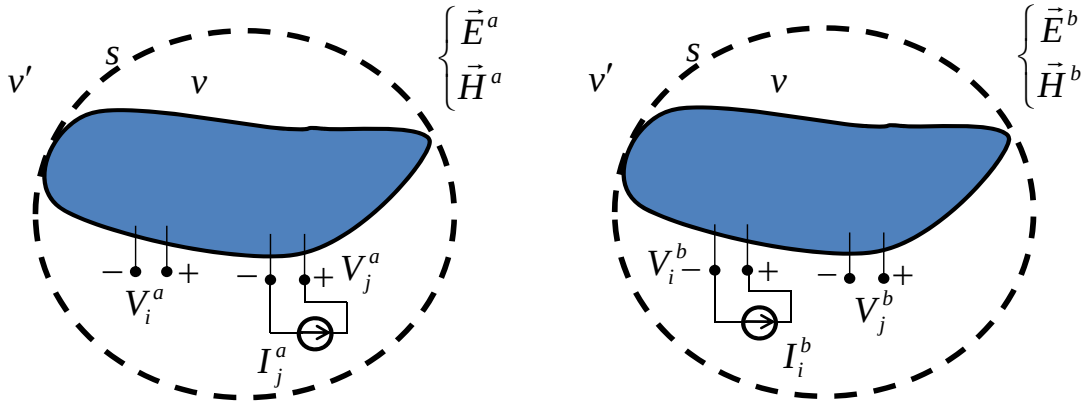

Problem (a) Problem (b)

Figure 4.1: The electromagnetic reciprocity between the two problems

The Maxwell equations can be written as follow for each problem:

$$\begin{cases} \vec{\nabla}\times\vec{H}^a = j\omega\varepsilon\vec{E}^a + \vec{J}^a \\ \vec{\nabla}\times\vec{E}^a = -j\omega\mu\vec{H}^a \end{cases} \qquad \begin{cases} \vec{\nabla}\times\vec{H}^b = j\omega\varepsilon\vec{E}^b + \vec{J}^b \\ \vec{\nabla}\times\vec{E}^b = -j\omega\mu\vec{H}^b \end{cases} \tag{4.13}$$

where the current source distributions are delta functions at the positions of port# *i* and *j*:

$$\vec{J}^a = I_j^a\,\delta(\vec{r}' - \vec{r}_j) \qquad \vec{J}^b = I_i^b\,\delta(\vec{r}' - \vec{r}_i) \tag{4.14}$$

Scalarly multiplying the conjugate of the first equation in problem (b) by $\vec{E}^a$ and the second equation in problem (a) by the conjugate of $\vec{H}^b$, the difference of the two resulting equations is obtained as:

$$\begin{aligned} \vec{E}^a.\vec{\nabla}\times\vec{H}^{b^*} - \vec{H}^{b^*}.\vec{\nabla}\times\vec{E}^a &= -\vec{\nabla}.(\vec{E}^a\times\vec{H}^{b^*}) \\ &= -j\omega\varepsilon\,\vec{E}^a.\vec{E}^{b^*} + j\omega\mu\,\vec{H}^a.\vec{H}^{b^*} + \vec{E}^a.\vec{J}^{b^*} \end{aligned} \tag{4.15}$$

Integrating throughout volume v and applying the divergence theorem, the following integral form is obtained:

$$\begin{aligned} V_i^a I_i^{b^*} &= -\iiint_v \vec{E}^a.\vec{J}^{b^*}\,dv \\ &= \oiint_s (\vec{E}^a\times\vec{H}^{b^*}).\hat{n}\,ds + j\omega\iiint_v \mu\vec{H}^a.\vec{H}^{b^*}\,dv - j\omega\iiint_v \varepsilon\vec{E}^a.\vec{E}^{b^*}\,dv \end{aligned} \tag{4.16}$$

where $\hat{n}$ is $\hat{r}$ for the spherical surface, s.

The first term on right hand side is the interaction power of problems (a) and (b) which is propagated outwards from the sphere s. The second and third terms also represent the interaction of the electric and magnetic energies stored in volume v. Since the surface s is chosen to be the smallest sphere surrounding the antenna structure, volume v would be a small volume over which the interaction energies are calculated. Assuming that the electric and magnetic fields are not singular, the interaction energies in volume v can be neglected:

$$V_i^a I_i^{b^*} \approx \oiint_s (\vec{E}^a \times \vec{H}^{b^*}).\hat{n}\, ds \tag{4.17}$$

Note that the EM fields are not singular in practical cases, and ignoring the difference between the magnetic and electric interaction energies would be a valid assumption except for the mathematically singular sources. The approximation (4.17) becomes an exact relationship if the interaction energies in volume v are exactly zero. Such a case can be considered when the volume v is filled with PEC or the spherical current sources form spherical antennas. Using the orthogonality relationships of the spherical waves, it can be observed that if the different sets of SVWs are excited in problem (a) and (b), (4.17) will be zero, and consequently, the voltage across port# i, V_i^a induced by the excitation of port# j, becomes zero. Hence, the aforementioned criterion in (4.12) not only maximizes the system capacity, but also alleviates the mutual coupling between the MIMO antenna elements. In the case that the antenna elements excite the same SVWs, (4.17) can be used to approximately estimate the mutual coupling between the antennas from the electromagnetic fields radiated by each MIMO antenna element. It is only required to expand the fields in terms of the SVWs, and obtain the coefficients. Then, using integrals known for the SVWs [46], the equation (4.17) provides an approximation for the mutual coupling between the antenna elements. As mentioned before, the weighting coefficients can also be adjusted so that the mutual coupling becomes zero even when the same SVWs are excited by different MIMO antenna elements.

It should be emphasized that the expression (4.17) is obtained thanks to the orthogonality of the SVWs in the near field region. The near field orthogonality of the SVWs lets us choose the smallest sphere making the interaction energies negligible. The near field orthogonality results from the fact that the electromagnetic fields are orthogonalized in the SVW approach, rather than the current sources (which is the case in the characteristic modes). This can be thought of as an important advantage of the SVW approach for the MIMO antenna design, which yields a low correlation coefficient for the antenna elements and good isolation of the excitation ports.

4.4 Spherical MIMO Antenna Design

As discussed before, it is desired to find the current sources for the MIMO antenna elements whose radiation field patterns satisfy the orthogonality condition given in (4.1). The current source construction problem can be thought of as an *inverse source problem* which is defined as constructing the current source localized within a limited space to generate a predefined radiated field [71-82]. In the MIMO antenna case, the desired radiation fields are orthogonal SVWs generated by each of the MIMO antenna elements. Consequently, by solving an inverse source problem for the radiated SVW fields, the required current sources would be obtained for MIMO antenna elements which should be located either inside the given volume space or on the surface surrounding the given space for the antenna structure. Since the SVWs are defined in a spherical coordinate system, the spherical source region is a convenient source domain to obtain the analytic solution of the current sources generating the orthogonal radiation patterns. Therefore, the aim is to take advantage of the inverse source problems in order to find the orthogonal current sources in the spherical volume and surface to be used as the MIMO antenna elements.

Assuming that the current source is a *square-integrable*, it is proposed that the current source is first expanded in terms of the prescribed vector functions, and then the coefficients of vector functions are determined so that the source generates the desired radiation SVW fields. This expansion is also consistent with the *Spectral Theorem* [83]. Based on the Spectral Theorem, if $\vec{J} = £(\vec{E})$ in which £ is a self-adjoint operator, $\vec{J}$ can be expanded in terms of the Eigen functions of the operator £, which is commonly known as *Eigen-decomposition*. Since the aforementioned $\vec{L}$, $\vec{M}$, and $\vec{N}$ are the vector Eigen-functions of the vector Helmholtz equation, it is possible to simply expand the $\vec{J}$ in terms of the VWFs in the spherical coordinate system. Notice that the current source can also be expanded in terms of the VWF in other coordinate systems as well, but since $\hat{a}_1$ cannot be chosen for constructing the VWF, the orthogonal properties of the VWF will be lost. Thus, the coefficient calculations in the current source will need more manipulations [80, 81].

The equations (4.10) and (4.11) show that the projections of the electric field on $\vec{M}^{(4)}$ and $\vec{N}^{(4)}$ are proportional to the projections of the electric current source on $\vec{M}^{(1)}$ and $\vec{N}^{(1)}$, respectively. This observation suggests that the source can be expanded in terms of those $\vec{M}^{(1)}$, $\vec{N}^{(1)}$, and $\vec{L}^{(1)}$ functions which are finite at the origin. Therefore, $\vec{J}$ is represented as:

$$\vec{J}(\vec{r}') = \sum_{n=1}^{\infty}\sum_{m=0}^{n}\left[c_{\substack{e_{mn}\\o_{mn}}} \vec{M}^{(1)}_{\substack{e_{mn}\\o_{mn}}}(\vec{r}') + d_{\substack{e_{mn}\\o_{mn}}} \vec{N}^{(1)}_{\substack{e_{mn}\\o_{mn}}}(\vec{r}') + e_{\substack{e_{mn}\\o_{mn}}} \vec{L}^{(1)}_{\substack{e_{mn}\\o_{mn}}}(\vec{r}') \right] \quad for \;\; r' < r_0 \tag{4.18}$$

Assuming a and b are the desired electric field expansion coefficients in equation (4.10) representing an electric field generated by an electric current source within the volume of a sphere with a radius of r_0 (V'), it is desired to determine the c, d and e coefficients. Replacing the expansion (4.18) in equation (4.11), one can obtain:

$$\begin{bmatrix} a_{\substack{e_{mn}\\o_{mn}}} \\ b_{\substack{e_{mn}\\o_{mn}}} \end{bmatrix} = \alpha\beta_{mn}\left(\begin{bmatrix} c_{\substack{e_{mn}\\o_{mn}}} I_{M'M'} \\ 0 \end{bmatrix} + \begin{bmatrix} 0 \\ d_{\substack{e_{mn}\\o_{mn}}} I_{N'N'} \end{bmatrix} + \begin{bmatrix} 0 \\ e_{\substack{e_{mn}\\o_{mn}}} I_{N'L'} \end{bmatrix} \right) = \alpha\beta_{mn} \begin{bmatrix} c_{\substack{e_{mn}\\o_{mn}}} I_{M'M'} \\ d_{\substack{e_{mn}\\o_{mn}}} I_{N'N'} + e_{\substack{e_{mn}\\o_{mn}}} I_{N'L'} \end{bmatrix} \tag{4.19}$$

$$I_{M'M'} = \int_{V'} \vec{M}'^{(1)}_{\substack{e_{mn}\\o_{mn}}} \cdot \vec{M}'^{(1)}_{\substack{e_{mn}\\o_{mn}}} dv' \;, \quad I_{N'N'} = \int_{V'} \vec{N}'^{(1)}_{\substack{e_{mn}\\o_{mn}}} \cdot \vec{N}'^{(1)}_{\substack{e_{mn}\\o_{mn}}} dv' \;, \quad I_{N'L'} = \int_{V'} \vec{N}'^{(1)}_{\substack{e_{mn}\\o_{mn}}} \cdot \vec{L}'^{(1)}_{\substack{e_{mn}\\o_{mn}}} dv'$$

where the integrals $I_{M'M'}$, $I_{N'N'}$, and $I_{N'L'}$ are given in [46]. Notice that, integrating over the spherical volume, the $\vec{M}$ vector function is orthogonal to both $\vec{L}$ and $\vec{N}$ even if the orders are the same, whereas the $\vec{L}$ and $\vec{N}$ vector functions are not orthogonal when the orders are identical (see Appendix B). Furthermore, if the VWFs of the different orders are not orthogonal, the right-hand side of the simple relationship (4.19) will have to include infinitely many terms. This is the case when the other coordinate systems other than the six aforementioned ones are chosen. The source expansion for the oblate and prolate spheroidal coordinate systems has been presented in [80-82].

As expected, the current source supporting the given electrical field is not unique. This is obvious from (4.19), because an infinite combination of d and e coefficients giving the same b coefficient generates the same radiation field. Hence, there are infinitely many solutions for the inverse source problem. Note that the c coefficients can be uniquely calculated from the a coefficients:

$$c_{\substack{e_{mn}\\o_{mn}}} = a_{\substack{e_{mn}\\o_{mn}}} / \left(\alpha\beta_{mn} I_{M'M'} \right) \tag{4.20}$$

The non-uniqueness of the current source can also be observed from the Green's function representation in (4.9), wherein the *non-radiating* sources (sources that are orthogonal to both $\vec{M}^{(1)}$ and $\vec{N}^{(1)}$ and therefore produce no field coefficient in equation (4.11)) can be added to radiating sources without affecting the radiated field. The non-radiating sources have been defined in [77] for

the general inverse source problems. Hence, in addition to the liberty in choosing the d and e coefficients, any combination of the non-radiating sources with the radiating ones can generate the same radiation field.

Among the infinitely many possible solutions for $\vec{J}$, there is a particular minimum energy source solution [76, 77]. To find this solution, let us assume that the source is square-integrable. The L^2 norm of the current source $\vec{J}$ is then calculated as:

$$\begin{aligned}
&\int_{V'} \left| \vec{J} \right|^2 dv' = \sum_{n=1}^{\infty} \sum_{m=0}^{n} \left[c^2_{\substack{e_{mn} \\ o_{mn}}} I_{M'M'} + d^2_{\substack{e_{mn} \\ o_{mn}}} I_{N'N'} + e^2_{\substack{e_{mn} \\ o_{mn}}} I_{L'L'} + 2 d_{\substack{e_{mn} \\ o_{mn}}} e_{\substack{e_{mn} \\ o_{mn}}} I_{N'L'} \right] \\
&I_{L'L'} = \int_{V'} \vec{L}'^{(1)}_{\substack{e_{mn} \\ o_{mn}}} \cdot \vec{L}'^{(1)}_{\substack{e_{mn} \\ o_{mn}}} dv'
\end{aligned} \tag{4.21}$$

As mentioned before, the a coefficients will determine the c coefficients, but one has the liberty to choose the d and e coefficients in such a way that the L^2 norm is minimized:

$$\begin{aligned}
&Min\left\{ \left| d^2_{\substack{e_{mn} \\ o_{mn}}} I_{N'N'} + e^2_{\substack{e_{mn} \\ o_{mn}}} I_{L'L'} + 2 d_{\substack{e_{mn} \\ o_{mn}}} e_{\substack{e_{mn} \\ o_{mn}}} I_{N'L'} \right| \right\} \\
&Const.: \; b_{\substack{e_{mn} \\ o_{mn}}} = \alpha\beta_{mn} \left(d_{\substack{e_{mn} \\ o_{mn}}} I_{N'N'} + e_{\substack{e_{mn} \\ o_{mn}}} I_{N'L'} \right)
\end{aligned} \tag{4.22}$$

Solving the above simple minimization problem, the following coefficients are obtained to have the minimum energy source:

$$\begin{aligned}
&e_{\substack{e_{mn} \\ o_{mn}}} = 0 \\
&d_{\substack{e_{mn} \\ o_{mn}}} = b_{\substack{e_{mn} \\ o_{mn}}} / \left(\alpha\beta_{mn} I_{N'N'} \right)
\end{aligned} \tag{4.23}$$

Consequently, the minimum energy current source is represented as follows:

$$\begin{aligned}
&\vec{J}_{\min}(\vec{r}') = \sum_{n=1}^{\infty} \sum_{m=0}^{n} \left[c_{\substack{e_{mn} \\ o_{mn}}} \vec{M}^{(1)}_{\substack{e_{mn} \\ o_{mn}}}(r', \theta', \phi') + d_{\substack{e_{mn} \\ o_{mn}}} \vec{N}^{(1)}_{\substack{e_{mn} \\ o_{mn}}}(r', \theta', \phi') \right] \quad for \quad r' < r_0 \\
&where: \quad c_{\substack{e_{mn} \\ o_{mn}}} = a_{\substack{e_{mn} \\ o_{mn}}} / \left(\alpha\beta_{mn} I_{M'M'} \right), \quad d_{\substack{e_{mn} \\ o_{mn}}} = b_{\substack{e_{mn} \\ o_{mn}}} / \left(\alpha\beta_{mn} I_{N'N'} \right)
\end{aligned} \tag{4.24}$$

The same result has been derived using both a mathematical theory for the *ill-posed inverse source problems* [76, 77] and the Lagrangian optimization [79] to obtain the minimum energy volume current distribution confined in a sphere. The main advantages of the new proposed derivation are: 1) the proposed method is a general approach and can deal with different types of constraints, and 2) both the longitudinal and transverse parts are included which makes the source solution more physically meaningful.

Using the inverse source problem mentioned here, it is found that the different current sources containing $\vec{M}$ and $\vec{N}$ vector functions with different orders produced orthogonal SVW functions in the electromagnetic fields. Therefore, by knowing the SVWs required for the orthogonal field radiation patterns, the modal current sources can be reconstructed to be used as MIMO antenna elements. However, $\vec{J}_{\min}$, as represented in (4.24), is a volume current distribution containing only the $\vec{M}$ and $\vec{N}$ vector functions which are divergence-less interior the sphere region excluding the boundary surface, whereas a current source is not divergence-less unless either charge density is zero ($\rho = 0$) or $\omega = 0$. Hence, the current distribution in (4.24) is not practically implementable. Thus, as mentioned in [75], it is not physically possible to realize $\vec{J}_{\min}$ without any non-radiating sources. The equation (4.18) suggests that by adding the $\vec{L}$ vector functions to the current source, it is possible to construct a non-zero divergence $\vec{J}$, which obviously is no longer a minimum energy source. In addition to having a non-zero divergence, the source expression now contains more coefficients, which can be used to apply the other desired constraints to the current source.

Since in most practical cases, the surface current density is preferred over the volume current source, it is desired to find a surface current distribution which can generate a predefined radiated field. For this purpose, the $\vec{L}$ vector functions are added in such a way that the normal component of the current source at the surface $\xi_1 = C$ becomes zero. Notice that it is desirable to add the minimum number of $\vec{L}$ vector functions to keep the source energy as small as possible, because adding any non-radiating source only changes the total energy of the current source and will not affect the radiated field. In a separable curvilinear coordinate system (ξ_1, ξ_2, ξ_3), only the $\vec{L}$ and $\vec{N}$ vector functions have non-zero components along the $\hat{a}_1$ direction:

$$\psi(\xi_1,\xi_2,\xi_3)=\psi_1(\xi_1)\psi_2(\xi_2)\psi_3(\xi_3)$$
$$(\vec{L})_{\xi_1}=\frac{1}{h_1}\psi_2\psi_3\frac{\partial}{\partial\xi_1}(\psi_1)$$
$$(\vec{N})_{\xi_1}=\left(\frac{1}{k}\vec{\nabla}\times\vec{\nabla}\times\left(\hat{a}_1\xi_1\psi\right)\right)_{\xi_1}= \tag{4.25}$$
$$-h_1\psi_1\psi_2\psi_3\frac{\xi_1}{k}\left\{\frac{1}{h_1h_2h_3}\frac{1}{\psi_2}\frac{\partial}{\partial\xi_2}\left[\frac{h_3}{h_1h_2}\frac{\partial}{\partial\xi_2}(h_1\psi_2)\right]+\frac{1}{h_1h_2h_3}\frac{1}{\psi_3}\frac{\partial}{\partial\xi_3}\left[\frac{h_2}{h_1h_3}\frac{\partial}{\partial\xi_3}(h_1\psi_3)\right]\right\}$$

Since ψ is the scalar Helmholtz equation solution, the following relationships can be written as [45]:

$$\frac{1}{h_1h_2h_3}\frac{1}{\psi_1}\frac{\partial}{\partial\xi_1}\left[\frac{h_2h_3}{h_1}\frac{\partial}{\partial\xi_1}(\psi_1)\right]+\frac{1}{h_1h_2h_3}\frac{1}{\psi_2}\frac{\partial}{\partial\xi_2}\left[\frac{h_1h_3}{h_2}\frac{\partial}{\partial\xi_2}(\psi_2)\right]+$$
$$\frac{1}{h_1h_2h_3}\frac{1}{\psi_3}\frac{\partial}{\partial\xi_3}\left[\frac{h_1h_2}{h_3}\frac{\partial}{\partial\xi_3}(\psi_3)\right]+k^2=0$$
or (4.26)
$$\frac{1}{h_1^2f_1}\frac{1}{\psi_1}\frac{\partial}{\partial\xi_1}\left[f_1\frac{\partial}{\partial\xi_1}(\psi_1)\right]+\frac{1}{h_2^2f_2}\frac{1}{\psi_2}\frac{\partial}{\partial\xi_2}\left[f_2\frac{\partial}{\partial\xi_2}(\psi_2)\right]+$$
$$\frac{1}{h_3^2f_3}\frac{1}{\psi_3}\frac{\partial}{\partial\xi_3}\left[f_3\frac{\partial}{\partial\xi_3}(\psi_3)\right]+k^2=0$$

Knowing $h_1=1$ and $f_1=\xi_1^2$, as it was required for expression (4.6), and substituting (4.26) into equation (4.25), the ξ_1 components of the $\vec{L}$ and $\vec{N}$ vector functions on the surface of $\xi_1=C$ are obtained as follows:

$$(\vec{L})_{\xi_1}=\psi_2\psi_3\frac{\partial}{\partial\xi_1}(\psi_1)\Big|_{\xi_1=C}$$
$$(\vec{N})_{\xi_1}=\psi_2\psi_3\frac{\xi_1}{k}\left(k^2\psi_1+\frac{1}{\xi_1^2}\frac{\partial}{\partial\xi_1}\left[\xi_1^2\frac{\partial}{\partial\xi_1}(\psi_1)\right]\right)\Big|_{\xi_1=C} \tag{4.27}$$

Therefore, the ξ_1 components of the $\vec{L}$ and $\vec{N}$ vector functions are in the form of $\psi_2(\xi_2)\psi_3(\xi_3)$ over the surface of $\xi_1=C$, and it is possible to add the $\vec{L}$ vectors to the minimum energy volume current source in such a way that the total ξ_1 component of the current source is canceled out. In the

spherical coordinate system which has orthogonal VWFs, the surface current source $\vec{J}_S$ is expanded in terms of the SVWs on the surface of the sphere shell with a radius of r_0:

$$\vec{J}_S = \sum_{n=1}^{\infty}\sum_{m=0}^{n}\left[c_{\substack{e_{mn}\\o}} \vec{M}^{(1)}_{\substack{e_{mn}\\o}}(r',\theta',\phi') + d_{\substack{e_{mn}\\o}} \vec{N}^{(1)}_{\substack{e_{mn}\\o}}(r',\theta',\phi') + e_{\substack{e_{mn}\\o}} \vec{L}^{(1)}_{\substack{e_{mn}\\o}}(r',\theta',\phi') \right] \delta(r'-r_0) \quad (4.28)$$

Substituting equation (4.28) in (4.11), the following equation is obtained:

$$\begin{bmatrix} a_{\substack{e_{mn}\\o}} \\ b_{\substack{e_{mn}\\o}} \end{bmatrix} = \alpha\beta_{mn} \begin{bmatrix} c_{\substack{e_{mn}\\o}} I_{M'M'} \\ d_{\substack{e_{mn}\\o}} I_{N'N'} + e_{\substack{e_{mn}\\o}} I_{N'L'} \end{bmatrix}$$

$$\begin{aligned} I_{M'M'} &= \int_{V'} \vec{M}'^{(1)}_{\substack{e_{mn}\\o}} \cdot \vec{M}'^{(1)}_{\substack{e_{mn}\\o}} \delta(r'-r_0)dv' = (1+\delta_0)\frac{2\pi}{2n+1}\frac{(n+m)!}{(n-m)!}\, n\,(n+1)\, r_0^2\, \left[j_n(k\,r_0)\right]^2 \\ I_{N'N'} &= \int_{V'} \vec{N}'^{(1)}_{\substack{e_{mn}\\o}} \cdot \vec{N}'^{(1)}_{\substack{e_{mn}\\o}} \delta(r'-r_0)dv' = \\ &\quad (1+\delta_0)\frac{2\pi}{(2n+1)^2}\frac{(n+m)!}{(n-m)!}\, n\,(n+1)\, r_0^2 \left\{(n+1)\left[j_{n-1}(k\,r_0)\right]^2 + n\left[j_{n+1}(k\,r_0)\right]^2\right\} \\ I_{N'L'} &= \int_{V'} \vec{N}'^{(1)}_{\substack{e_{mn}\\o}} \cdot \vec{L}'^{(1)}_{\substack{e_{mn}\\o}} \delta(r'-r_0)dv' = \\ &\quad (1+\delta_0)\frac{2\pi}{(2n+1)^2}\frac{(n+m)!}{(n-m)!}\, n\,(n+1)\, k\, r_0^2 \left\{\left[j_{n-1}(k\,r_0)\right]^2 - \left[j_{n+1}(k\,r_0)\right]^2\right\} \end{aligned} \quad (4.29)$$

where δ_0 has been defined in equation (4.9), and the integrals are presented in [46]. Again, the c coefficients are uniquely determined from a, whereas there are infinite choices for the d and e coefficients. To have the a coefficients in the radiated fields, those radii for which $j_n(k\,r_0)=0$ should be avoided to ensure non-zero $I_{M'M'}$. Furthermore, $I_{N'L'}$ should be non-zero to have the liberty of choosing the e coefficients. Therefore, those radii for which $j_{n-1}(k\,r_0) = \pm j_{n+1}(k\,r_0)$ should also be avoided.

As before, $e=0$ gives the minimum energy source, but the minimum energy source is not a surface current distribution. Therefore, the minimum energy condition should be relaxed. Using equation (4.27) for the spherical coordinate system and (4.29), the two following equations are obtained:

$$\alpha\beta_{mn}\left(d_{\substack{e\\o}mn} I_{N'N'} + e_{\substack{e\\o}mn} I_{N'L'} \right) = b_{\substack{e\\o}mn}$$
$$d_{\substack{e\\o}mn} \frac{n(n+1)}{k r_0} j_n(k r_0) + e_{\substack{e\\o}mn} \left. \frac{\partial}{\partial r'} j_n(k r') \right|_{r'=r_0} = 0 \tag{4.30}$$

The first equation is a result of (4.29), and the second one is imposed to cancel the radial component of the current source. Notice that the radial deferential equation in the spherical coordinate is used to convert the ξ_1 component of $\vec{N}$ to the simple form in (4.30). Solving the equation (4.30), the following surface current distribution is found on a spherical shell with the radius of r_0, which generates the predefined electromagnetic field presented in equation (4.10) [84]:

$$\vec{J}_S = \sum_{n=1}^{\infty}\sum_{m=0}^{n} \vec{J}_{Smn} = \sum_{n=1}^{\infty}\sum_{m=0}^{n} \left[c_{\substack{e\\o}mn} \vec{M}^{(1)}_{\substack{e\\o}mn}(r_0,\theta',\phi') + d_{\substack{e\\o}mn} \vec{N}^{(1)}_{\substack{e\\o}mn}(r_0,\theta',\phi') + e_{\substack{e\\o}mn} \vec{L}^{(1)}_{\substack{e\\o}mn}(r_0,\theta',\phi') \right]$$
$$where: \quad c_{\substack{e\\o}mn} = \frac{a_{\substack{e\\o}mn}}{\alpha\beta_{mn} I_{M'M'}}, \qquad d_{\substack{e\\o}mn} = \frac{b_{\substack{e\\o}mn}}{\alpha\beta_{mn}\left(I_{N'N'} + I_{N'L'}\tau_n\right)}, \tag{4.31}$$
$$e_{\substack{e\\o}mn} = \frac{b_{\substack{e\\o}mn}}{\alpha\beta_{mn}\left(I_{N'L'} + \frac{I_{N'N'}}{\tau_n} \right)}, \qquad \tau_n = \frac{e_{\substack{e\\o}mn}}{d_{\substack{e\\o}mn}} = -\frac{\frac{n(n+1)}{k r_0} j_n(k r_0)}{\left. \frac{\partial}{\partial r'} j_n(k r') \right|_{r'=r_0}}$$

where τ_n is the ratio of the coefficient of the n^{th} order $\vec{L}$ to the coefficient of the n^{th} order $\vec{N}$ vector function. If τ_n was zero for all n s, the minimum energy spherical surface current source would be obtained. However, since the radii for which $j_n(k r_0) = 0$ are avoided, τ_n would not be zero, and generally speaking, it is impossible to obtain the minimum energy current source on the spherical surface for arbitrarily given radiated electromagnetic fields. Although $\vec{J}_S$ contains all three SVWs, the amplitudes of the $\vec{L}$ vector functions have been adjusted so that the total current distribution only has $\hat{\theta}-$ and $\hat{\phi}-$ components. In [84], it is proven that the surface current source presented in (4.31) is a unique solution for the spherical surface electric current source in the homogenous media.

Note that for certain radii, $\partial j_n(k\,r')/\partial r'\big|_{r'=r_0} = 0$, which means that the radial component of $\vec{L}$ is zero and it is impossible to cancel the radial component of the $\vec{N}$ vector function. Hence, to obtain the surface current distribution on the sphere, the radii for which the radial component of $\vec{L}$ is equal to zero must be avoided. As it was emphasized before, a finite number of SVWs appear at the far field. Thus, $j_{n-1}(k\,r_0) \neq \pm j_{n+1}(k\,r_0)$, $j_n(k\,r_0) \neq 0$ and $\partial j_n(k\,r')/\partial r'\big|_{r'=r_0} \neq 0$ should be satisfied for only a finite number of modes ($n < N = kr_0$). Hence, these conditions are not too restrictive.

The surface current sources $\vec{J}_{Smn}$ in (4.31) are more practical than the volumetric source, and generate orthogonal radiating EM fields. Consequently, any element or any disjoint subset (any subset with no element in common) of the derived $\vec{J}_{Smn}$ current sources where $n < N$ can be used as a MIMO antenna element in the uniform PAS. Moreover, any combination of $\vec{J}_{mn}$ and non-radiating sources will create a new arrangement of MIMO antenna elements. Although the practical implementation of the spherical current sources is not discussed here, there are various practical approaches in the literature to implement spherical antennas [85-88]. The recent fabrication technologies and procedures proposed in [87] and [88] can be employed to implement surface current sources on a spherical dielectric. The derived formulation (4.31) can be used to determine the surface current distributions required to design spherical antennas for orthogonal MIMO radiations.

Considering a proper non-radiating source, it is possible to form and design the MIMO antenna elements to be compatible with the desired constraints. The constraint considered here is set to have a spherical surface source, but the non-radiating source can be employed for other constraints such as reactive power [79]. Including the numerical analysis of the VWFs, the proposed approach can be generalized for the arbitrary shape of the antennas in which the non-radiating sources are considered to satisfy the required constraint for the given geometry.

4.5 Planar MIMO Antenna Design

In comparison to 3-dimentional (3D) antennas such as the spherical sources, the planar antennas of various shapes are of greater interest due to their inherent advantages, such as the ease of construction and integration, the low cost, the low profile configuration, and the compactness. Therefore, the investigation to how the planar current source can be used as a MIMO antenna element and how the

physical characteristics of the planar structure will affect the SVW excitations generating the field radiation patterns of MIMO antenna elements is indispensable.

Assuming a planar antenna lying in the *x-y* plane, the planar current source can be represented in the spherical coordinate system in the following form:

$$\vec{J}(\vec{r}') = \left\{ J_r(r',\varphi')\,\hat{r} + J_\varphi(r',\varphi')\,\hat{\varphi} \right\} \; \delta\!\left(\theta - \frac{\pi}{2}\right) \tag{4.32}$$

Replacing (4.32) in relationship (4.11), one can obtain:

$$\begin{aligned} a_{\substack{e\\o}mn} &= -\alpha\beta_{mn} \left.\frac{\partial P_n^m(\cos\theta')}{\partial\theta'}\right|_{\theta'=\frac{\pi}{2}} \int_{S'} j_n(kr') \begin{matrix}\cos\\ \sin\end{matrix} m\varphi'\, J_\varphi(r',\varphi')\, ds' \\ b_{\substack{e\\o}mn} &= \alpha\beta_{mn}\; P_n^m(0) \{ \int_{S'} \frac{n(n+1)}{kr}\, j_n(kr) \begin{matrix}\cos\\ \sin\end{matrix} m\varphi\, J_r(r',\varphi')\, ds' \\ &\qquad \mp \int_{S'} \frac{m}{kr\sin\theta} \frac{\partial}{\partial r}[r j_n(kr)] \begin{matrix}\sin\\ \cos\end{matrix} m\varphi\, J_\varphi(r',\varphi')\, ds' \} \end{aligned} \tag{4.33}$$

Referring to [89], the Legendre function and its derivative have the following values at $\theta = \pi/2$:

$$P_n^m(0) = \begin{cases} 0 & m+n: odd \\ \neq 0 & m+n: even \end{cases} \quad and \quad \left.\frac{\partial P_n^m(\cos\theta)}{\partial\theta}\right|_{\theta=\frac{\pi}{2}} = \begin{cases} \neq 0 & m+n: odd \\ 0 & m+n: even \end{cases} \tag{4.34}$$

Substituting (4.34) in (4.33) to calculate the coefficients of the spherical vector waves excited by a general planar antenna, the following radiated field is obtained [90]:

$$\vec{E}_J(r,\theta,\varphi) = \sum_{\substack{n=1\\ m+n:odd}}^{N}\sum_{m=0}^{n} a_{\substack{e\\o}mn}\, \vec{M}_{\substack{e\\o}mn}^{(4)}(r,\theta,\varphi) + \sum_{\substack{n=1\\ m+n:even}}^{N}\sum_{m=0}^{n} b_{\substack{e\\o}mn}\, \vec{N}_{\substack{e\\o}mn}^{(4)}(r,\theta,\varphi) \quad for\ r_0 < r \tag{4.35}$$

where *N* is determined according Chu's theorem ($n < N = k\,r_0$). Using the *Duality Theorem*, a similar expression can be obtained for the magnetic field *H* radiated by the planar magnetic current source $\vec{M}(\vec{r}')$ lying in the same plane (*x-y* plane). Then, by applying the curl operator on the magnetic field, the following electric field radiated by the planar magnetic current source $\vec{M}(\vec{r}')$ will be obtained:

$$\vec{E}_M(r,\theta,\varphi) = \sum_{\substack{n=1\\ m+n:odd}}^{N}\sum_{m=0}^{n} c_{\substack{e\\o}mn}\, \vec{N}_{\substack{e\\o}mn}^{(4)}(r,\theta,\varphi) + \sum_{\substack{n=1\\ m+n:even}}^{N}\sum_{m=0}^{n} d_{\substack{e\\o}mn}\, \vec{M}_{\substack{e\\o}mn}^{(4)}(r,\theta,\varphi) \quad for\ r_0 < r \tag{4.36}$$

Equations (4.35) and (4.36) show that a planar electric or magnetic current source is not able to excite particular SVWs [90]. For a given bandwidth and the size of an antenna, the planar antenna structure will excite approximately half of the spherical harmonics which can potentially be excited by a 3D current source. Since the field radiation pattern of the antenna elements are dependent on the SVWs propagated by the antenna, the degrees of freedom to orthogonalize the field radiation pattern of the MIMO antenna elements is decreased for a planar current source (antenna).

More importantly, since at least one of the orders, either *m* or *n*, is different in (4.35) and (4.36), it can be concluded that the planar electric and magnetic current sources lying in the same plane radiate orthogonal electromagnetic fields. This conclusion can be used for the MIMO antenna designs. If the electric and magnetic current sources can be implemented on the same plane, each current source can be used as one MIMO antenna element. To verify this idea, one simple antenna, compromising of both magnetic and electric current sources in the same plane is depicted in Figure 4.2. The designed MIMO antenna contains a ring slot antenna, modeled by the ring magnetic current, and a half-wavelength dipole antenna which can be represented by the electric current source. The S-parameters of the designed MIMO antenna are illustrated in Figure 4.3.

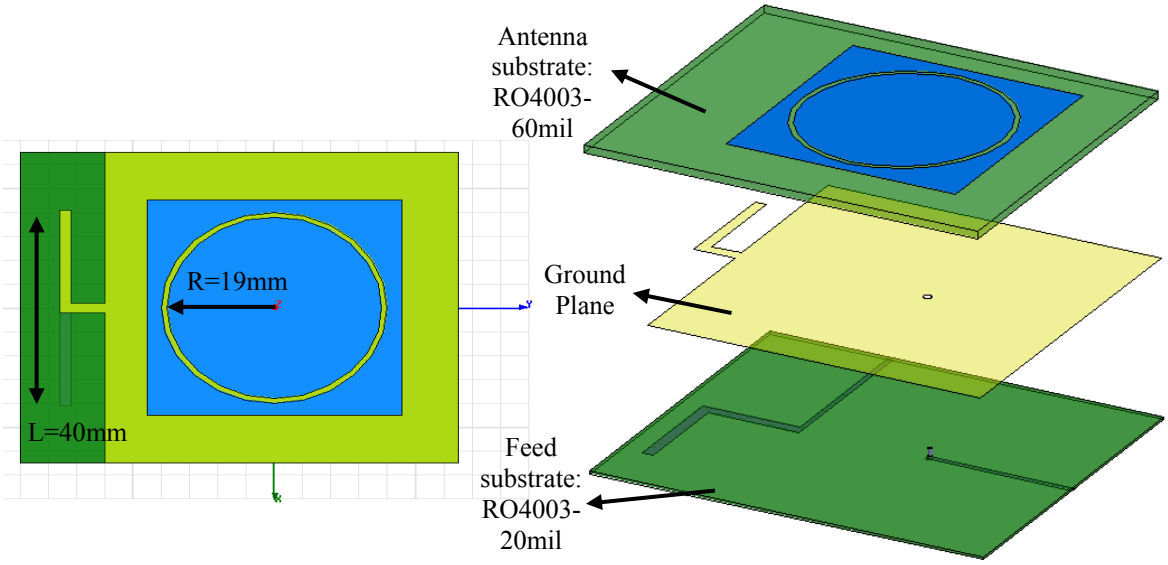

Figure 4.2: MIMO antenna design containing magnetic and electric currents in the x-y plane

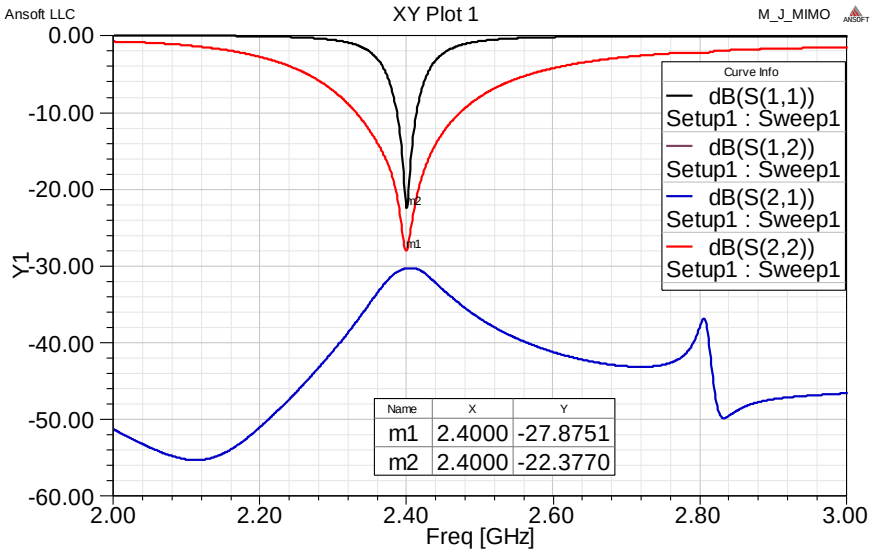

Figure 4.3: S-parameters of the MIMO antenna shown in Figure 4.2

In this design, the effort is devoted to match the input impedance of two MIMO antenna elements, and as can be seen, the two inputs are appropriately isolated thanks to the orthogonality of the EM field radiated by the co-planar magnetic and electric current sources. Note that the suitable isolation can also be observed for other implementations of co-planar magnetic and electric current sources. The two-port MIMO antenna shown in Figure 4.2 is only one simple example of such an implementation.

The gain radiation patterns of two MIMO antenna elements are illustrated in Figure 4.4.

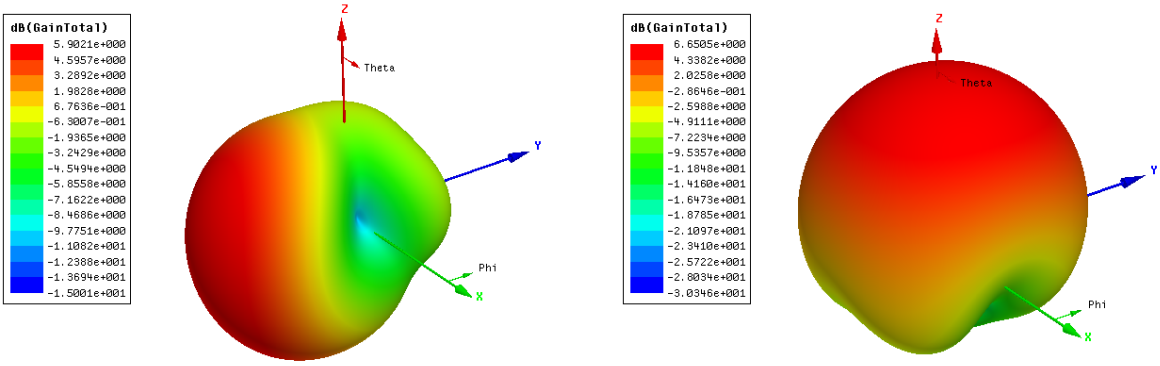

(a) (b)

Figure 4.4: The gain radiation patterns of the two MIMO antennas shown in Figure 4.2

To investigate the orthogonality of the field radiation patterns in the physical MIMO channels, a Monte Carlo simulation is required to study the statistical behaviour of the correlation coefficient. In this simulation, the Laplacian wireless channel is modeled by four clusters with equal power coefficients, $\sigma_{\phi n} = 30^{\circ}$, $\sigma_{\theta n} = 30^{\circ}$, and with uniformly distributed mean angles of arrival. The cumulative density function of the correlation coefficient is plotted in Figure 4.5. As can be observed, the correlation coefficient between the signals received by the two MIMO antenna elements is less than 0.3 for 98% of the time. The statistical analysis of the correlation coefficient shows that the idea of the co-planar magnetic and electric current source implementation can be effectively applied to obtain orthogonal field radiation patterns.

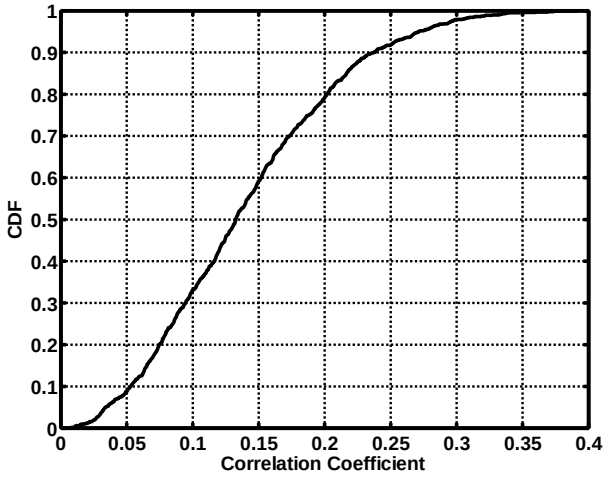

Figure 4.5: The cumulative density function of the correlation coefficient in the Laplacian channel

4.6 Conclusion

The spherical vector waves approach was introduced as an analytical tool to analyze and design current sources for MIMO antenna applications. The SVWs establish an orthogonal set of vector wave functions for electromagnetic fields. Thus, the transformation of the radiated fields into the SVW spectrum provides a physical insight into the antenna design problems. The orthogonality properties of the SVWs can also be employed to generate orthogonal field radiation patterns for MIMO antennas. Although the SVW orthognality is valid for the free space, the SVW behaviour through an arbitrary physical channel model can be investigated (this will be discussed in Chapter 5 with more details). Once the orthogonal SVWs through the given channel are know, it is required to

obtain the current sources (antennas) which excite the predefined SVWs as vector field radiations of the MIMO antenna elements. One of the main contributions of this research is to analytically solve the inverse surface source problem by including the non-radiating sources in current source solution. Using the non-radiating current sources, the modal surface current sources are obtained on a sphere to excite the desired SVWs. The spherical surface source formulation contributes in the designing of the spherical antennas for MIMO applications.

Additionally, the analytical representations of the current source distributions were studied for planar antennas, and it is shown that the co-planar magnetic and electric current sources generate orthogonal vector field radiation patterns. This observation was used to design a two-port planar MIMO antenna. A statistical analysis of the correlation coefficient was also presented for the Laplacian channel model to investigate the orthogonality of the vector field radiation patterns in different realizations of the non-uniform channels.

Chapter 5
Systematic Spherical Vector Wave Method

In Chapter 4, the orthogonality of the SVWs was utilized to obtain the orthogonal current source distributions which provide a physical insight to analytically design the MIMO antenna elements. Since the SVWs are orthogonal in the free space, the uniform PAS was considered to obtain the orthogonal current distributions, whereas it is crucial to include an arbitrary physical channel model in the orthogonalization procedure. Meanwhile, the spherical nature of the SVWs leads to analytical derivations that are limited to the spherical shape antennas, though in many practical cases the arbitrary shapes of the antennas are of more interest. In this chapter, a systematic methodology based on the SVW formulation is proposed not only to include the arbitrary MIMO wireless channel model in the MIMO antenna design, but to also obtain the optimal current distributions (antenna elements) for a given arbitrary shape of the antenna structure. Additionally, the SVW formulation is utilized to determine the degrees of freedom in the MIMO antenna design for a given wireless channel and antenna structure.

5.1 Spherical Vector Wave Formulation

Since SVW functions establish a complete orthogonal set of vector functions for radiated electromagnetic fields, it is advantageous to analyze the correlation coefficient in (2.11) in terms of the SVWs. Considering a multi-antenna configuration using N_a antenna elements in the MIMO system, the vector angular dependence of the radiated field of the k^{th} antenna element excited by the unit current (vector radiation pattern), $\vec{E}_k$, can be expanded in terms of the angular part of the SVWs:

$$\vec{E}_k(\theta,\phi) = \sum_{n=1}^{N} a_n^k \, \vec{u}_n(\theta,\phi) \tag{5.1}$$

where $\vec{u}$ is the angular part of the far field spherical vector wave functions ($\vec{M}^{(4)}$ and $\vec{N}^{(4)}$ vector wave functions defined in Chapter 3), the a_n^k coefficients are the weights of the n^{th} SVW function in the radiated electromagnetic field by the k^{th} antenna element, and N is the maximum number of spherical waves which can appear in the far field region according to Chu's Theorem.

In general, there is no guarantee that the vector field radiation patterns of the MIMO antenna elements, $\vec{E}_k$, are orthogonal in the given PAS of the wireless channel. One possible approach for

orthogonalization is to combine the vector field radiations of the MIMO antenna elements with different sets of current excitations to obtain the orthogonal vector field radiation patterns through the given PAS. Hence, the *MIMO system mode*, denoted by $\vec{F}_i$, is defined as the vector field radiation pattern of the MIMO antenna structure when the vector field radiation patterns of the MIMO antenna elements are weighted by the complex current excitations and combined to form an orthogonal vector field radiation pattern. Assuming I_i^k is the current excitation of the k^{th} antenna elements in the i^{th} MIMO system mode, $\vec{F}_i$ can be written as:

$$\vec{F}_i = \sum_{k=1}^{N_a} I_i^k \vec{E}_k = \sum_{k=1}^{N_a} I_i^k \left(\sum_{n=1}^{N} a_n^k \vec{u}_n(\theta,\phi) \right) = \sum_{n=1}^{N} \left(\sum_{k=1}^{N_a} I_i^k \, a_n^k \right) \vec{u}_n(\theta,\phi) = = \sum_{n=1}^{N} \alpha_n^i \, \vec{u}_n(\theta,\phi) \qquad (5.2)$$

where a^k is the SVW expansion coefficients of $\vec{E}_k$, and α_n^i is the contribution of the n^{th} spherical wave in the vector radiation pattern of the i^{th} MIMO system mode. If the vector field radiation pattern of each antenna element is supposed to be used as one MIMO system mode, $\vec{F}_i$ is simply $\vec{E}_k$.

Note that if $\vec{E}_k$ is considered as the radiated field of an individual antenna in the presence of other antenna elements, the mutual coupling effects can also be included in the SVW expansion coefficients, a^k. Thus, the proposed formulation is general and can effectively include the electromagnetic interactions between the antenna elements and other objects in the vicinity.

Rewriting (5.2) in the matrix form as shown in (5.3), the matrix $\mathbf{M}$ is constructed such that the k^{th} row of $\mathbf{M}$ contains the coefficients of the SVWs excited by the k^{th} antenna element [54]:

$$\mathbf{F} = \mathbf{IMW}$$

$$\mathbf{F} = \begin{bmatrix} \vec{F}_1 \\ \vdots \\ \vec{F}_i \\ \vdots \\ \vec{F}_M \end{bmatrix} \quad \mathbf{I} = \begin{bmatrix} I_1^1 & \cdots & I_1^{N_a} \\ \vdots & & \vdots \\ I_i^1 & \cdots & I_i^{N_a} \\ \vdots & & \vdots \\ I_M^1 & \cdots & I_M^{N_a} \end{bmatrix} \quad \mathbf{M} = \begin{bmatrix} a_1^1 & \cdots & a_N^1 \\ \vdots & & \vdots \\ a_1^k & \cdots & a_N^k \\ \vdots & & \vdots \\ a_1^{N_a} & \cdots & a_N^{N_a} \end{bmatrix} \quad \mathbf{W} = \begin{bmatrix} \vec{u}_1(\theta,\phi) \\ \vdots \\ \vec{u}_k(\theta,\phi) \\ \vdots \\ \vec{u}_N(\theta,\phi) \end{bmatrix} \qquad (5.3)$$

where M is the number of orthogonal MIMO system modes (M sets of current excitations), which should be considered as the degrees of freedom for the MIMO antenna system. Using the SVW

representation (5.3), the inner product of $\vec{F}_i$ and $\vec{F}_j$, which is defined in (2.11), can be written as follows [54]:

$$< \vec{F}_i , \vec{F}_j >_P = \sum_{n=1}^{N} \sum_{p=1}^{N} \alpha_n^i \, \alpha_p^{j\,*} < \vec{u}_n , \vec{u}_p >_P = (\mathbf{IM})_i \; \mathbf{G} \; (\mathbf{IM})_j^{\dagger}$$

$$\mathbf{G} = \begin{bmatrix} < \vec{u}_1 , \vec{u}_1 >_P & \cdots & < \vec{u}_N , \vec{u}_1 >_P \\ \vdots & & \vdots \\ < \vec{u}_1 , \vec{u}_p >_P & \cdots & < \vec{u}_N , \vec{u}_p >_P \\ \vdots & & \vdots \\ < \vec{u}_1 , \vec{u}_N >_P & \cdots & < \vec{u}_N , \vec{u}_N >_P \end{bmatrix} \tag{5.4}$$

where $(\mathbf{IM})_i$ stands for the i^{th} row of matrix $\mathbf{IM}$, and contains α_n^i. The defining interaction matrix, $\mathbf{R}$, whose element, R_{ij}, is the interaction of the i^{th} and j^{th} MIMO system modes through the given PAS, $< \vec{F}_i , \vec{F}_j >_P$, one can obtain:

$$\mathbf{R} = (\mathbf{IM})\mathbf{G}(\mathbf{IM})^{\dagger} \qquad \mathbf{R} = \begin{bmatrix} R_{11} & \cdots & R_{M1} \\ \vdots & & \vdots \\ R_{1i} & \cdots & R_{iM} \\ \vdots & & \vdots \\ R_{1M} & \cdots & R_{MM} \end{bmatrix} \tag{5.5}$$

After calculating the interaction matrix, $\mathbf{R}$, the correlation coefficients between the MIMO system modes can be obtained by (2.11). Therefore, the correlation coefficient is represented in terms of the inner products of known spherical vector waves, and once the inner products are investigated for a specific PAS associated with a specific wireless environment, the α coefficients, which are entries of the matrix $\mathbf{IM}$, are enough to calculate the cross-correlation between the MIMO system modes.

Notice that the a_n^k coefficients in the matrix $\mathbf{M}$ depend on the physical properties including the size, the location, the orientation and the material of the MIMO antenna elements. Also, the matrix $\mathbf{G}$ entries, which are the inner products of the SVWs through the given PAS, are independent of the MIMO antennas. Hence, the SVW representation (5.5) separates the complex current excitations (feed circuit), the physical properties of antenna elements, and the wireless communication environment effects into $\mathbf{I}$, $\mathbf{M}$, and $\mathbf{G}$ matrices, respectively. Therefore, for a given PAS, the

matrix $\mathbf{G}$ can be evaluated independently of MIMO antenna design, and the optimization criteria can be imposed on the $\mathbf{M}$ and $\mathbf{I}$ entries rather than $\vec{F}_i$ and $\vec{F}_j$ which are θ- and φ-dependent functions. Accordingly, the $\mathbf{M}$ matrix can be optimized first, and once an optimal choice for the antenna configuration and physical properties is made in terms of the practical restrictions, the current excitations can either be optimized to generate different MIMO system modes or be adaptively changed in a time-varying environment (adaptive MIMO antenna system).

The SVW representation can be used to find the maximum number of MIMO system modes, *M*, and the *M* sets of the current excitations, matrix $\mathbf{I}$, which results in the diagonal matrix $\mathbf{R}$ to achieve maximum system capacity. For this purpose, the matrix orthogonalization methods such as the Eigen-value decomposition can be used to find the conditions on the matrix $\mathbf{I}$ so that the matrix $\mathbf{R}$ is diagonal [91, 92].

Since $<\vec{u}_i,\vec{u}_j>_P=(<\vec{u}_j,\vec{u}_i>_P)^*$, $\mathbf{G}$ is the Hermitian matrix [83]. Additionally, since the inner product of $<\vec{F}_i,\vec{F}_i>=(\mathbf{IM})_i\ \mathbf{G}\ (\mathbf{IM})_i^\dagger$ is physically interpreted as the received power by the i^{th} MIMO system mode for the given PAS, the matrix $\mathbf{G}$ is a positive-definite matrix [48, 83]. Therefore, the singular value decomposition of matrix $\mathbf{G}$ can be written as:

$$\mathbf{G}=\mathbf{QDQ}^\dagger \tag{5.6}$$

where $\mathbf{Q}$ is the unitary matrix and $\mathbf{D}$ is a diagonal matrix whose diagonal entries are real positive values. Then replacing (5.6) in representation (5.5) and defining matrix $\mathbf{Z}$, one can obtain:

$$\mathbf{R}=(\mathbf{IZ})(\mathbf{IZ})^\dagger \qquad \textit{where} \quad \mathbf{Z}=\mathbf{MQD}^{1/2} \tag{5.7}$$

For a given PAS, the matrix $\mathbf{G}$ can be calculated, and the $\mathbf{Q}$ and $\mathbf{D}$ matrices can be obtained through singular value decomposition. The matrix $\mathbf{M}$ is also constructed from the SVW expansion of the vector field radiation patterns of the MIMO antenna elements. Thus, the matrix $\mathbf{Z}$ can be obtained for the MIMO antenna structure in a certain wireless environment. The SVD of matrix $\mathbf{Z}$ can be used to diagonalize the matrix $\mathbf{R}$:

$$\mathbf{Z}=\mathbf{USV}^\dagger \tag{5.8}$$

where $\mathbf{U}$ and $\mathbf{V}$ are unitary matrices and $\mathbf{S}$ is a diagonal matrix whose diagonal entries are singular values of $\mathbf{Z}$ (the root of Eigen values of the matrix $\mathbf{R}$). Therefore, choosing $\mathbf{I}=\mathbf{U}^\dagger$ for the complex

current excitations makes the rows of the matrix $\mathbf{IZ}$ orthogonal yielding to the diagonal matrix $\mathbf{R}$ [91, 92]. Note that the calculated current excitations are implemented through an RF feed circuit rather than via baseband signal processing. Thus, the proposed approach optimizes the EM characteristics of the MIMO antenna system to make the channel transfer matrix diagonal, whereas in conventional spatial multiplexing, the antenna properties are fixed and considered as part of wireless channel.

The rank of the matrix $\mathbf{Z}$ determines the maximum achievable number of MIMO system modes. The singular values of $\mathbf{Z}$, which are the diagonal elements of the matrix $\mathbf{S}$, also represent the root of the power gains of the corresponding MIMO system modes. Therefore, the calculated singular values show how strong the designed MIMO system mode is in receiving or transmitting the signals through the wireless environment. In the case that a transmitter has the knowledge of the channel, the water-filling may be used to allocate higher or lower power levels to lower or higher power gain MIMO system modes, respectively [1, 2, 10], in order to maximize the system capacity. However, in the case of the formulation (2.5) in which it is assumed the transmitter does not know the channel state information, the maximum capacity is obtained when the power gains of the MIMO system modes are equalized as much as possible. To increase the rank of the matrix $\mathbf{Z}$ and equalize the singular values, the matrix $\mathbf{M}$ can be manipulated by optimizing the physical properties of the MIMO antenna elements. Since there are restrictions to optimize the physical properties in many practical cases, the best effort should be performed to achieve the maximum number of MIMO system modes with equalized power gains.

To summarize the proposed systematic method to find the optimal MIMO system modes supported by the given antenna structure, the design procedure would entail in the following steps [54]:

1- For the given wireless environment, the matrix $\mathbf{G}$ should be evaluated, and the $\mathbf{Q}$ and $\mathbf{D}$ matrices should be obtained by the SVD of the matrix $\mathbf{G}$.

2- Using the physical properties of the MIMO antenna elements, the radiated field of the individual MIMO antenna elements should be expanded in terms of the SVWs to form matrix $\mathbf{M}$ as represented in (5.3). The rank and singular values of the matrix $\mathbf{Z} = \mathbf{MQD}^{1/2}$ determine the maximum number of effective MIMO system modes, *M*. Therefore, the physical properties of the MIMO antenna elements included in the matrix $\mathbf{M}$ can be designed so that *M* is increased and the power gains of the *M* MIMO system modes are equalized. If the matrix $\mathbf{M}$

can be optimized so that the orthogonal MIMO system modes are achieved with the identity matrix $\mathbf{I}$, there is no need to obtain optimal current excitations. However, the physical properties of the antenna elements may be constrained in many practical cases so that the diagonal matrix $\mathbf{R}$ may not be achieved by manipulating the matrix $\mathbf{M}$ only.

3- Once the physical properties of the antenna elements are fixed, the complex current excitations in the matrix $\mathbf{I}$ should be determined to obtain the diagonal matrix $\mathbf{R}$. Decomposing the matrix $\mathbf{Z}$ into $\mathbf{Z} = \mathbf{USV}^{\dagger}$ using the SVD method, it is found the optimal choice for current excitations is $\mathbf{I} = \mathbf{U}^{\dagger}$ which makes the rows of the matrix $\mathbf{IZ}$ orthogonal and maximizes the system capacity. Since there are *M* number of orthogonal MIMO system modes, the optimal sets of current excitation are achieved by *M* different rows of the matrix $\mathbf{I} = \mathbf{U}^{\dagger}$. Note that the matrix $\mathbf{I}$ will be a unitary matrix. Therefore, $\sum_{k=1}^{N_a} \left| I_i^k \right|^2$ remains identical for the current excitations fed into the antenna elements in various MIMO system modes.

This formulation provides a systematic method to designing the MIMO antenna elements to achieve orthogonal signals through the given wireless environment. As mentioned before, the SVW formulation separates the MIMO channel effect, the physical properties of MIMO antenna elements, and the complex current excitations provided by the feed circuit into three cascaded matrices. In the next sections, it will be shown how each matrix presented in the SVW formulation can be used to design and analyze the MIMO antenna systems in wireless environments.

5.2 MIMO Channel Analysis

The matrix $\mathbf{G}$ represented in (5.4) contains the inner products of the SVWs through the PAS for a wireless environment. Therefore, the inner products can be evaluated independently of the MIMO antenna structure, and the MIMO channel effects on the orthogonality of the SVWs can be investigated prior to designing the MIMO antenna elements. Once the SVW behaviour through the physical environment is known, the MIMO antenna elements can be intelligently designed so that the orthogonal signals are obtained through the MIMO system modes. For instance, in the case of the uniform PAS, the matrix $\mathbf{G}$ is a diagonal matrix. Therefore, different sets of SVWs can provide the orthogonal field radiation patterns for the MIMO antenna elements, as discussed in Chapter 4.

For the non-uniform PAS, the orthogonality of the SVWs is not necessarily held, and non-zero inner products will be obtained. In this case, the design criterion can be set to excite those SVWs which can make the inner products as small as possible for different non-uniform PAS realizations. For example, consider that the PAS is only φ-dependent as presented in [61, 64]. Using the SVWs of $\vec{M}^{(4)}$ and $\vec{N}^{(4)}$, four possible inner products, $<\vec{M}^{(4)},\vec{M}^{(4)}>$, $<\vec{M}^{(4)},\vec{N}^{(4)}>$, $<\vec{N}^{(4)},\vec{M}^{(4)}>$, and $<\vec{N}^{(4)},\vec{N}^{(4)}>$, would have one of the following two forms:

$$\begin{aligned} I_1 &= A_1\int_0^{\pi}\frac{m}{\sin\theta}P_n^m(\cos\theta)\frac{\partial P_q^p(\cos\theta)}{\partial\theta}\sin\theta\,d\theta + \\ &\quad A_2\int_0^{\pi}\frac{p}{\sin\theta}P_q^p(\cos\theta)\frac{\partial P_n^m(\cos\theta)}{\partial\theta}\sin\theta\,d\theta \\ I_2 &= B_1\int_0^{\pi}\frac{mp}{\sin^2\theta}P_n^m(\cos\theta)P_q^p(\cos\theta)\sin\theta\,d\theta + \\ &\quad B_2\int_0^{\pi}\frac{\partial P_n^m(\cos\theta)}{\partial\theta}\frac{\partial P_q^p(\cos\theta)}{\partial\theta}\sin\theta\,d\theta \end{aligned} \tag{5.9}$$

where the *A* and *B* coefficients are the resultants of integrals with respect to φ, and therefore, are the functions of PAS. According to the orthogonality relationships presented in [46] for the Legendre functions, the above integrals are zero for particular *m*, *n*, *p*, and *q*. Zero and non-zero inner products of a few SVWs are shown in Table 5.1 and 5.2 by using "0" and "×", respectively. Notice that $\vec{M}_{o0n}=0$ and $\vec{N}_{o0n}=0$ in general, and therefore, these vector wave functions are excluded from Table 5.1 and 5.2.

Table 5.1: The inner Products of SVW functions [55]

$<\vec{M}_{e\,mn}^{(4)},\vec{M}_{e\,pq}^{(4)}>$ / $<\vec{N}_{o\,mn}^{(4)},\vec{N}_{o\,pq}^{(4)}>$		*pq*				
		01	**11**	**02**	**12**	**22**
mn	**01**	×	0	0	×	0
	11	0	×	×	0	×
	02	0	×	×	0	×
	12	×	0	0	×	0
	22	0	×	×	0	×

Table 5.2: The inner Products of SVW functions [55]

$<\vec{M}^{(4)}_{e_{o}^{mn}}, \vec{N}^{(4)}_{e_{o}^{pq}}>$ $<\vec{N}^{(4)}_{e_{o}^{mn}}, \vec{M}^{(4)}_{e_{o}^{pq}}>$		*pq*				
		01	**11**	**02**	**12**	**22**
mn	**01**	0	×	0	0	×
	11	×	0	0	×	0
	02	0	0	0	×	0
	12	0	×	×	0	×
	22	×	0	0	×	0

If those SVWs which provide the orthogonality in the elevation angle, θ, are excited as vector field radiation patterns of the MIMO antenna elements, the orthogonality is held independent of the probability density function of the φ-dependent PAS. Of course, this would be the case only when the probability of incoming signals from all elevation angles is one.

For the case where the inner products are not zero, the random behaviour of the *A* and *B* parameters can be investigated to gain insight into the spherical vector wave interactions in the Laplacian cluster channel. A Monte-Carlo simulation can be performed using the Laplacian probability density function to investigate the statistical behaviour of the correlation coefficient for different SVWs in a non-uniform PAS. In the Monte-Carlo simulation, four clusters are considered which have an azimuth angular spread of 30 degrees, and the mean angle of arrival for each cluster has a uniform distribution over 0 to 2π. The cumulative density function of the correlation coefficient for different pair of SVWs is illustrated in Figure 5.1.

As can be seen in Figure 5.1, the orthogonality of the different pairs of SVWs would be differently affected in the Laplacian channel. For instance, if the correlation coefficient of 0.1 is of interest, the probability that the correlation coefficient for $\vec{M}_{e11}$ and $\vec{N}_{e01}$ vector functions is less than 0.1 is only 20%. This means that the desired correlation coefficient (equivalently, the system capacity) cannot be obtained for 80% of the time. Hence, in order to avoid large correlation coefficients, these two modes should not be excited by two MIMO antenna elements. Therefore, the statistical behaviour of the inner products provides an insight to observe which SVWs hold the otrthogonality for most of the time.

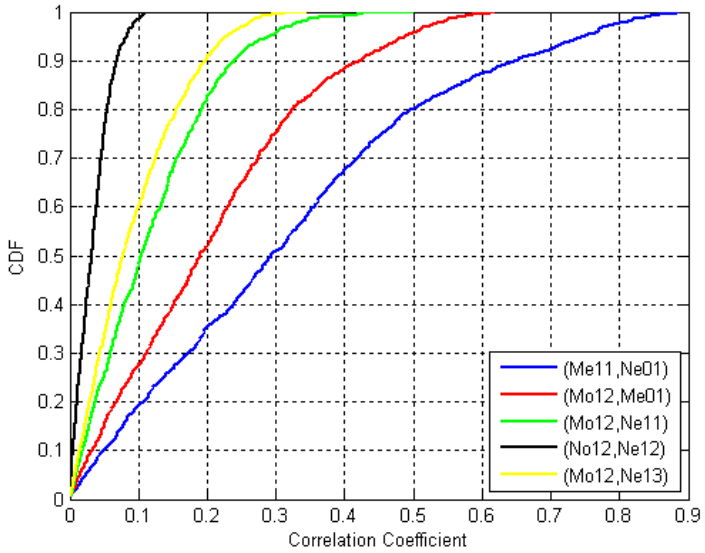

Figure 5.1: The CDF of the correlation coefficient between various SVWs for a Laplacian PAS [55]

The advantage of the SVW method is the fact that the CDF curves are independent of the antenna elements. It is only required to calculate these curves once for each SVW pair to construct the matrix $\mathbf{G}$, and then design the MIMO antenna elements in such a way that they excite the appropriate SVWs. For instance, the analytic method proposed in Chapter 4 can be used to obtain the current distributions exciting those SVWs whose orthogonality is not sensitive to the wireless channel. This way, low correlation coefficients will be obtained for an acceptable percentage of time. However, in order to have an efficient MIMO system, it should be possible to adaptively update current excitations according to the channel variations by using phase shifters and switches in the feed circuit of the MIMO antennas. Alternatively, deterministic physical channel models such as the ray tracing model can be used to rigorously calculate the PAS for specific classes of wireless environments. In this case, a deterministic matrix $\mathbf{G}$ is obtained and can be used for calculating the $\mathbf{Q}$ and $\mathbf{D}$ matrices in (5.6).

5.3 Optimal Current Excitations of MIMO Antennas

In this section, the approach formulated in Section 5.1 is applied to practical multi-antenna configurations where the MIMO antenna elements are given, and it is desired to find optimal current excitations generating the orthogonal MIMO system modes for the given MIMO antenna structure and wireless channel.

5.3.1 Four-Element MIMO Antenna System

The first configuration comprises four half wavelength dipoles (N_a=4) centered at the *x*-*y* plane and directed in the *z*-direction, as depicted in Figure 5.2.

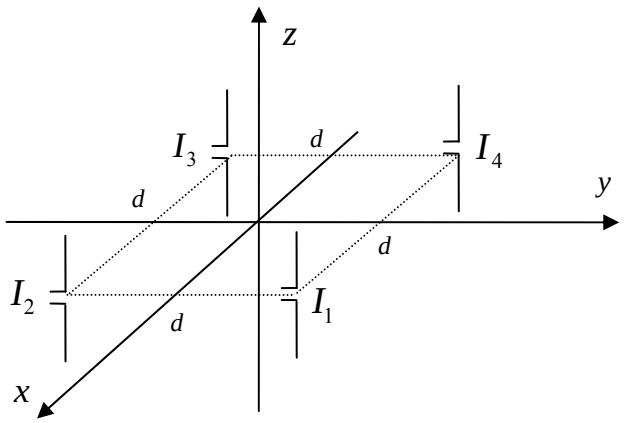

Figure 5.2: The MIMO system comprising of four half wavelength dipole antennas [54]

The matrix $\mathbf{G}$ is calculated for both the uniform PAS ($P(\Omega)=1$) and the double directional Laplacian clustered channel model presented in (2.13). For the non-uniform PAS, it is assumed there are four clusters centered at $\bar{\phi}_k = 0, 90, 180, 270^\circ$ and $\bar{\theta}_k = 90^\circ$, and $\sigma_{\phi k}$ and $\sigma_{\theta k}$ are chosen to be 30°, as depicted in Figure 5.3. As mentioned before, depending on the wireless environment, any other arbitrary PAS could be used for calculating the matrix $\mathbf{G}$.

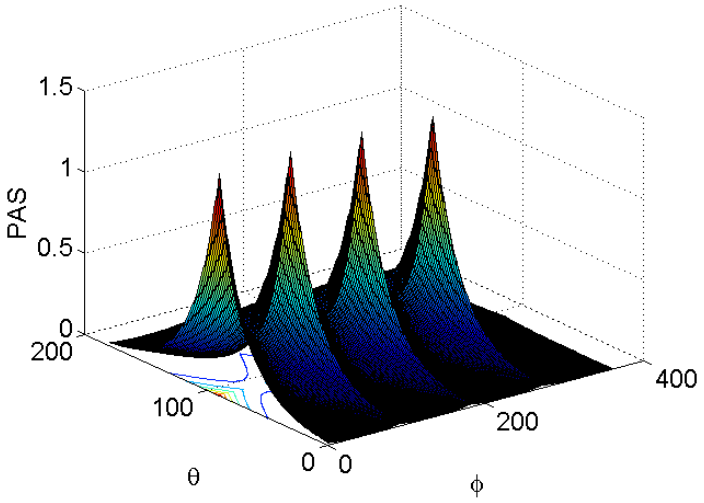

Figure 5.3: The Laplacian power angular spectrum

Similar to the discussion presented in Section 5.1, it is obvious that the optimal SVW spectrum for the MIMO antennas, i.e. the optimal matrix $\mathbf{IM}$, is obtained when $\mathbf{IM} = \mathbf{Q}^{\dagger}$. Therefore, the rows of the matrix $\mathbf{Q}^{\dagger}$ and the diagonal elements of the matrix $\mathbf{D}$ are respectively SVW coefficients and the power gains of optimal MIMO system modes which can be achieved by the antenna (current sources) enclosed in a sphere. Each row of the matrix $\mathbf{Q}^{\dagger}$ can be used as the coefficients of SVWs in (4.10), and analytic method presented in Chapter 4 can be employed to find the optimal spherical surface current source to generate the optimal MIMO system modes. However, the antenna architecture here is limited to four dipole antennas which may not be capable of producing the optimal SVW spectrum.

Next step is to construct the matrix $\mathbf{M}$. To include mutual coupling effects in the correlation calculations, the SVW coefficients in each row of the matrix $\mathbf{M}$ should be calculated for each antenna element excited in the presence of three other antenna elements. To consider the mutual couplings, the MoM presented in Appendix A, is used to include the influence of parasitic antenna elements (with the short circuit terminations) on the vector field radiation pattern of the excited antenna element. Note that the formulation is general and the other effects such as antenna interactions with the enclosure can also be included into the SVW coefficient calculations.

If the output of each half wavelength dipole is supposed to be used to provide a MIMO system mode, the matrix $\mathbf{I}$ would be an identity matrix. For this case, the correlation coefficient between a pair of half wavelength dipoles separated by *d* is calculated when the mutual coupling effects are also included. The blue and red lines in Figure 5.4 depict the magnitude of the correlation coefficient for the uniform and Laplacian clustered PAS versus *d*, respectively, with an identity matrix $\mathbf{I}$.

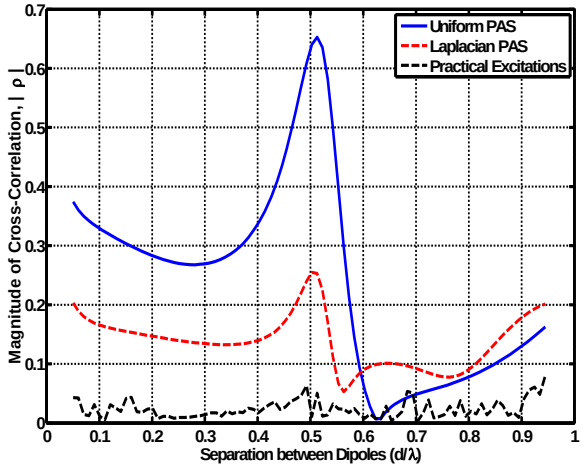

Figure 5.4: The correlation coefficient for two dipoles in a 4-element MIMO system [54]

As can be seen, due to the mutual coupling of the four MIMO antenna elements, the correlation coefficient is significantly increased even for half a wavelength separation. However, the optimal current excitations can be obtained so that the orthogonal MIMO system modes are achieved for a given separation of d and a non-uniform Laplacian PAS.

To perform orthogonalization, the matrix $\mathbf{Z} = \mathbf{M}\mathbf{Q}\mathbf{D}^{1/2}$ should be calculated, and using the SVD method, the optimal current excitations, $\mathbf{I} = \mathbf{U}^{\dagger}$, generate four orthogonal modes. The calculated current excitations for the four MIMO system modes are given in Table 5.3 for the particular separation of $d = \lambda/4$ and the given Laplacian PAS. Note that the amplitudes are in terms of dB, with I_1 as the normalization reference.

Table 5.3: The exact current excitations for the four MIMO system modes [54]

Mode #	I_1	I_2	I_3	I_4
1	0	$-8.53\angle 63.44^{\circ}$	$8.15\angle -12.46^{\circ}$	$4.53\angle -8.44^{\circ}$
2	0	$-4.70\angle -175.91^{\circ}$	$-7.46\angle -4.44^{\circ}$	$1.45\angle -178.64^{\circ}$
3	0	$2.21\angle 11.36^{\circ}$	$-5.19\angle 152.12^{\circ}$	$-29.08\angle -1.71^{\circ}$
4	0	$1.39\angle -156.97^{\circ}$	$-0.20\angle -173.99^{\circ}$	$0.46\angle 8.11^{\circ}$

When implementing the optimal current excitations with a feed circuit, the correlation coefficient becomes exactly zero, but the exact values of the phase and the amplitude of the complex currents achieved by $\mathbf{I} = \mathbf{U}^{\dagger}$ are difficult to practically implement. For realizability, the current excitations can be deviated from the exact solution so that the correlation coefficient remains below a reasonable threshold. Assuming that 0.5 dB and 10 degrees resolution can be provided in adjusting the amplitude and the phase of the current excitations, respectively, the rounded current excitations are given in Table 5.4 for the separation of $d = \lambda/4$.

Table 5.4: The rounded current excitations for the four MIMO system modes [54]

Mode #	I_1	I_2	I_3	I_4
1	0	$-8.5\angle 60^{\circ}$	$8\angle -10^{\circ}$	$4.5\angle -10^{\circ}$
2	0	$-4.5\angle -180^{\circ}$	$-7.5\angle 0^{\circ}$	$1.5\angle 180^{\circ}$
3	0	$2\angle 10^{\circ}$	$-5\angle 150^{\circ}$	$-29\angle 0^{\circ}$
4	0	$1.5\angle -160^{\circ}$	$0\angle -170^{\circ}$	$0.5\angle 10^{\circ}$

The current excitations in Table 5.4 result in a correlation coefficient equal to 0.01 for the Laplacian PAS given in Figure 5.3. The black line in Figure 5.4 also shows the correlation coefficient obtained for MIMO system modes in the Laplacian PAS when the optimal current excitations are realized at 0.5 dB and 10 degrees of resolution in the amplitude and phase adjustments. As it can be seen, the optimal MIMO system modes provide negligible correlation coefficients even after considering the practical imperfections. Of course, if lower resolutions are used for the phase and amplitude implementations, the correlation coefficient will increase.

The four optimal MIMO system modes generated by the current excitations given in Table 5.4 are shown in Figure 5.5. Note that although the antenna structure and PAS are symmetric with respect to the *x*- and *y*- axis, the field radiation patterns of the optimal MIMO system modes are not symmetrically distributed. This shows that the four dipole antennas arranged as in Figure 5.2 cannot generate the optimal SVW spectrum obtained by $\mathbf{IM} = \mathbf{Q}^{\dagger}$ which would be directive beams toward four clusters. Due to the limitations imposed by the geometry of the four dipole antennas, the optimal MIMO system modes are obtained as asymmetric vector field radiation patterns shown in Figure 5.5.

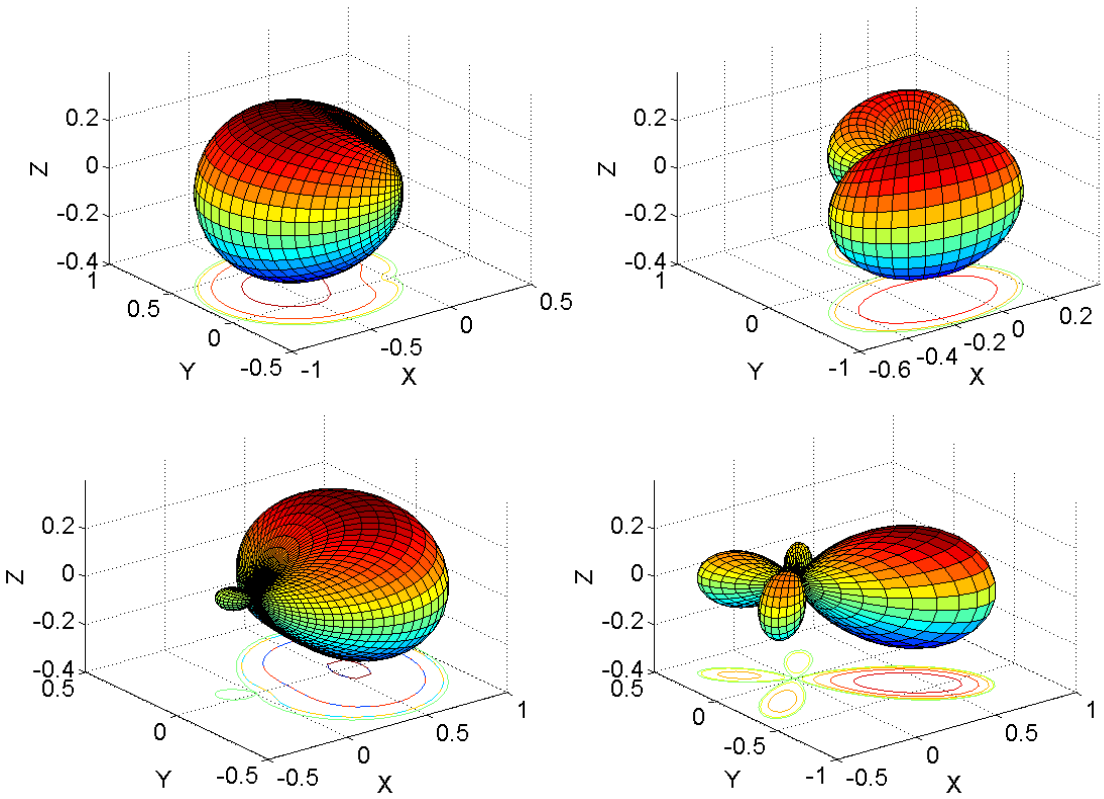

Figure 5.5: The four optimal MIMO system modes for the 4-element MIMO system

The normalized SVW spectra of the four MIMO system modes are also given in Figure 5.6 (the mode index corresponds to $mn = 01, 11, 02, 12, 22, ...$). As can be observed, the identical SVWs may be excited for different MIMO system modes in order to achieve orthogonality through a non-uniform PAS. In the case that the channel is dynamically changed, the SVW coefficients should be updated with new sets of current excitations to adaptively update the orthogonal MIMO system modes.

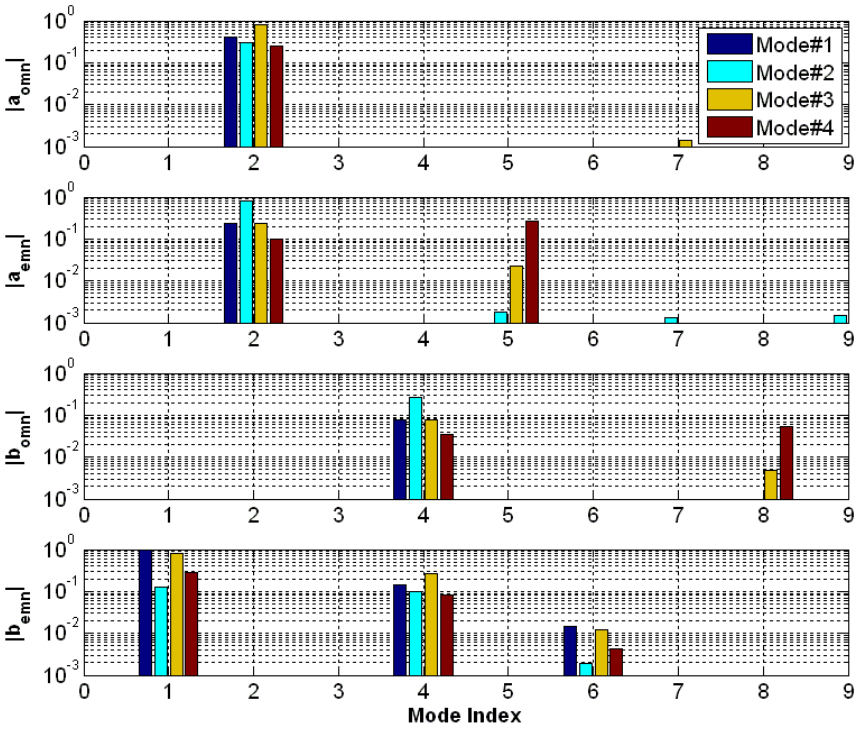

Figure 5.6: The normalized SVW coefficients obtained for the four MIMO system modes [54]

Note that although small correlation coefficients are obtained using optimal MIMO system modes for the antenna separations as small as $d = 0.1\lambda$, the system capacity is not guaranteed to be maximum. As discussed before, the power gains of the MIMO system modes should also be taken into account for the capacity evaluations. The four singular values of the matrix $\mathbf{Z} = \mathbf{M}\mathbf{Q}\mathbf{D}^{1/2}$ obtained for the four MIMO system modes versus the antenna separation of d are plotted in Figure 5.7. Accordingly, the singular values of the MIMO system modes are increased when the antenna separations become larger. Hence, although four MIMO system modes are obtained for small antenna separations, the low amount of mode power gains yield to a lower system capacity in comparison to the capacity achieved by larger separations.

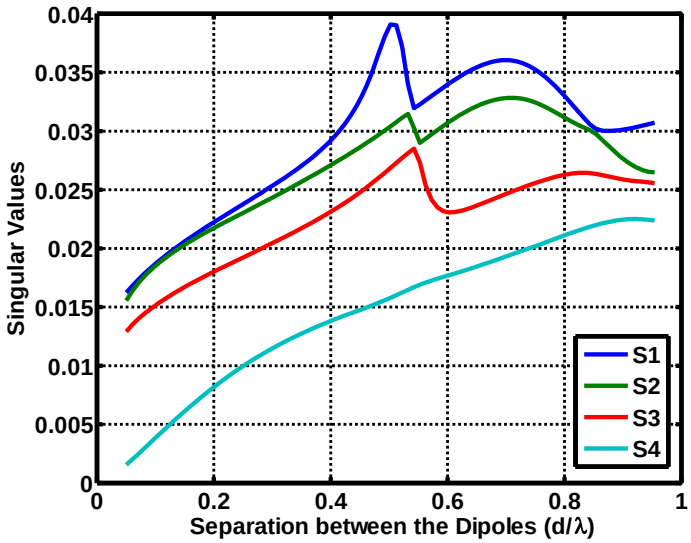

Figure 5.7: The singular values of optimal MIMO system modes in the Laplacian PAS

It is also notable that three of the MIMO system modes are dominant in very small antenna separations and that the other mode becomes stronger when the antennas' separation is increased. Therefore, even though the rank of the matrix $\mathbf{Z}$ is four for small separations, there are three MIMO system modes that dominantly contribute in increasing the system capacity of MIMO system. For design purposes, those antenna separations should be chosen so that the power gains of all the MIMO system modes are as identical as possible.

5.3.2 Multi-port Patch Antenna

In the previous example, a fixed PAS was considered, and the optimal MIMO system modes were obtained to achieve the maximized system capacity for the given structure. However, in various environments, the wireless channel dynamically varies over the time and there is no guarantee that the calculated MIMO system modes for a certain channel would be orthogonal in other channel realizations. As mentioned, the current excitations can be adaptively updated to maintain the orthogonality over the time. Alternatively, the statistical behaviour of the channel realizations can be investigated, and the MIMO system modes can be obtained accordingly.

In this subsection, the SVW approach is employed to effectively optimize the feed circuit of the MIMO antenna system for a dynamic channel environment. The multi-port patch antenna is a suitable candidate for the MIMO antenna elements which provide the pattern orthogonality. Multi-port patch

antennas have been investigated in [68, 93]. It has been shown that the orthogonal radiation patterns can be obtained by exciting the different modes of the patch antennas. Using the orthogonal properties of the radiation patterns, the MIMO antennas can be designed to provide small correlation coefficients. As a practical example, a two-port circular patch antenna has been designed at 2.4 GHz in HFSS. The circular patch geometry and simulated S-parameters are shown in Figure 5.8.

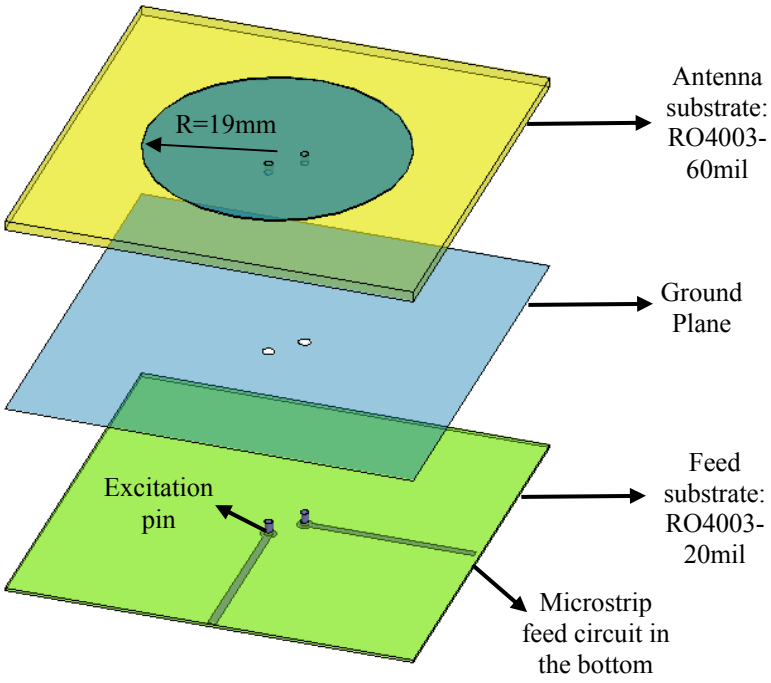

(a)

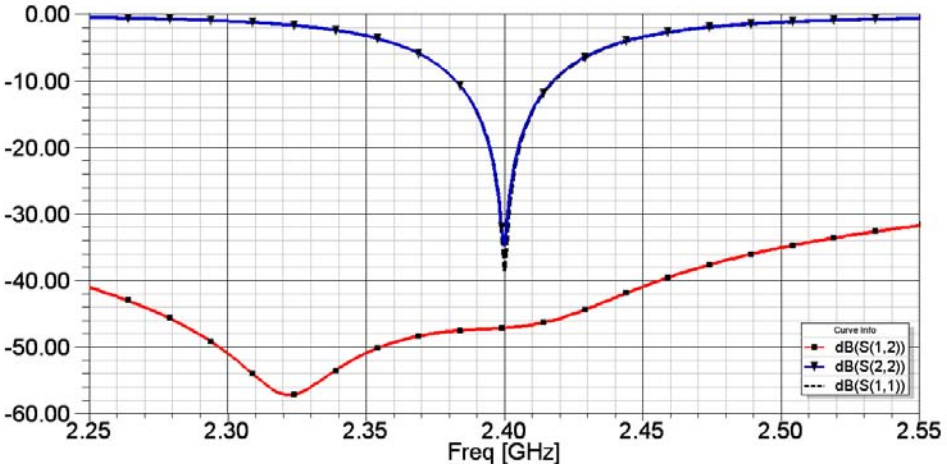

(b)

Figure 5.8: A two-port circular patch antenna; (a) antenna geometry (b) simulated S-parameters

As can be seen, both ports are matched at the operating frequency, and the isolation between the ports is more than 45dB. Using (2.12), the correlation coefficient of the MIMO signals provided by the two-port circular patch is almost zero. Accordingly, the vector field radiation patterns should be orthogonal in the uniform PAS. The simulated gain radiation patterns are presented in Figure 5.9 and 5.10 when port# 1 and 2 are excited, respectively. The simulated gain radiation patterns verify that the two MIMO system modes, generated by the two ports of the circular patch antenna are orthogonal in both polarization and the space. Accordingly, a low correlation coefficient is expected in even the non-uniform channels. To investigate how the MIMO system performance is affected in the physical wireless channel, the statistical behaviour of the correlation coefficient is studied for the Laplacian clustered channel model.

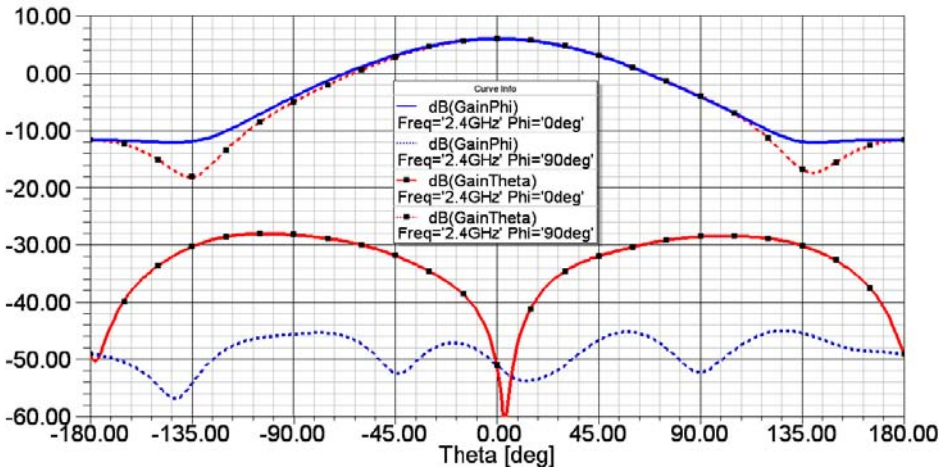

(a)

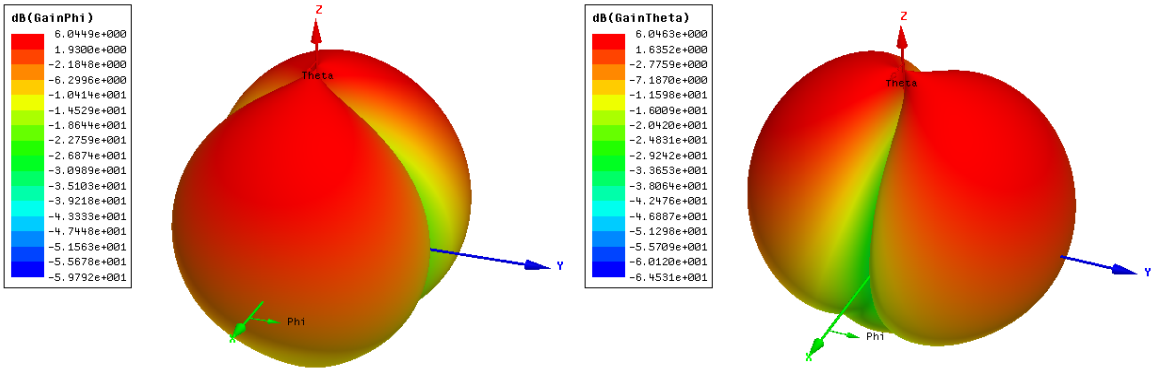

(b)

Figure 5.9: (a) The gain radiation patterns for two φ-planes when port#1 in Figure 5.8.a is excited, (b) The 3D gain radiation patterns when port#1 in Figure 5.8.a is excited

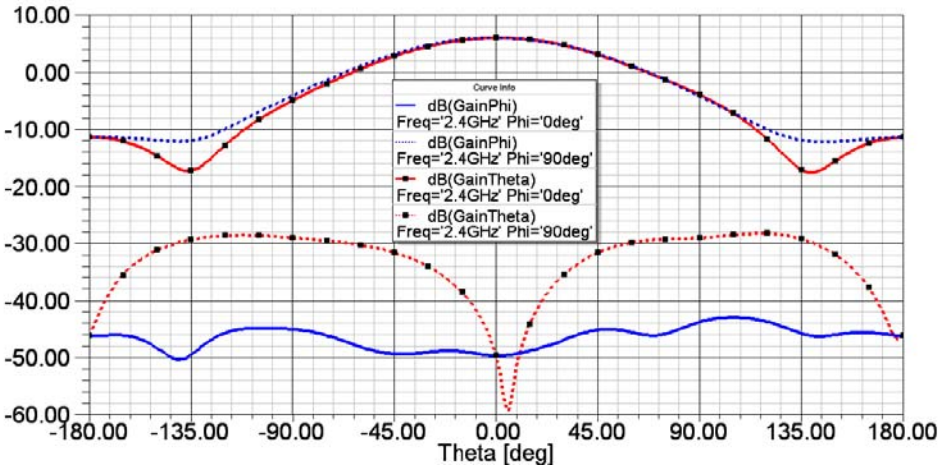

(a)

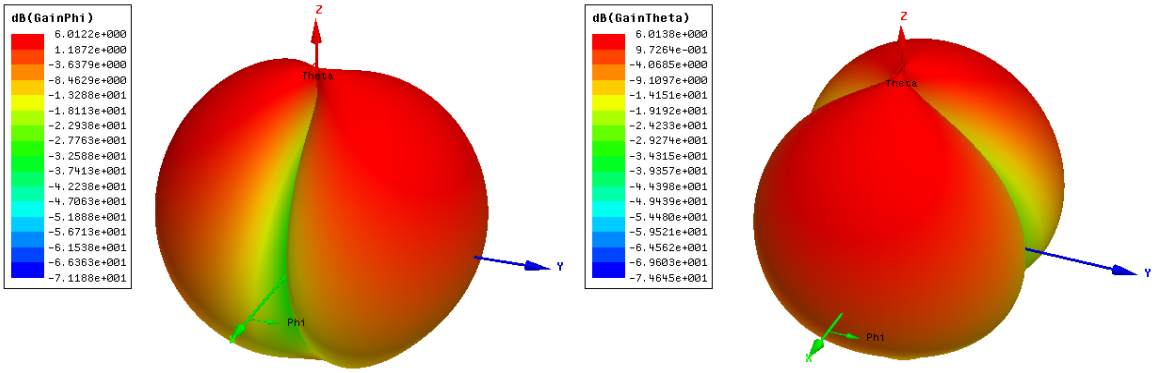

(b)

Figure 5.10: (a) The gain radiation patterns for two φ-planes when port#2 in Figure 5.8.a is excited, (b) The 3D gain radiation patterns when port#2 in Figure 5.8.a is excited

Since $P(\Omega)$ is a random function varying for different random parameters of the Laplacian distribution, the correlation coefficient should be calculated for various channel realizations. In the statistical simulations, 1000 channel realizations are considered. For each channel realization, the mean angles of arrival of the clusters are randomly changed, and the corresponding correlation coefficient is calculated. Through this Mont-Carlo simulation, the CDF of correlation coefficient is illustrated in Figure 5.11 for different number of clusters and various angular spreads. As can be seen, when there is a lower number of clusters and smaller angular spread, a higher correlation coefficient is achieved.

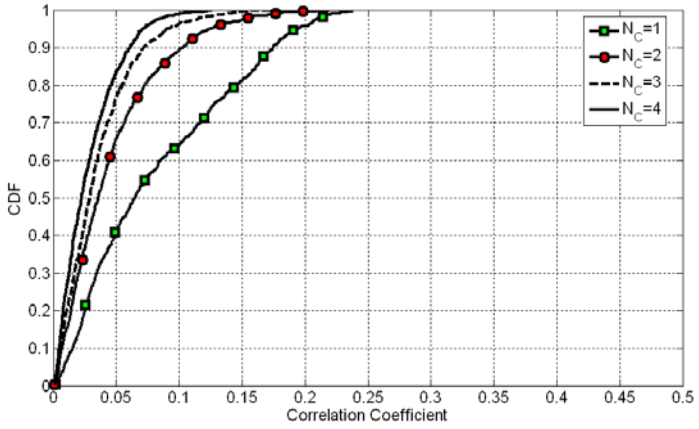

(a)

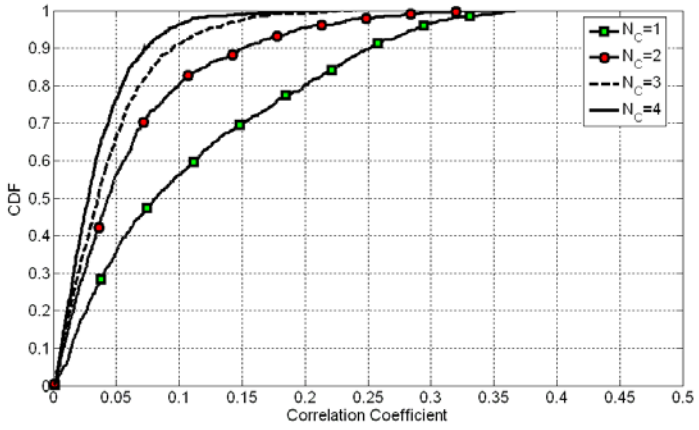

(b)

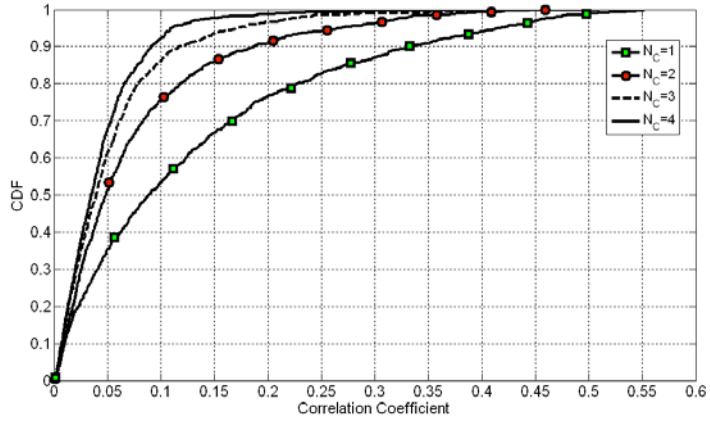

(c)

Figure 5.11: The CDF of the correlation coefficient obtained from the two-port circular patch antenna (a) $\sigma_{\phi n} = \sigma_{\theta n} = 30^{\circ}$ (b) $\sigma_{\phi n} = \sigma_{\theta n} = 20^{\circ}$ (c) $\sigma_{\phi n} = \sigma_{\theta n} = 10^{\circ}$

Accordingly, if the desired correlation coefficient is chosen to be 0.1, the correlation coefficient is less than 0.1 for 64%, 56%, and 53% of the time for one cluster channel with an angular spread of 30^o, 20^o, and 10^o, respectively. Therefore, in the worst case scenario, which is one cluster with an angular spread of 10^o, the desired system capacity cannot be achieved for 47% of the time, and the maximum correlation of 0.55 may occur. Hence, even though the MIMO vector radiation patterns are orthogonal in the uniform PAS, the desired system capacity is lost for a high percentage of the time in the physical wireless channel.

Obtaining the optimum complex current excitations for the two-port circular patch antenna, it is shown that the percentage of time for which the correlation coefficient is less than the desired value can be enhanced. Following the proposed SVW formulation, the first step is to find the matrix $\mathbf{G}$ for a certain channel realization, and then, determine the complex currents accordingly. Since the calculated current excitations result in a zero correlation coefficient for the corresponding channel realization, it is critical to choose the appropriate channel realization for which the matrix $\mathbf{G}$ should be calculated. One reasonable choice is the worst channel realization in which the highest value of correlation coefficient is achieved. According to Figure 5.11, three largest correlation coefficients are 0.55, 0.52, and 0.51 for 1, 2, and 3 clusters with an angular spread of 10^o. Hence, the Laplacian distribution in (2.13) with the PAS parameters corresponding to the three chosen large correlation coefficients are used as $P(\Omega)$ to calculate the entries of the matrix $\mathbf{G}$. Notice that the calculated matrices $\mathbf{G}$ are attributed to the chosen PASs and are independent of the MIMO antenna elements.

The next step is to construct the matrix $\mathbf{M}$ for a two-port circular patch. In this case, the MIMO antenna elements are the identical circular patch antenna excited through different ports. Therefore, the matrix $\mathbf{M}$ will have two rows; each row contains SVW coefficients of the vector field radiation pattern excited by each port when the other port is matched. The SVW coefficients are obtained by expanding the HFSS simulation results given in Figure 5.9 and 5.10 in terms of the SVWs. Knowing the matrix $\mathbf{M}$ for the two-port circular patch and the $\mathbf{G}$ matrices for the three severe channel realizations, the optimal complex currents of the exciting ports are obtained, and the feed circuit can be designed appropriately.

To obtain $\mathbf{I} = \mathbf{U}^{\dagger}$ as the optimum current excitation matrix, the matrix $\mathbf{Z}$ should be calculated. Calculating the matrix $\mathbf{Z}$ and using SVD, the three optimal complex current excitations to achieve zero correlation coefficient through three chosen channel realizations are obtained.

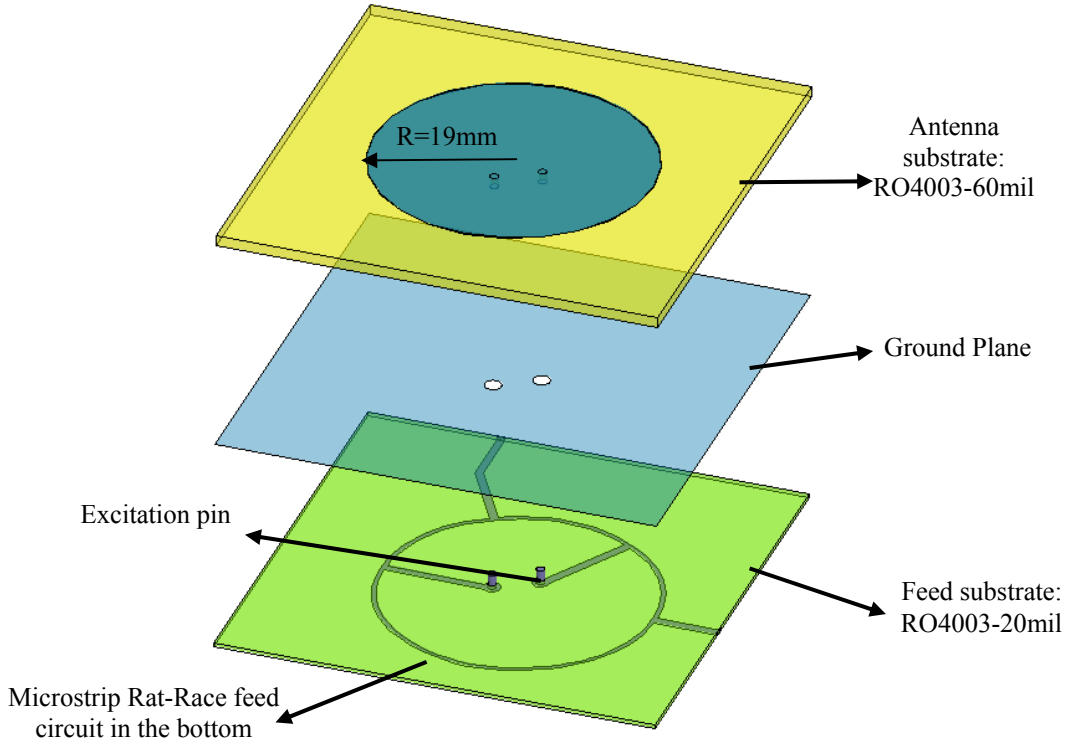

(a)

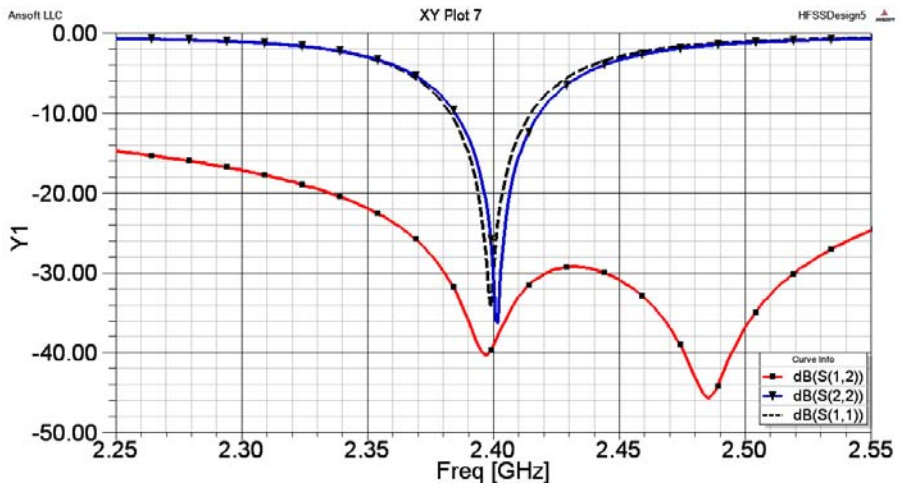

(b)

Figure 5.12: The two-port circular patch antenna with the optimal feed circuit;

(a) antenna geometry (b) simulated S-parameters

The average of the current excitations obtained for severe channel realizations is calculated as:

$$\mathbf{I} = \begin{bmatrix} 0.705 \angle 0^{\circ} & 0.707 \angle 178.2^{\circ} \\ 0.707 \angle 0^{\circ} & 0.705 \angle -1.8^{\circ} \end{bmatrix} \tag{5.10}$$

The calculated current excitation matrix can be implemented by the Rat-Race circuit. The Rat-Race circuit is designed and optimized in the *Advanced Design System* (ADS), and then is imported into the HFSS. Attaching the designed feed circuit to the two-port circular patch antenna, the antenna geometry and simulated S-parameters are shown in Figure 5.12. Since the two ports are matched and isolated, the S-parameter based formulation results in an almost zero correlation coefficient. By exciting each input port of the feed circuit when the other port is matched, the vector field radiation patterns of two MIMO system modes are obtained. The simulated gain radiation patterns are shown in Figure 5.13 and 5.14.

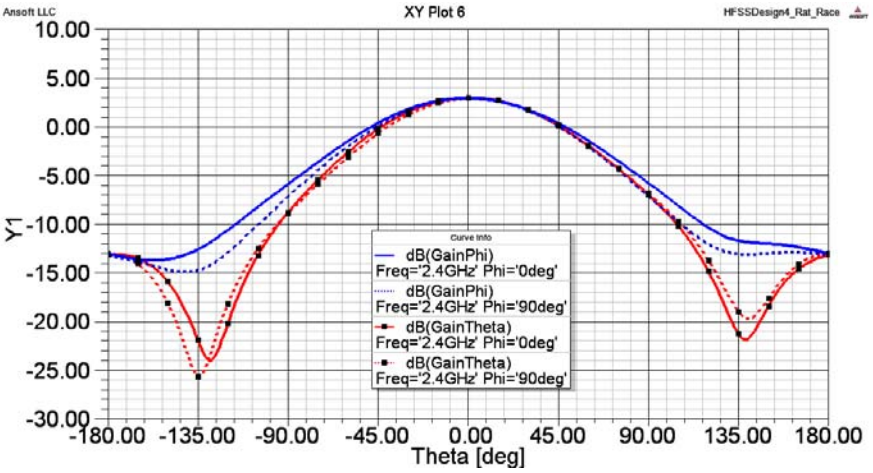

(a)

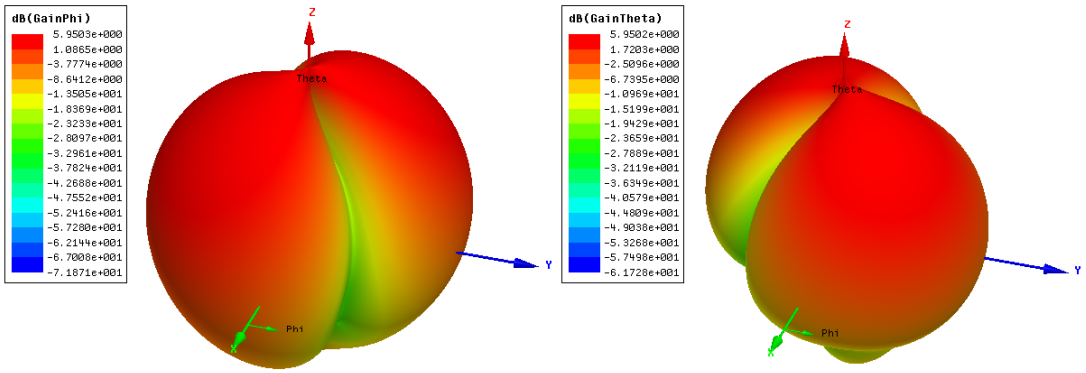

(b)

Figure 5.13: (a) The gain radiation patterns for two φ-planes when port#1 in Figure 5.12.a is excited, (b) The 3D gain radiation patterns when port#1 in Figure 5.12.a is excited

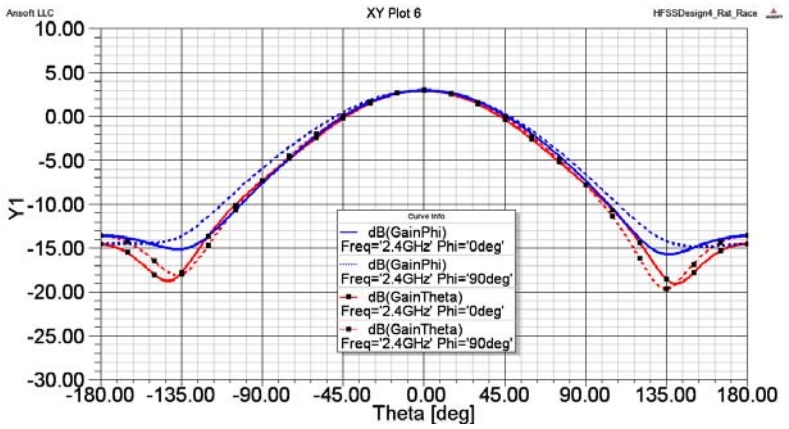

(a)

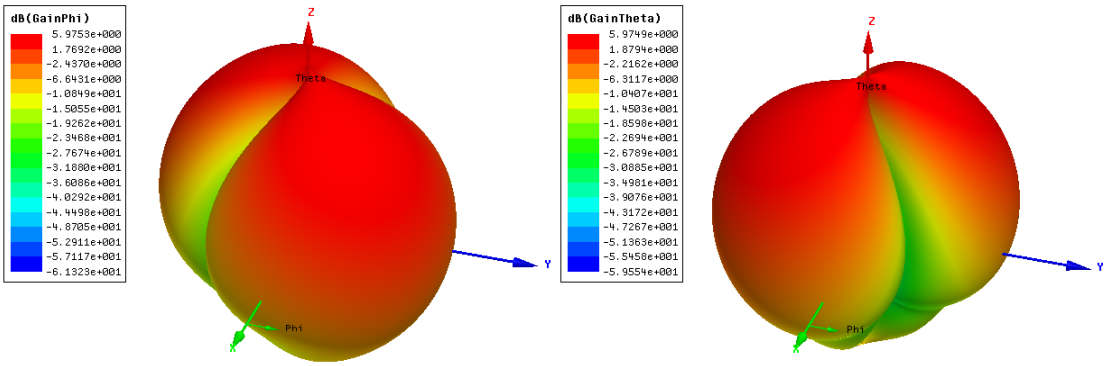

(b)

Figure 5.14: (a) The gain radiation patterns for two φ-planes when port#2 in Figure 5.12.a is excited, (b) The 3D gain radiation patterns when port#2 in Figure 5.12.a is excited

Expanding the field radiation patterns given in Figure 5.13 and 5.14 in terms of the SVWs and performing the Mont-Carlo simulation for the Laplacian clustered channel model, the CDF curves of the correlation coefficient are depicted in Figure 5.15. As can be seen, the correlation coefficient is less sensitive to the number of clusters in comparison to the case where no feed circuit was used. The maximum possible value of the correlation coefficient is also decreased to 0.43. More importantly, the percentage of time for which the correlation is less than 0.1 has been significantly increased. For instance, the correlation coefficient is less than 0.1 for 93%, 78%, and 73% of the time, for one cluster channel that has an angular spread of 30^{o}, 20^{o}, and 10^{o}, respectively. Significant improvements in the time percentages are also observed for other number of clusters as well. Therefore, including the wireless channel effects in the MIMO system mode design can efficiently provide the desired system capacity for higher percentage of time in the MIMO antenna system.

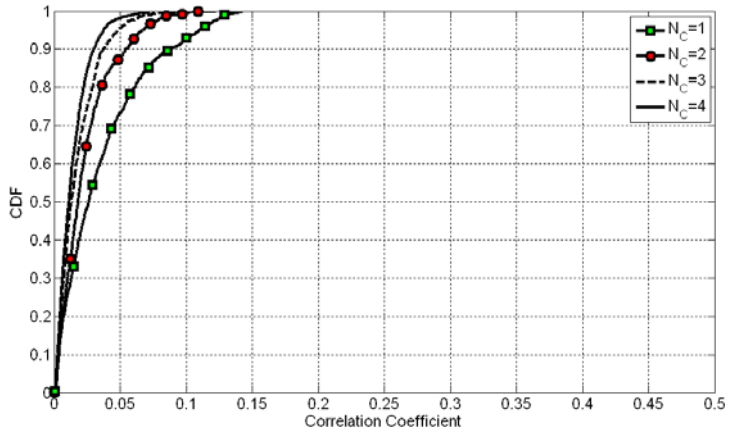

(a)

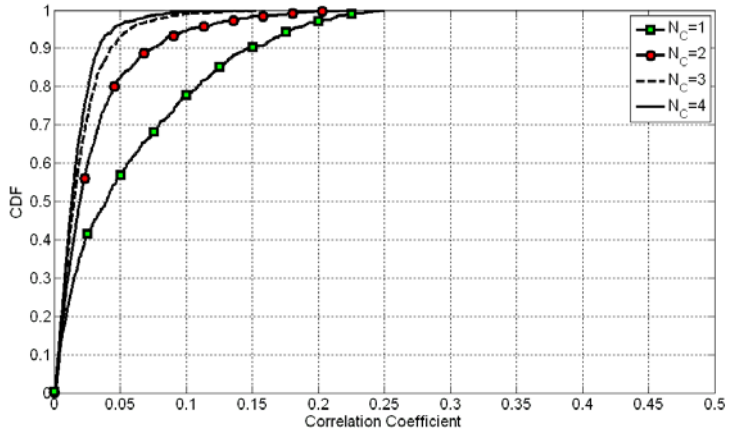

(b)

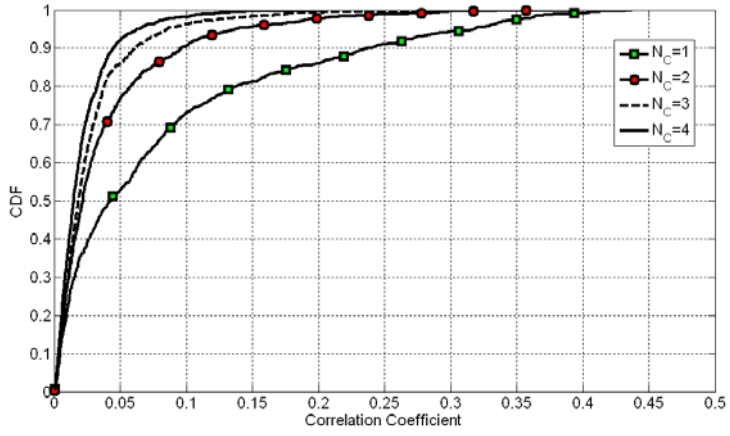

(c)

Figure 5.15: The CDF of the correlation coefficient for the two-port circular patch antenna with an optimal feed circuit (a) $\sigma_{\phi n} = \sigma_{\theta n} = 30^{\circ}$ (b) $\sigma_{\phi n} = \sigma_{\theta n} = 20^{\circ}$ (c) $\sigma_{\phi n} = \sigma_{\theta n} = 10^{\circ}$

5.4 Optimal Current Distributions for MIMO Antenna Systems

In the previous section, the physical geometry of the antenna elements are known, and the SVW approach is utilized to exploit the maximum degrees of freedom of the wireless channel for communicating the information data. However, one important aspect of the MIMO antenna design is to investigate what antenna elements are optimal in terms of practical restrictions for the MIMO application. To design the optimal MIMO antenna elements, the starting point is obtaining the optimal current distributions radiating the optimal MIMO system modes for the given antenna geometry and the physical channel. Once the optimal currents are known, the MIMO antenna elements should be designed in such a way that each antenna element or a combination of them imitates one optimal current source. Hence, the optimal current distributions can essentially provide a benchmark for the MIMO antenna design in terms of the given restrictions.

The proposed SVW approach can also be employed to achieve the optimal current distributions if the current distributions in the given geometry are generally represented in terms of infinitesimal current sources:

$$\vec{J}_{opt}^{(i)} = \sum_{p=1}^{P} I_{x,p}^{(i)} \frac{\delta(\vec{r}-\vec{r}_p)}{r^2 \sin\theta}\hat{x} + I_{y,p}^{(i)} \frac{\delta(\vec{r}-\vec{r}_p)}{r^2 \sin\theta}\hat{y} + I_{z,p}^{(i)} \frac{\delta(\vec{r}-\vec{r}_p)}{r^2 \sin\theta}\hat{z} \tag{5.11}$$

where $\vec{J}_{opt}^{(i)}$ is the optimal current distribution for the i^{th} MIMO system mode, $\vec{r}_p$ is the position vector pointing the geometry in which the current distributions are to be obtained, P is the number of grid points to represent the current distributions, and $I_{l,p}^{(i)}$ is the weighting coefficient of infinitesimal current source directed in the $\hat{l}$ direction ($\hat{l} = \hat{x}, \hat{y}$, or $\hat{z}$) at the p^{th} grid point. Note that if the number of grid points is more than a certain threshold the current results would not change as expected based on the *Sampling Theorem*. Assuming an arbitrary volume or surface, Figure 5.16 shows the infinitesimal current sources placed at the grid points for two examples. Considering representation (5.11), each delta function current source can play the role of one antenna element in the SVW formulation, and the weighting coefficients can be thought of as the current excitations of the MIMO antenna elements. Accordingly, each row of the matrix $\mathbf{M}$, which are the SVW coefficients of the radiated field by each delta function source, can be directly obtained from (4.11) in which $\vec{J}$ is replaced by $\delta(\vec{r}-\vec{r}_p)\hat{l}$. Therefore, the matrix $\mathbf{M}$ will only depend on the grid point

positions representing the given geometry. Since three delta functions are placed at each grid point, the matrix $\mathbf{M}$ would contain $3P$ rows.

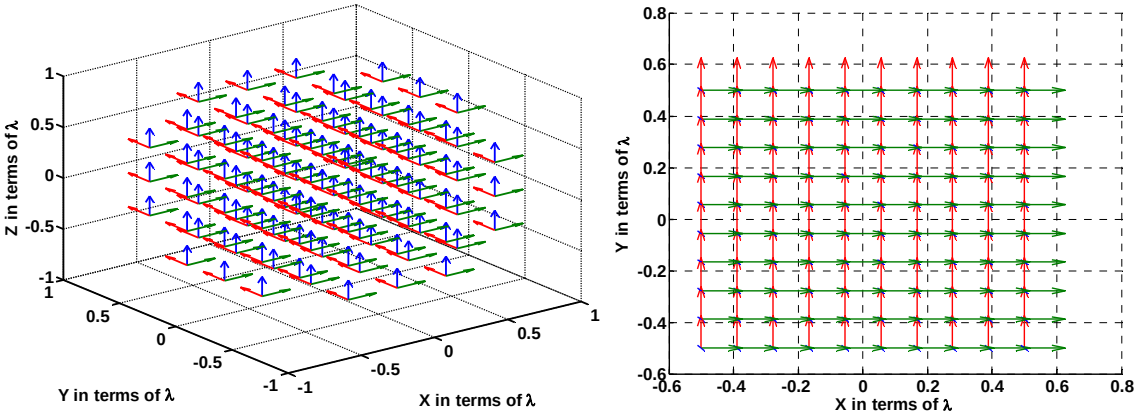

Figure 5.16: The delta function current sources covering the given volume or surface

Applying the SVW approach, the optimal weighting current coefficients are obtained to generate the optimal MIMO system modes. Additionally, the singular values given by the matrix $\mathbf{S}$ determine the power gains of the current distributions to investigate how many efficient MIMO system modes can be achieved for the given geometry.

5.4.1 System Capacity versus MIMO Antenna Shape

Consider the square plane shown in Figure 5.17. Considering the infinitesimal current sources covering the entire plane and applying the SVW formulation in the uniform PAS, the normalized power gains of the MIMO system modes are shown in Figure 5.18 for four different sizes of the square plane. As can be seen, the number of MIMO system modes with significant power gains is decreased when the plane size is smaller.

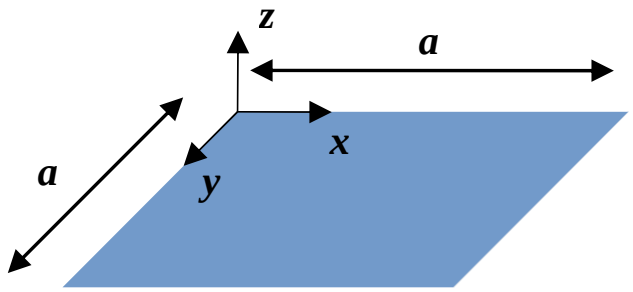

Figure 5.17: The square plane for current distributions

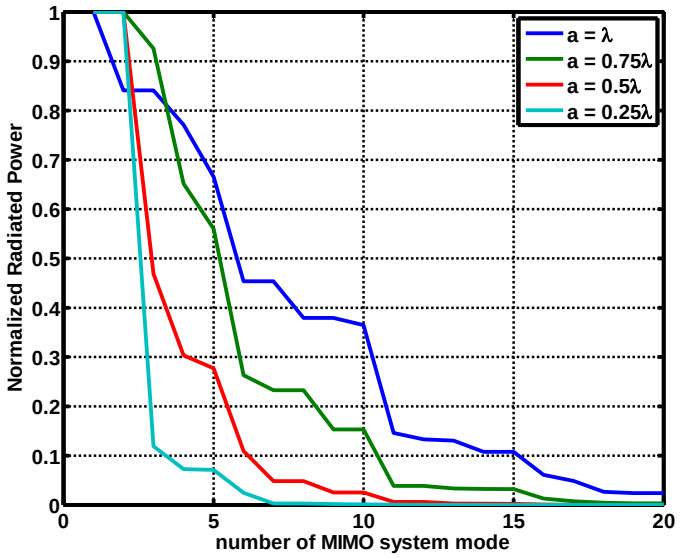

Figure 5.18: The normalized power gains of the optimal MIMO system modes for different sizes of a square plane

The expression (2.6) can be used to evaluate the effect of the MIMO system modes on the system capacity. Note that the λ_is in (2.6) are the singular values of the channel transfer matrix. Assuming that $N_T > N_R$ and the power gains of the MIMO system modes in the transmitter side are equal, λ_is would be only affected by the wireless channel variations and the power gains of the MIMO system modes in the receiver side. This assumption lets us evaluate the influence of the MIMO system modes designed in one side of transceiver (the receiver is considered here), on the system capacity.

Considering that the required SNR is equal to 10dB for the desired MIMO system performance, the system capacity can be calculated by (2.6). Figure 5.19 shows the system capacity versus the number of MIMO system modes for various plane sizes. Accordingly, the system capacity will increase by using more MIMO system modes up to a certain number. After the optimum number of MIMO system modes is passed, the system capacity decreases. The capacity trend shown in Figure 5.19 can be attributed to the fact that the weaker Eigen channels are also included to communicate the data when the MIMO system modes with low power gains are employed. Therefore, increasing in the number of MIMO system modes would not enhance the system capacity. However, if the power gains of MIMO system modes can be balanced, the contributions of all Eigen channels will be significant, yielding to an ever increasing system capacity.

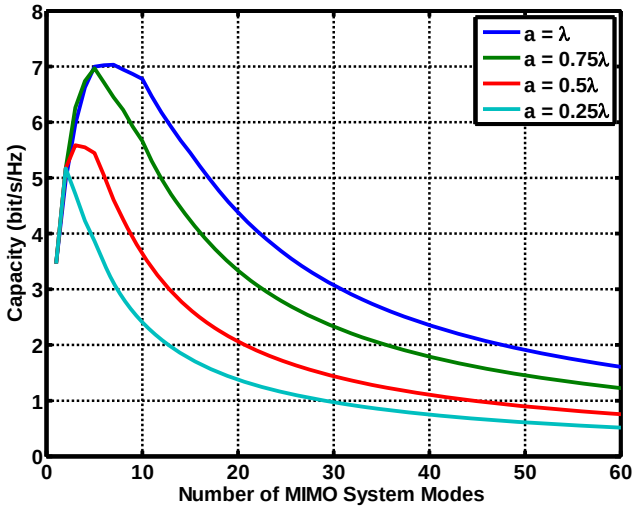

Figure 5.19: The system capacity versus the number of MIMO system modes used for different sizes of a square plane

Notice that in the limit case, where SNR goes to infinity, the system capacity linearly increases by the number of MIMO system modes. Thus, it is expected that the peak of capacity is moved to a higher number of MIMO system modes when a higher SNR is chosen [1, 2, 10]. However, for each particular SNR, the system capacity would be optimum for a certain number of MIMO system modes employed in the MIMO communication. According to Figure 5.19, the optimum capacity is obtained by 2, 3, 5, and 7 number of MIMO system modes for the side length of $a = 0.25\lambda$, $a = 0.5\lambda$, $a = 0.75\lambda$, and $a = \lambda$, respectively. As expected, more degrees of freedom can be exploited from the free space when the size of the geometry is increased. Although the uniform PAS is used for Figure 5.18 and 5.19, any arbitrary physical environment can be also considered. Thus, the SVW approach provides a general methodology to determine the maximum number of achievable MIMO system modes for the given geometry of the antenna structure and the given wireless environment.

5.4.2 Optimal Current Distributions on Antenna Geometry

To obtain the optimal current distributions, a more practical surface geometry is considered which is in the same size as a typical mobile handset, as shown in Figure 5.20. The goal is to obtain the optimal current distributions over the mobile handset plane for the MIMO applications at 2.4GHz. Note that the thickness of the handset is assumed to be negligible. However, the arbitrary volume and z-directed delta function sources could also be included, but due to the small thickness the results would not be different from the surface source.

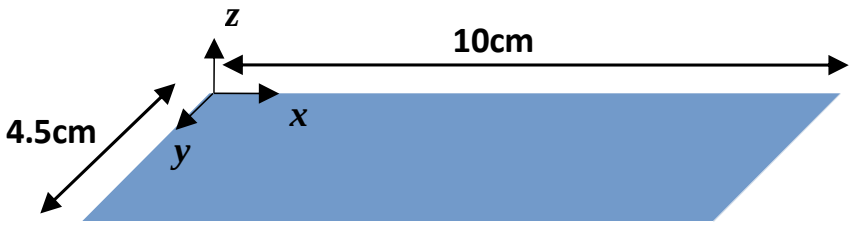

Figure 5.20: The plane of the mobile handset

The power gains of the MIMO system modes are plotted in Figure 5.21. Considering the required SNR is equal to 10dB, the system capacity would be maximized by choosing four MIMO system modes (Figure 5.22). Note that the difference in system capacity is slight when the number of MIMO system modes is increased from 3 to 4. Hence, although the maximum capacity is obtained by four MIMO system modes, the forth mode does not provide significant improvement.

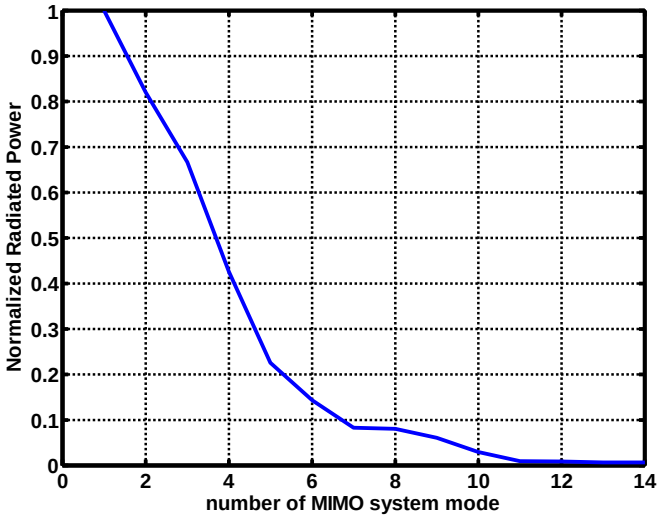

Figure 5.21: The normalized power gains of the optimal MIMO system modes at 2.4GHz for the mobile handset plane

The current distributions of four optimal MIMO system modes are depicted in Figure 5.23. The optimal current distributions can be employed as a benchmark to design or optimize the MIMO antenna elements. If four MIMO antenna elements are designed in such a way that each antenna element imitates one of the optimal current distributions illustrated in Figure 5.23, then the optimal MIMO antenna elements can be obtained for the given size of handset. Figure 5.24 also illustrates the radiation patterns of four optimal MIMO system modes.

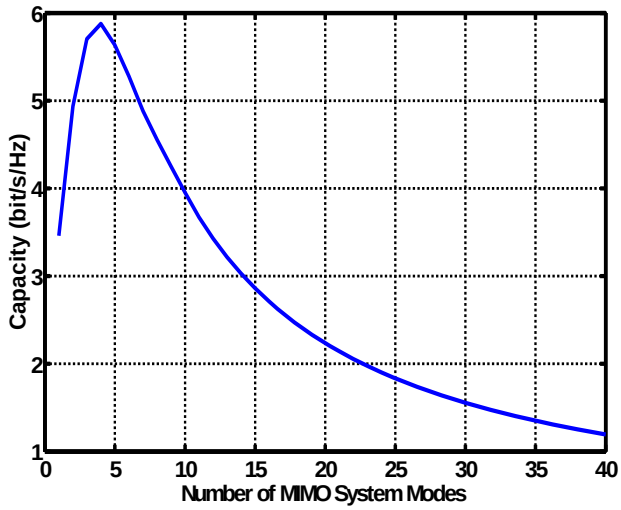

Figure 5.22: The system capacity versus the number of MIMO system modes at 2.4GHz for the mobile handset plane

The optimal current distributions and radiation patterns given in Figure 5.23 and 5.24 are obtained for the uniform PAS, and it is required to investigate if the number of optimal MIMO system modes would change for the other PAS channel realizations. For this purpose, a Monte-Carlo simulation can be performed for various wireless channel realizations to study the maximum degrees of freedom achievable through a non-uniform PAS.

For the statistical analysis of the wireless channel, the Laplacian channel model is used with four clusters and $\sigma_{\phi k} = 30^\circ$ and $\sigma_{\theta k} = 30^\circ$. Before finding the number of optimal MIMO system modes for the plane of the mobile handset, the degrees of freedom of the Laplacian channel can be investigated through the SVD of the matrix $\mathbf{G}$. As mentioned before, the optimal SVW spectrum is obtained for the PAS channel when $\mathbf{IM} = \mathbf{Q}^\dagger$. Considering the size of the plane in Figure 5.20, the smallest sphere enclosing the plane will have a radius of 0.44λ. According to Chu's theorem, the number of modes appearing at the far field would be limited by $n < kr_0 \approx 3$ which results in 36 SVWs in total. The matrix $\mathbf{G}$ with the size of 36×36 can be calculated for each random channel realization. Using the SVD of the matrix $\mathbf{G}$ in each channel realization, the optimal SVW spectrums and their singular values can be calculated. Considering SNR=10dB, the capacity is calculated versus the number of MIMO system modes for each channel realization. The histogram in Figure 5.25 shows the recording of the optimum number of MIMO system modes for 250 different channel realizations.

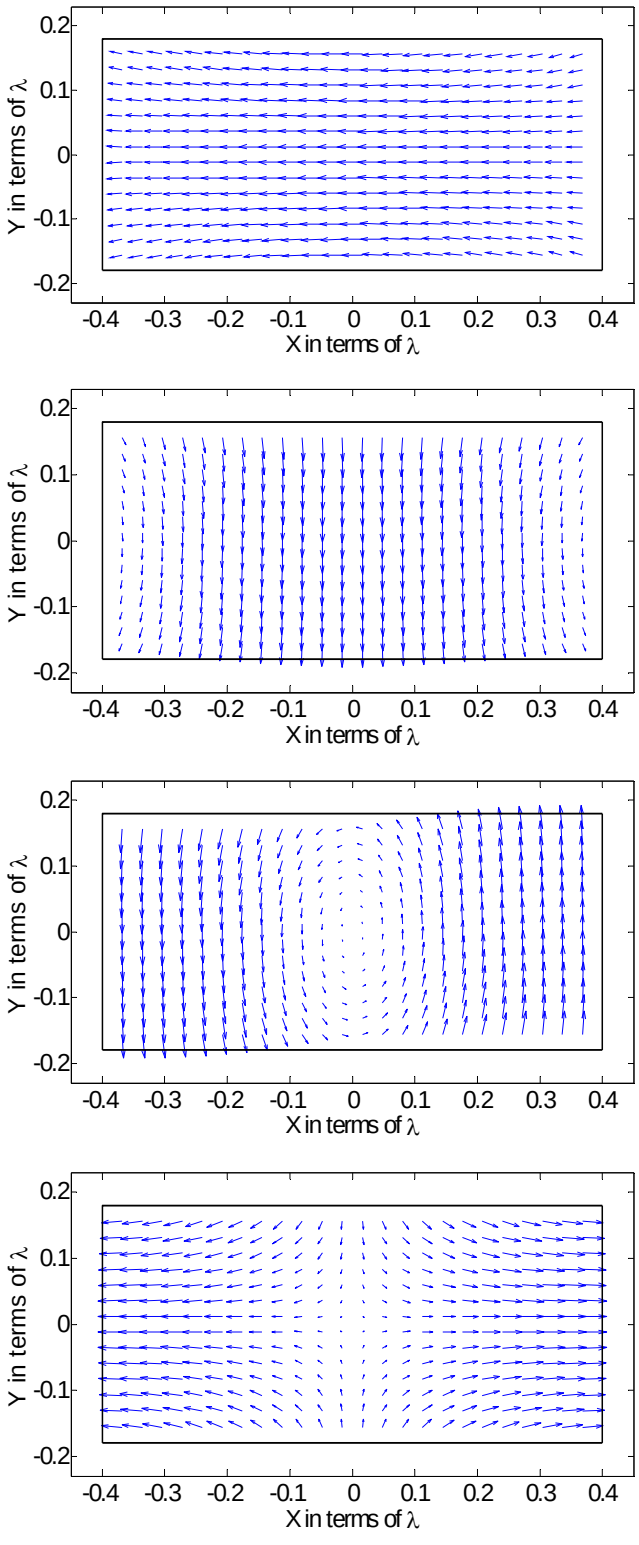

Figure 5.23: The optimal current distributions on the mobile handset plane at 2.4GHz

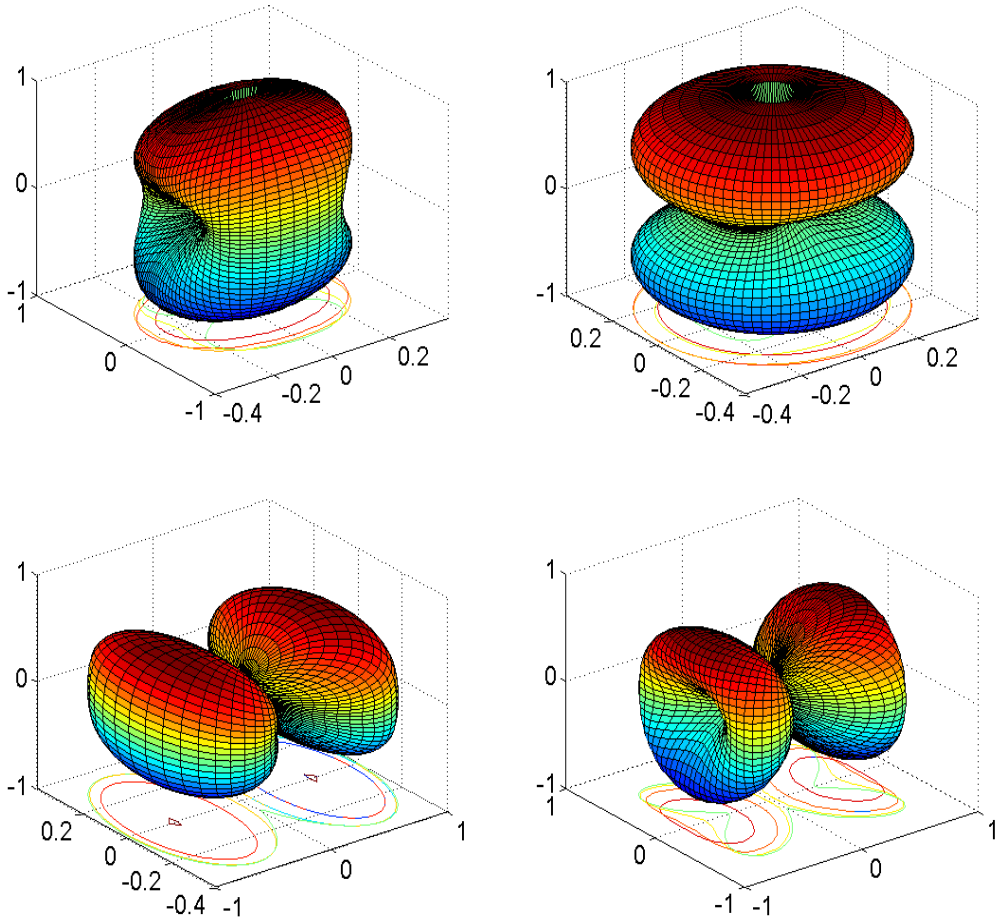

Figure 5.24: The radiation patterns of optimal current distributions for the handset plane

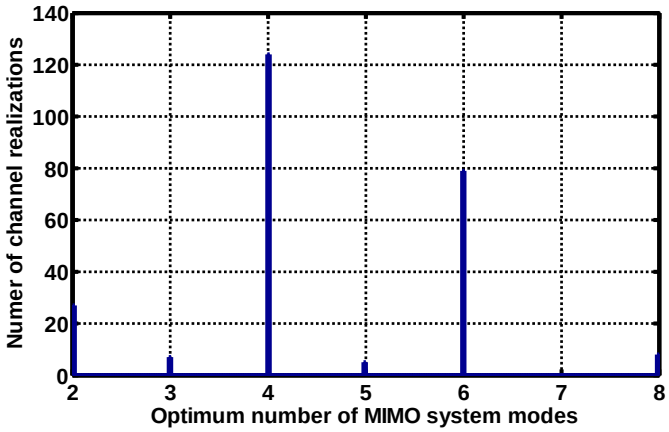

Figure 5.25: The optimum number of MIMO system modes for the Laplacian channel realizations

Figure 5.25 shows that the optimum number of MIMO system modes for which the channel capacity is maximized, is obtained as 4 for 124 different channel realizations out of 250. It also reaches to 6 and 8 numbers of MIMO system modes, but the most reliable number of effective MIMO system modes is 4 through the simulated Laplacian channel.

Note that the number of degrees of freedom shown in Figure 5.25 is only limited by the size of the sphere enclosing the antenna structure, but there is no limitation on the antennas' (current distributions) shapes. Therefore, it provides an upper bound for the number of MIMO system modes generated by the antennas inside a sphere with a radius of 0.44λ. The upper limit can be achieved by a spherical antenna (source distribution) which can generate the desired SVWs in the radiating fields, as presented in Chapter 4. If the current source is imposed to be distributed on the given plane, a lower number of MIMO system modes is expected. The limitations due to the shape of the antenna can be included by considering the matrix $\mathbf{M}$ constructed for infinitesimal dipoles placed on the antenna geometry. Using the SVD of the matrix $\mathbf{Z}$ and calculating the singular values (consequently, the power gains) for 250 different channel realizations, the histogram of the optimum number of MIMO system modes for which the capacity with SNR=10dB is maximized for the given antenna geometry and wireless channel is illustrated in Figure 5.26.

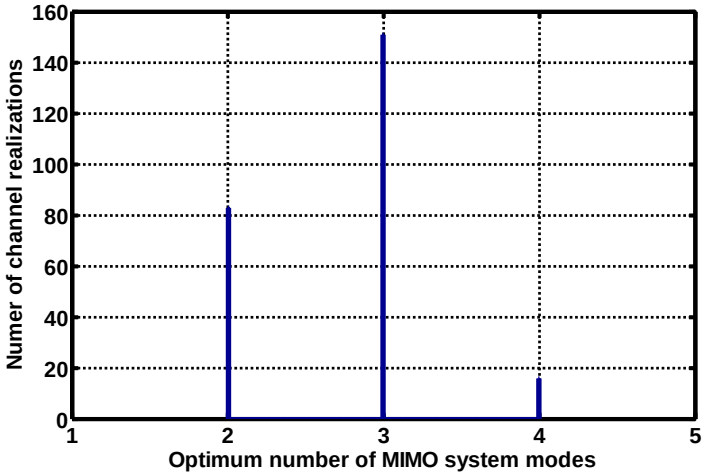

Figure 5.26: The optimum number of MIMO system modes for the Laplacian channel and the antenna geometry given in Figure 5.20

As expected, due to the limitations imposed by the antenna geometry, the number of degrees of freedom is decreased to 3 MIMO system modes for 151 different channel realizations out of 250. The lower number of effective MIMO system modes can be attributed to the fact that a planar source is

not able to excite particular SVWs, whereas a 3D source such as a spherical antenna can excite all possible SVWs for the smallest sphere (as discussed in Chapter 4).

In addition to the optimum number of MIMO system modes, it is important to investigate how much improvement the different modes can provide for the MIMO system performance. For instance, Figure 5.22 suggests four MIMO system modes for maximizing the system capacity, whereas the capacity improvement is very negligible when number of modes is increased from 3 to 4. To find the efficient MIMO system modes, a Monte-Carlo simulation can be performed to statistically calculate the correlation coefficients between optimal MIMO system modes for various channel realizations. Figure 5.27 illustrates the CDF of the correlation coefficients for four MIMO system modes shown in Figure 5.24.

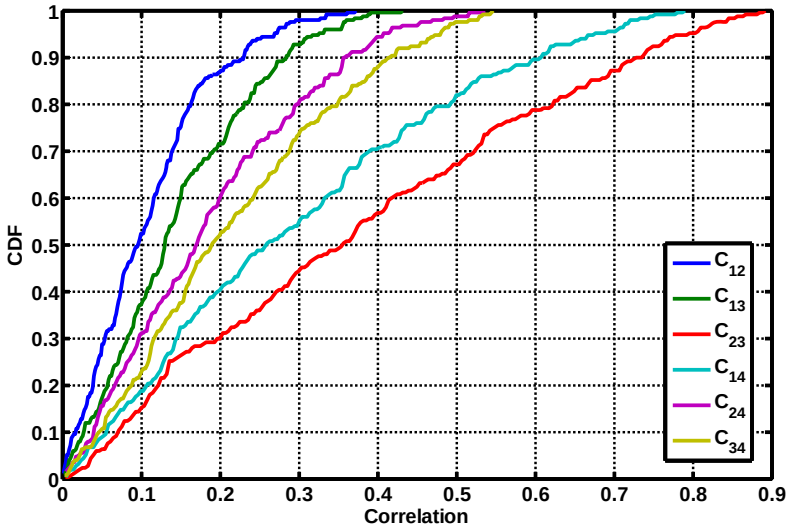

Figure 5.27: The CDF of the correlation coefficients between the optimum MIMO system modes shown in Figure 5.24

As can be seen, MIMO system mode#1 and #2 provide better orthogonality through the Laplacian channel in comparison with the other MIMO system modes (the correlation coefficient is less than 0.3 for 98% of the time). Hence, including the dynamic variations of the MIMO channel, it can be concluded that the first and second current distributions given in Figure 5.23 are optimal for the MIMO system.

Two optimal current distributions can be used as a benchmark to practically design optimal MIMO antenna elements. As a practical example, consider two half-wavelength dipole antennas located on

the rectangular plane given in Figure 5.20. It is desired to obtain the optimal shape of the dipole antennas so that the orthogonal MIMO system modes are obtained. To find the optimal shape, a MATLAB code is written to generate different possible shapes of a half-wavelength dipole on the grid points defined for the rectangular plane.

Note that the current distribution along the dipoles can be approximated as a sinusoidal function independent of the shape of the dipoles. Projecting the sinusoidal current distributions with various shapes onto the optimal current distributions shown in Figure 5.23, those dipole shapes are chosen that can imitate the optimal current distributions as much as possible. The four optimal dipole shapes, which have the most similarity with optimal current distributions, are shown in Figure 5.28 in red, blue, black, and green, respectively.

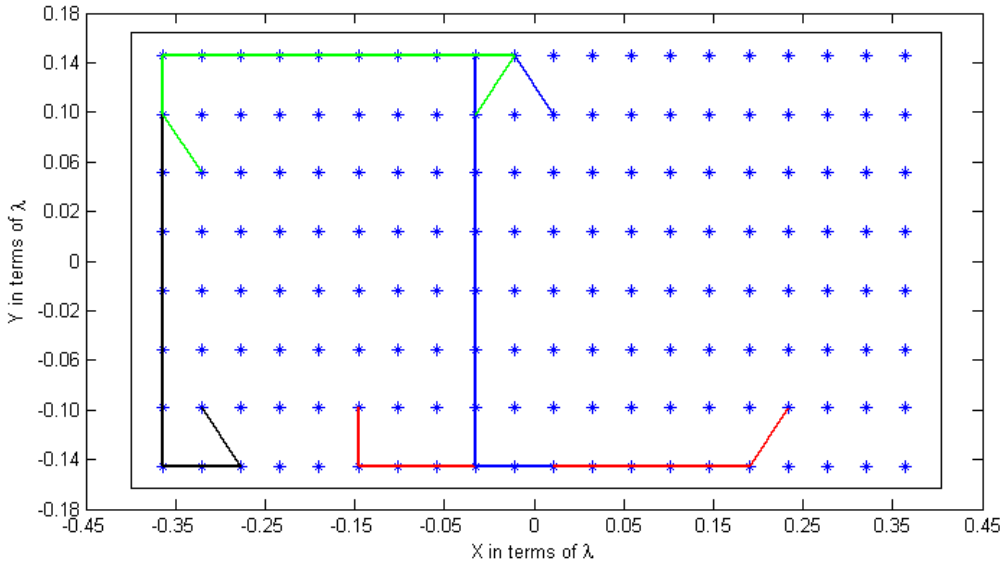

Figure 5.28: The four optimal half-wavelength dipoles

Since the MIMO system mode#1 and #2 are optimal in the given Laplacian channel (Figure 5.27), the corresponding dipole shapes (red and blue curves) are chosen to design the two dipole antennas on a thin dielectric substrate. The designed dipole antennas, their simulated S-parameters, and the radiation patterns of the two MIMO system modes are illustrated in Figure 5.29. As can be seen, using the optimal shapes of the dipole antennas, the two antennas are suitably isolated and the return losses are more than 10dB for 150MHz bandwidth.

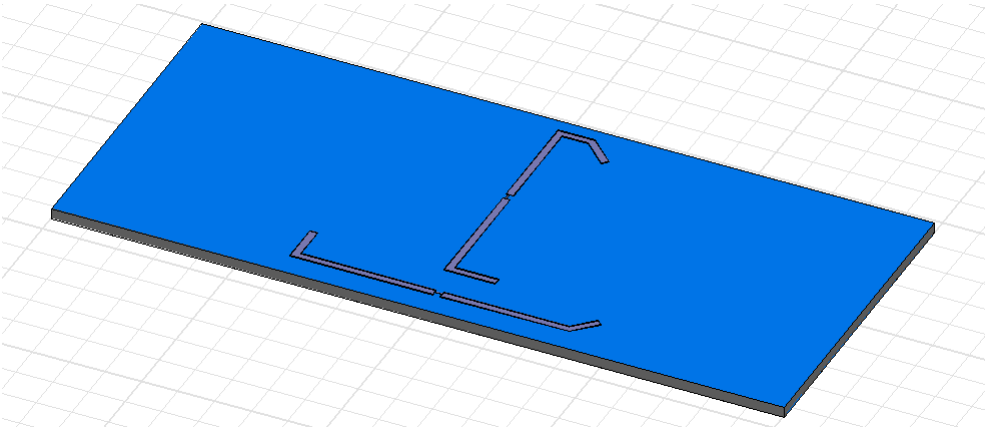

(a)

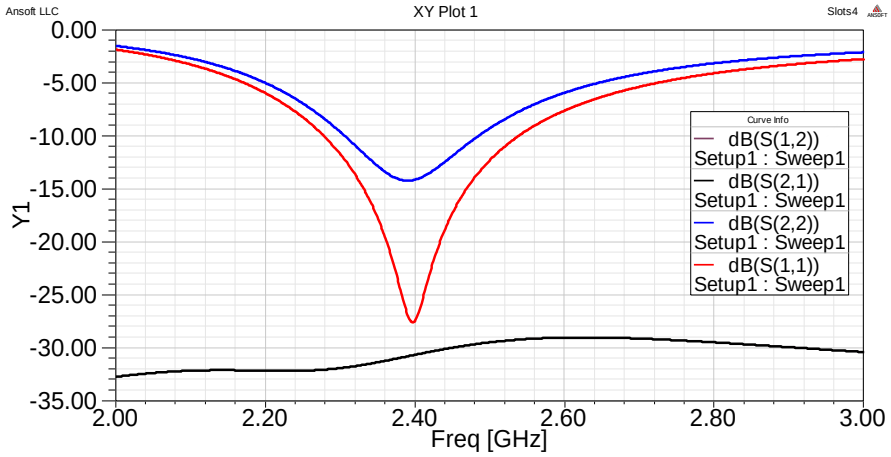

(b)

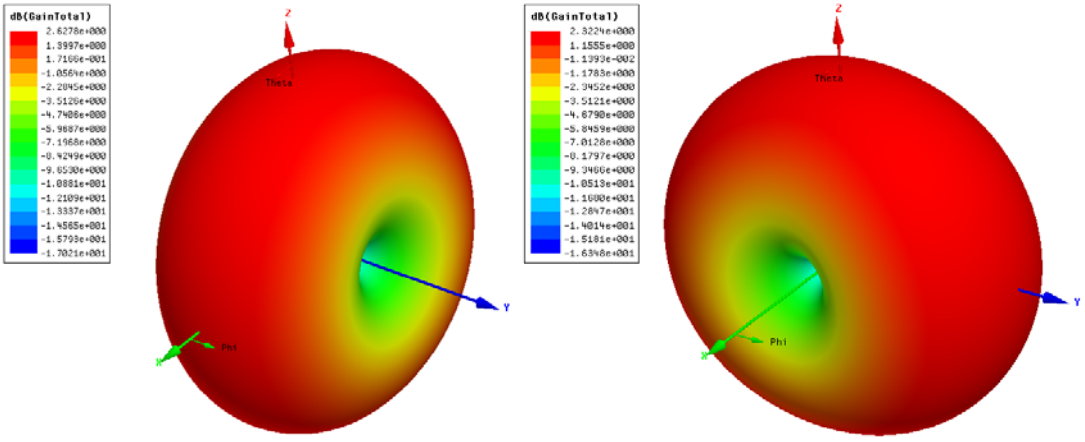

(c)

Figure 5.29: (a) Two optimal shapes of the half-wavelength dipoles, (b) simulated S-parameters, (c) gain radiation patterns of the two MIMO antenna elements

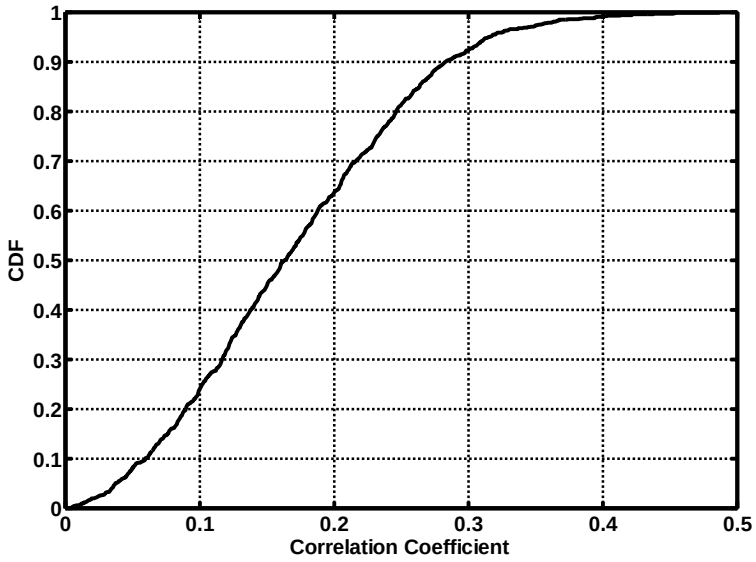

Figure 5.30: The CDF of the correlation coefficient between the MIMO system modes obtained by two optimal dipole shapes

The CDF of the correlation coefficient obtained by two optimal dipole shapes is also shown in Figure 5.30. Accordingly, the correlation coefficient is less than 0.3 for 93% of the time.

Obviously, the sinusoidal distributions of dipole antennas cannot create the exact radiation patterns of the optimal MIMO system modes shown in Figure 5.24, but the optimal current distributions and MIMO system modes provide a benchmark to design or optimize the other current distributions which are limited to be located on the given geometry.

Note that, for the sake of simplicity, the feed circuit is not included in this example, and only the shape of the dipole antennas are considered to investigate how the proposed method works. Of course, if the feed circuit of antennas was also included, the field radiation patterns and consequently the correlation coefficient would be affected.

5.4.3 Optimal Current Distribution on Ground Plane

The optimal current distributions in Figure 5.23 are obtained on a hypothetical plane, whereas the more practical scenario would be the case where the antennas are located on the handset's ground plane. In this case, the optimal magnetic current distributions on the ground plane are of interest. Similar to the expression (5.11), the magnetic current distributions can be written in terms of delta

functions. The reciprocity and the MoM approach developed in Chapter 3 can be effectively employed to calculate the vector field radiation patterns of each magnetic delta function in presence of the handset's ground plane. Expanding the calculated field radiation patterns in terms of the SVWs, the matrix $\mathbf{M}$ can be constructed for the magnetic delta functions in the presence of the handset's ground plane. Calculating the power gains of the optimal MIMO system modes generated by the magnetic currents on the handset's ground plane through 250 different channel realizations, the histogram of the optimum number of MIMO system modes is shown in Figure 5.31. As can be observed, the optimum number of MIMO system modes is 3.

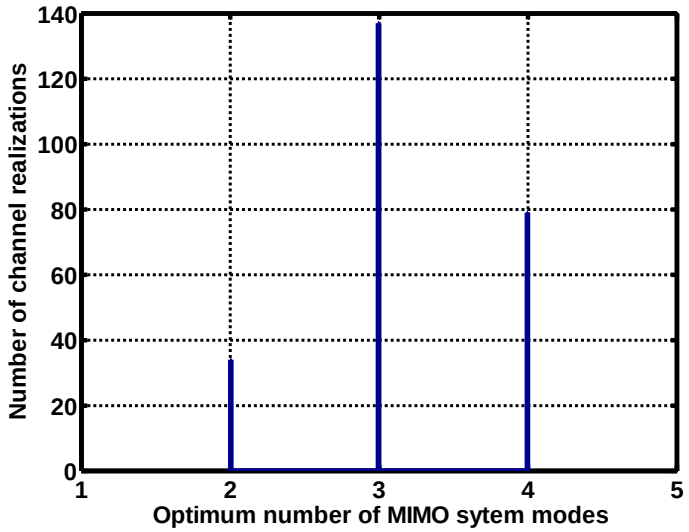

Figure 5.31: The optimum number of MIMO system modes for the magnetic current sources on the handset's ground plane in the Laplacian channel

The four dominant current distributions for the optimal magnetic sources on the handset's ground plane are shown in Figure 5.32. The corresponding radiation patterns are also illustrated in Figure 5.33. As can be seen, the radiation patterns of the magnetic currents are distorted due to the effect of the finite ground plane. The statistical analysis of the correlation coefficient between the optimal MIMO system modes in the Laplacian channel is also presented in Figure 5.34.

According to Figure 5.34, the orthogonality of the current mode pairs (1,3) and (2,4) are not held in the Laplacian channel, as they excite the SVWs which are not orthogonal in the various Laplacian channel realizations for a high percentage of time. Hence, for design purposes it is required to avoid exciting the correlated SVWs for different MIMO system modes.

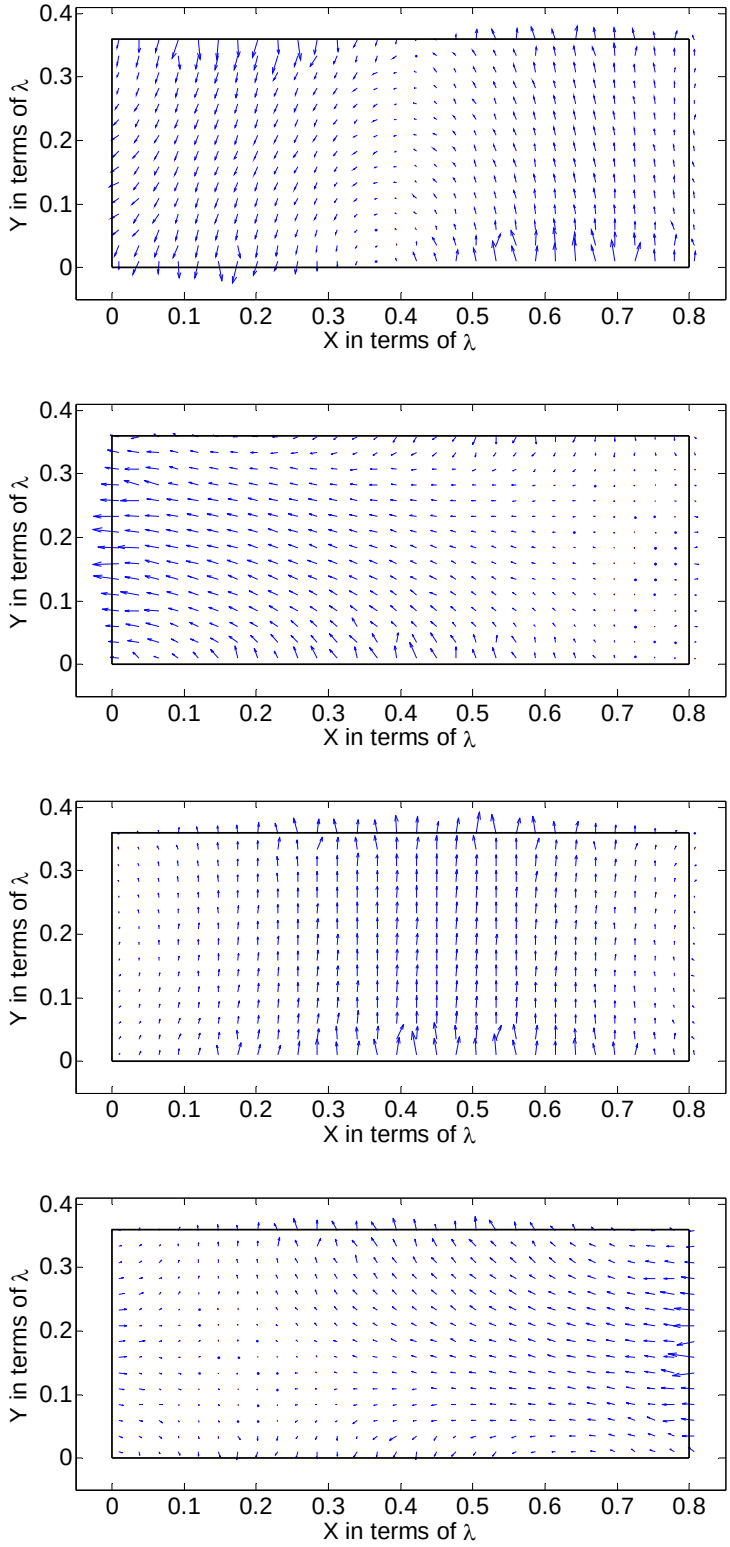

Figure 5.32: The optimal magnetic current distributions on the handset's ground plane at 2.4GHz

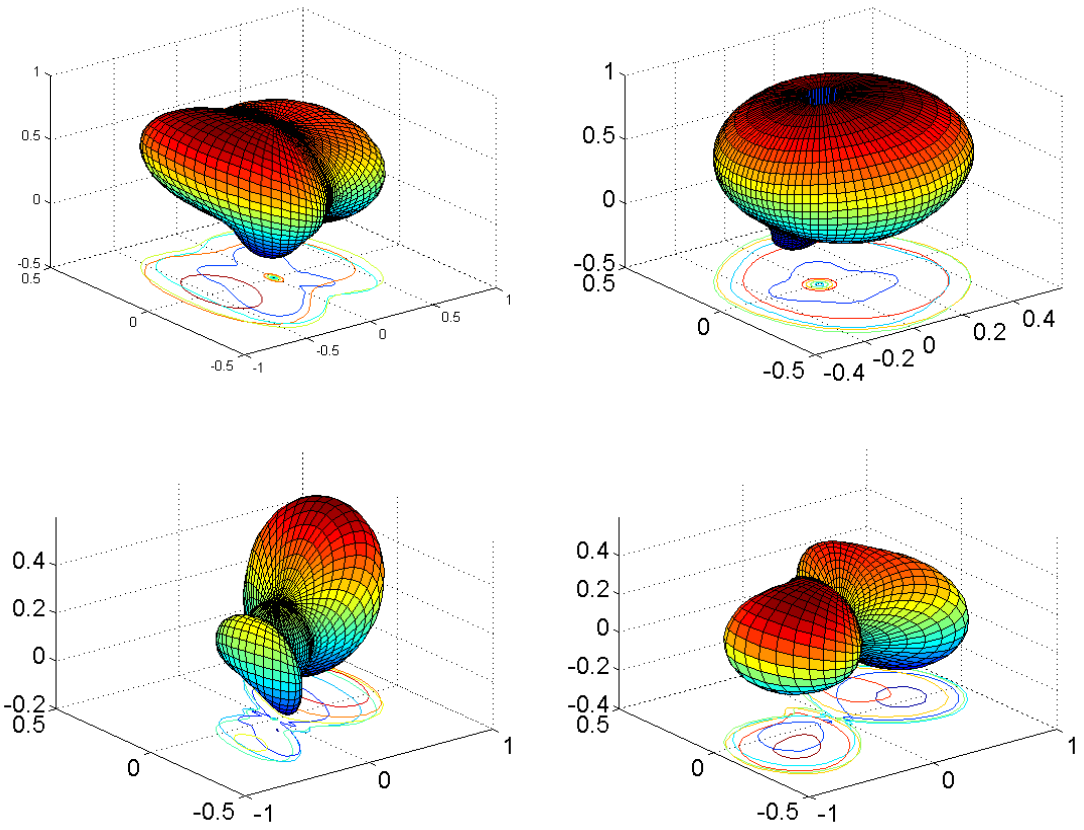

Figure 5.33:The radiation patterns of optimal magnetic currents on the handset's ground plane

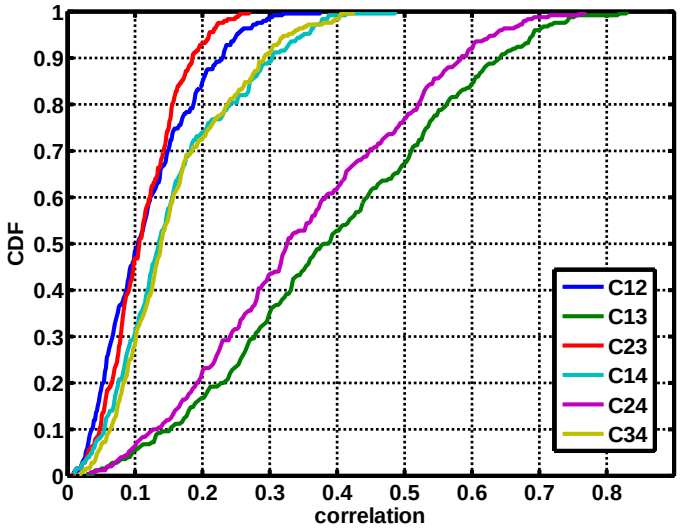

Figure 5.34: The CDF of the correlation coefficients between the optimal MIMO system modes generated by the magnetic currents on the handset's ground plane

Implementing the optimal magnetic currents given in Figure 5.32 requires locating the MIMO antenna elements over the whole ground plane, whereas the antenna region is usually restricted to a certain area over the ground plane. To consider a more practical case, it is assumed that two regions with a size of 30mm×17mm are given for accommodating the MIMO antenna elements on the handset's ground plane, as shown in Figure 5.35. Since the size of the antennas is decreased in comparison to the previous examples, the operating frequency is chosen to be 5.8GHz for the MIMO application so that the larger area is obtained in terms of the wavelength.

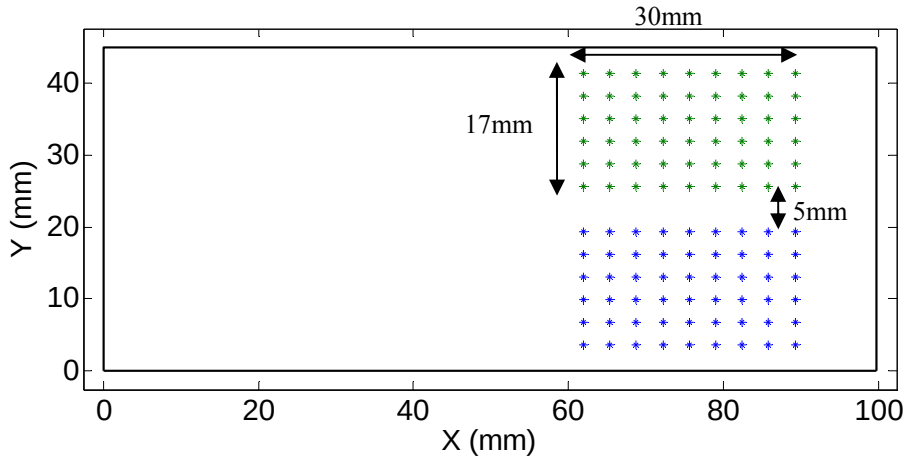

Figure 5.35: The two regions on the handset's ground plane for the MIMO antenna elements

Note that this example is different from the previous ones in the sense that the two current distributions are not co-located. Since the two optimal current sources are supposed to be obtained for two different regions, two sets of delta function sources should be considered. Hence, the two matrices $\mathbf{M}_1$ and $\mathbf{M}_2$ are constructed for the delta function sources located in two different regions. The optimal current source for each region can separately obtained by the SVD of matrix $\mathbf{Z}_1 = \mathbf{M}_1\mathbf{Q}\mathbf{D}^{1/2}$ and $\mathbf{Z}_2 = \mathbf{M}_2\mathbf{Q}\mathbf{D}^{1/2}$. The singular values of the $\mathbf{Z}_1$ and $\mathbf{Z}_2$ matrices determines which current modes are dominantly radiating from region#1 and #2, respectively.

Separately applying the orthogonalization procedure to the current sources in each region would not guarantee that the MIMO system modes obtained by two different regions are orthogonal. However, it provides an orthogonal basis for the magnetic current sources which are dominantly radiating from each particular region.

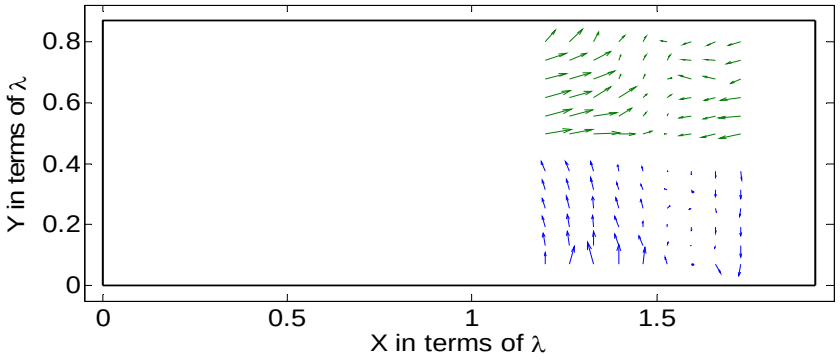

(a)

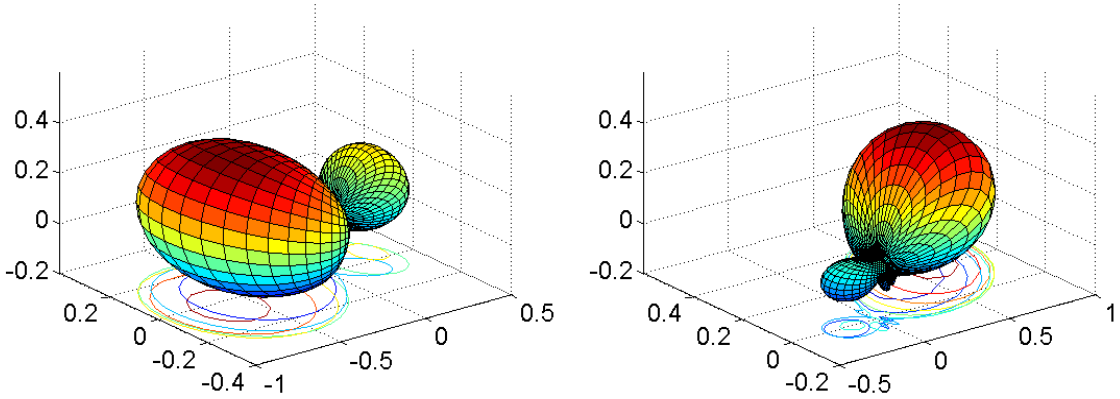

(b)

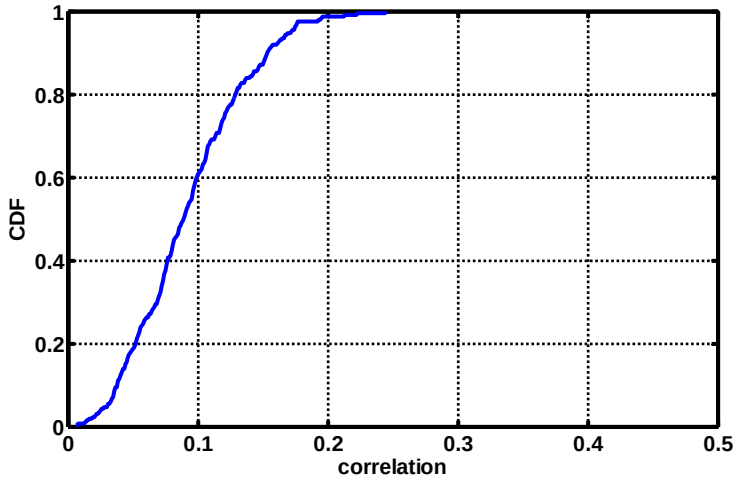

(c)

Figure 5.36: (a) The optimal magnetic currents for the given regions, (b) radiation patterns of two MIMO system modes, (c) CDF of the correlation coefficient for two MIMO system modes

For instance, in order to select four dominant current modes included in each region, four rows of $\mathbf{I}_1 = \mathbf{U}_1^{\dagger}$ and $\mathbf{I}_2 = \mathbf{U}_2^{\dagger}$ with the highest corresponding singular values can be chosen, where $\mathbf{I}_1$ and $\mathbf{I}_2$ are the coefficients of the optimal magnetic currents on the handset's ground plane in region#1 and #2, respectively. Then, it is required to calculate $\mathbf{R}_{12} = (\mathbf{I}_1\mathbf{M}_1)\,\mathbf{G}\,(\mathbf{I}_2\mathbf{M}_2)^{\dagger}$ to investigate which current modes among the four selected ones in each region provide the orthogonal MIMO system modes through the given wireless channel.

Using the proposed procedure, the optimal magnetic currents are shown in Figure 5.36.a. The radiation patterns of the magnetic currents and the statistical analysis of the correlation coefficient between them are also presented in Figure 5.36.b and 5.36.c. Note that the Laplacian channel parameters are similar to the previous examples.

To implement the optimal magnetic current distributions, one approach is to use *Dielectric Resonator Antennas* (DRA) [94]. The EM field modes excited in the dielectric resonator can imitate the magnetic current distributions in Figure 5.36.a. Figure 5.37 shows the designed DRAs at 5.8GHz for the MIMO application. The dielectrics are made of alumina ($\varepsilon_r = 9.4$) with the height of 5mm and the dimensions given in Figure 5.35, and the slots are excited using two microstrip lines mounted on the back of the handset's ground plane.

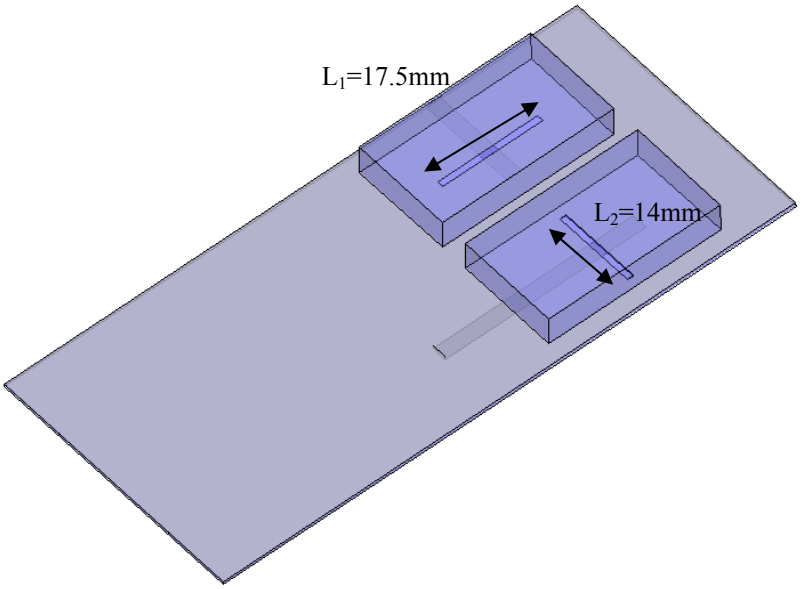

Figure 5.37: The dielectric resonator antennas to generate the MIMO system modes

The simulated S-parameters and radiation patterns of the DRAs are also illustrated in Figure 5.38. As can be seen, the two ports are isolated and the return losses are more than 10dB over a large bandwidth. The CDF of the correlation coefficient between the DRA radiation patterns is also shown in Figure 5.39 for the Laplacian channel model.

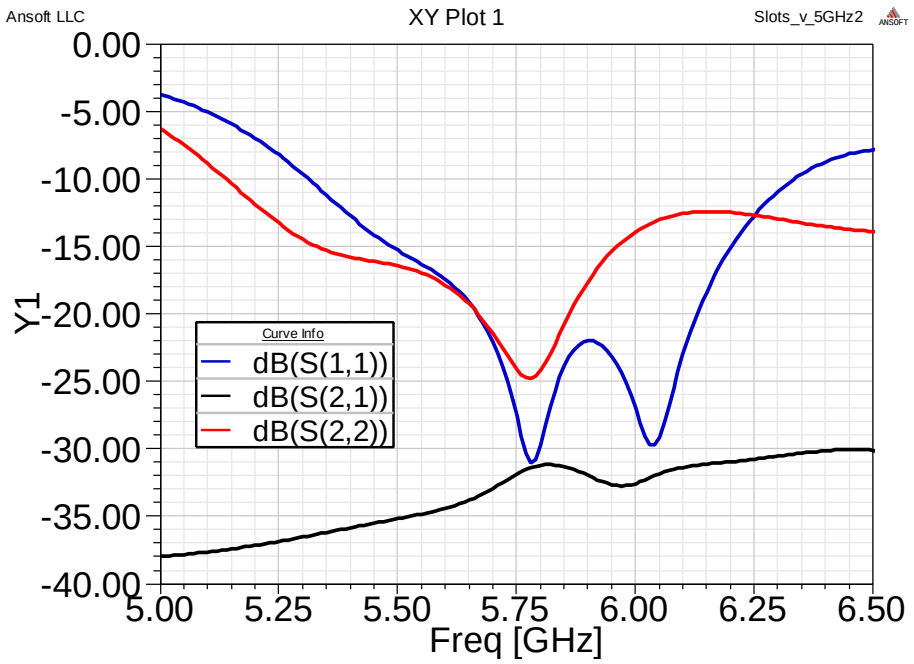

(a)

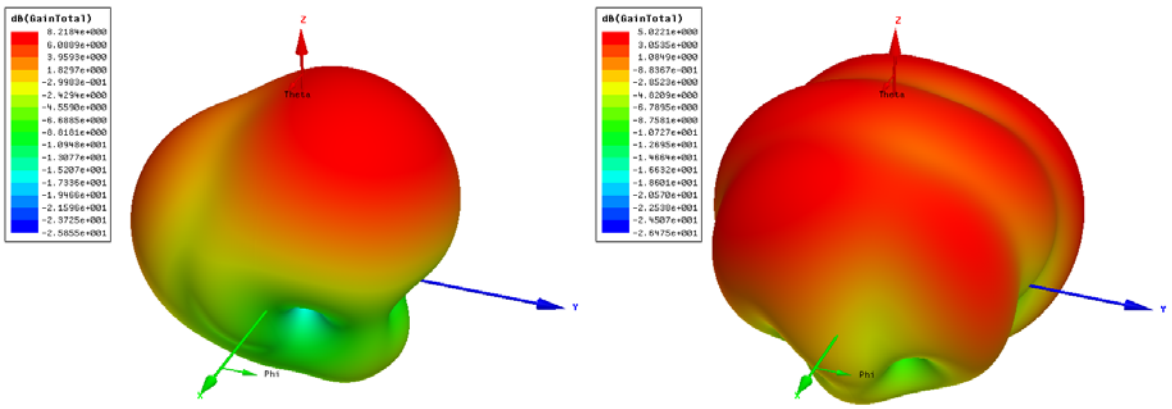

(b)

Figure 5.38: The DRA simulation results (a) S-Parameters (b) gain radiation patterns

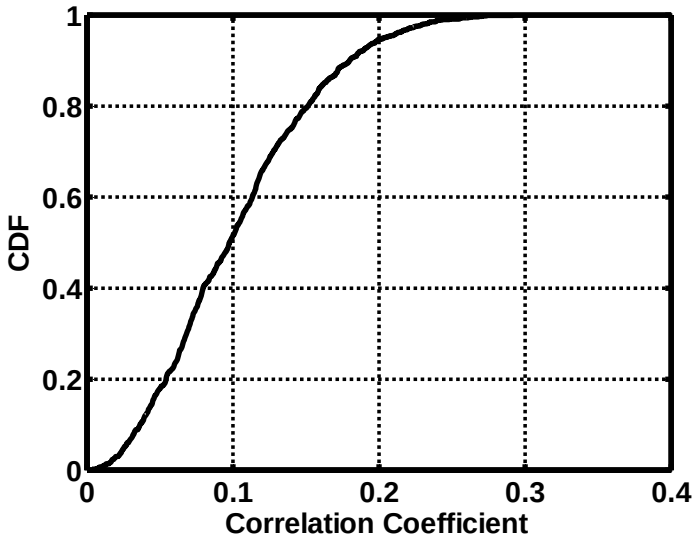

Figure 5.39: The CDF of the correlation coefficient between DRAs

The DRA design is inspired from the optimal magnetic currents calculated for the given regions on the handset's ground plane. Although the DRAs do not exactly represent the optimal magnetic sources, the calculated magnetic currents provide an initial step to design the DRA elements. Note that the other types of magnetic current implementations can also be employed to design the MIMO antenna elements. For instance, the optimal magnetic currents can be practically implemented by various slot shapes over the ground plane.

Although the fixed current distributions are selected here to implement MIMO antenna elements, the methodology can be utilized to derive the optimal current distributions corresponding to the severe channel realizations. Having a bank of optimal currents, the adaptive techniques [26] can be employed to either switch between the optimal MIMO antennas or change the current excitations corresponding to the channel variations.

5.5 Conclusion

The SVW representation of the correlation coefficients between the MIMO antenna system modes was derived, and a matrix formulation was presented to separate the channel effects from the current excitations and the physical properties of antenna elements. Using the SVD method, the degrees of freedom were obtained and the optimal current excitations were calculated to generate the orthogonal radiation modes for maximizing the system capacity. The proposed SVW formulation was employed to analyze wireless channel, and obtain the optimal current excitations for the given antenna

structures, as well as to determine the optimal current distributions for a few practical examples. The SVW formulation was also used to determine the maximum number of MIMO system modes achievable for an arbitrary antenna structure. The impact of the antenna shapes and dynamic wireless channels on the effective number of MIMO system modes were also investigated. The proposed approach offers a flexible and systematic method which can be applied to more realistic scenarios in practical applications by taking more complex electromagnetic interactions (the interaction with the package and complex objects close to the antennas) into consideration. The proposed formulation is one of main contributions of this research in the MIMO antenna design and analysis.

Chapter 6
Concluding Remarks

The MIMO system is recognized as an efficient solution to enhance the system capacity and combat the multipath fading effects of the wireless communication channels. The correlation coefficient between the received/transmitted signals is a crucial parameter which determines the MIMO system performance. The electromagnetic effects of the wireless channel and the MIMO antenna elements can significantly affect the correlation coefficients between the antenna elements. To include the EM properties in the MIMO antenna design and analysis, the general MIMO antenna system model and the appropriate correlation coefficient formulation were discussed. The physical channel models were also reviewed, and without the loss of generality, the statistical Laplacian cluster channel model was introduced to be used for MIMO antenna analysis and design throughout this research.

In addition to the far field effects modeled by the power angular spectrum of the wireless channel, the scattering objects in the vicinity of the MIMO antenna elements were considered. A fast and efficient approach was proposed to include the EM effects of scattering objects located in the near field region. The proposed method is beneficial for optimization problems in the sense that the EM effect of scattering objects can be numerically calculated independent of the MIMO antenna elements. Hence, the optimizations of the physical properties of the MIMO antenna elements in the presence of a scattering object would be numerically fast and efficient. Considering the PEC fixture effects on the radiation patterns of the MIMO antenna elements, the physical properties of the antenna elements were optimized in a few practical examples to achieve the minimum correlation coefficient. The proposed approach, which is a hybrid of the analytical reciprocity formulation and the numerical MoM, is a notable contribution in the MIMO antenna optimizations.

The spherical vector waves are Eigen vector solutions of the Helmholtz equation and establish an orthogonal set of vector basis functions for electromagnetic fields. The orthogonal properties of the SVWs were utilized to achieve orthogonal vector field radiation patterns of the MIMO antennas. To excite the desired SVWs for the MIMO application, it is required to obtain current sources radiating a particular SVW. Source reconstruction for a predefined EM field is known as the inverse source problem which also has other applications such as near field scanning, inverse scattering, imaging, and etc. For the sake of the analytical solution, the inverse source problem was solved on a spherical geometry for the predefined SVWs. To add more liberties into the inverse source problems, the non-

radiating sources were included so that a certain constraint was satisfied. Imposing the condition of spherical surface source, the current distributions were obtained on a sphere for the given SVW coefficients. The derived formulation for the spherical current source is a major contribution in the inverse source problem which was utilized for the MIMO antenna applications in this research. The analytical SVW analysis was also applied to the planar antennas, and the orthogonal properties of the co-planar electric and magnetic sources were also explored. This orthogonality was employed to design one simple MIMO antenna. The statistical analysis of the correlation coefficient showed that the vector field radiations of the designed magnetic and electric currents remain orthogonal for an appropriate percentage of the time.

The SVW approach was formulated in a general matrix form in which the inner product matrix of the MIMO system modes was separated into three cascaded matrices representing the SVW interactions through the wireless channel, the physical properties of the antenna elements, and the current excitations in the feed circuit. The SVW formulation provides the possibility of studying the wireless channel independent of the MIMO antenna elements. Investigating the SVW interaction in the wireless channel explores the possible degrees of freedom of the channel in the sense that the SVWs whose orthogonality is less sensitive to the wireless channels can be determined. Once the desired SVWs are known for the given channel, the analytical SVW method can be employed to determine the corresponding surface current distributions. The SVW formulation was also applied to a few practical examples to determine the optimal current excitations of the given MIMO antenna elements in both the fixed and statistically varying Laplacian channels. It was shown that the feed circuit design that provides the optimal current excitations can significantly improve the MIMO system performance. Ultimately, the SVW approach was applied to an arbitrary geometry of antennas in order to obtain the optimal current distributions for the orthogonal MIMO system modes, and also determine the maximum number of effective MIMO system modes which can maximize the system capacity for the given physical restrictions. The proposed reciprocity and the MoM method was linked with the SVW formulation to achieve the optimal magnetic current distributions on the given ground plane. The calculated current distributions inspired an initial step for designing the MIMO antenna elements. While designing the MIMO antenna elements according to the optimal current distributions, two practical examples of MIMO antennas were discussed for mobile handset communications. The statistical analysis of the correlation coefficients was also presented to evaluate the performance of the designed MIMO antenna elements in different wireless channels.

6.1 Future Work

The following directions are suggested as future work following this research:

1) For MIMO antenna optimizations, the method of moments was developed for PEC objects in this research. Extending the developed MATLAB code to calculate the impedance matrix for dielectric objects, it would be possible to include the EM influences of different types of fixture packages made of various materials on the vector field radiation patterns of the MIMO antenna elements. Combining the extended MoM with the reciprocity formulation, the MIMO antennas can be optimized in the presence of more practical enclosures.

2) The analytic source reconstruction presented in this research to excite the desired SVW was accomplished for spherical surfaces. The idea of including the non-radiating sources to satisfy the surface source constraint can be extended to the other coordinate systems such as the spheroidal coordinates. Although the spheroidal vector wave functions are not orthogonal on a spheroid, the orthognalization procedures can be employed to determine the coefficients of spheroidal waves in the current distributions. By solving the inverse surface problem for spheriodal structures, more general antenna shapes including the linear antennas can be considered to excite the SVWs for MIMO applications. Meanwhile, the non-radiating sources can be employed to satisfy the other practical constraints than the surface source constraint.

3) Although a few proof-of-concept examples were discussed in this research, the SVW formulation is a general methodology and can be applied to other practical problems. As an interesting application of the SVW approach, the physical shapes of the MIMO antenna elements can be optimized in such a way that the desired SVWs are excited for the given wireless channel. Additionally, the other types of current implementations than those proposed in this research can be investigated for the MIMO antenna designs in different practical scenarios.

4) In this research, the wireless channel was statistically modeled to obtain fixed MIMO system modes which were optimal for the various wireless channel realizations. The ultimate solution for the MIMO antenna designs is the adaptive or reconfigurable antenna structure which adapts the vector field radiation patterns of the MIMO system modes to the wireless channel variations. The compatibility of the MIMO antenna elements with the dynamic environment provides an efficient antenna design which guarantees the maximum system capacity in various

communication environments. The SVW approach proposed in this research can be employed in adaptive MIMO systems in order to achieve the optimal MIMO system modes in different wireless environments.

Appendix A
Method of Moments for Conducting Bodies

A.1 Theory of Scattering

If an electromagnetic wave incident upon a PEC body, the total electric field can be written as sum of the known incident field $\vec{E}_{inc}$ and the unknown scattered electric field $\vec{E}_S$ so that the total field satisfies the boundary condition on the PEC body:

$$\hat{n}\times(\vec{E}_S+\vec{E}_{inc})=0 \tag{A.1}$$

The scattered field $\vec{E}_S$ may be derived in the usual way from its electromagnetic potentials, in the following form [48, 56, 95]:

$$\begin{aligned}\vec{E}_S &= -j\omega\vec{A}-\nabla\phi \\ &= -\frac{j\omega\mu_0}{4\pi}\int_S \frac{\exp(-jkR)}{R}\vec{J}_S(\vec{r}\,')\,dS' - \frac{j}{4\pi\omega\varepsilon_0}\nabla\int_S \frac{\exp(-jkR)}{R}\nabla'\cdot\vec{J}_S(\vec{r}\,')\,dS' \\ R &= \left|\vec{r}-\vec{r}\,'\right|\end{aligned} \tag{A.2}$$

in which $\vec{J}_S$ is the unknown current density in the scattering PEC body, and $R=\left|\vec{r}-\vec{r}\,'\right|$ is the distance between the source point $\vec{r}\,'$ and the field point $\vec{r}$. Thus, an *Electric Field Integral Equation* (EFIE) can be established in terms of $\vec{J}_S$ and the solution of the scattering problem will conveniently be obtained in terms of the currents that flow in the scattering body.

A.2 Method of Moment Equations for PEC Bodies

To solve the EFIE using the MoM, the induced current is represented by a linear superposition of the suitable basis functions of the prescribed spatial variation so that the current density may be written in the approximated form [56, 95]:

$$\vec{J}_S=\sum_{n=1}^{N} I_n\vec{S}_n(\vec{r}) \tag{A.3}$$

where N is the total number of basis functions, the scalar quantities I_n are unknown constants to be determined, and the vector quantities $\vec{S}_n(\vec{r})$ are the individual basis functions.

If equation (A.3) is substituted into the integral equation (A.1), the EFIE is multiplied by a test function of $\vec{S}_n(\vec{r})$ (Galerkin's method), and the resultant is integrated over the PEC surfaces, the MoM equations will be derived as follow [56, 95]:

$$\sum_{n=1}^{N} Z_{nm} I_n = V_m \tag{A.4}$$

where

$$V_m = \int \vec{S}_m(\vec{r}) \cdot \vec{E}_{inc} dS \tag{A.5}$$

and

$$\begin{aligned} Z_{mn} = & \left(\frac{j\omega\mu_0}{4\pi} \right) \int_S \int_S \vec{S}_m(\vec{r}) \cdot \vec{S}_n(\vec{r}\,') \frac{\exp(-jkR)}{R} dS' dS \\ & - \left(\frac{j}{4\pi\omega\varepsilon_0} \right) \int_S \int_S \left(\nabla \cdot \vec{S}_m(\vec{r}) \right) \cdot \left(\nabla' \cdot \vec{S}_n(\vec{r}\,') \right) \frac{\exp(-jkR)}{R} dS' \end{aligned} \tag{A.6}$$

Each element of the impedance matrix is essentially a double integral of the Green's function multiplied by known basis functions over the PEC surface. Equation (A.4) can be written as the matrix form:

$$[Z_{nm}]_{N\times N} [I_n]_{N\times 1} = [V_m]_{N\times 1} \tag{A.7}$$

In the following section, an appropriate basis function is introduced which is popular in the Method of Moments, and it will be discussed how to calculate the double integrals in the impedance matrix.

A.3 MoM using RWG Basis Functions

Based on equation (A.6), the basis function $\vec{S}_i(\vec{r})$ is needed to have a nonsingular divergence. In other words, the elements should be *divergence-conforming* which means that its normal component is continuous across the element boundaries. A popular basis function in the MoM is often referred to as the *Rao–Wilton–Glisson* (RWG) elements on triangles. The RWG basis function illustrated in Figure A.1 contains a pair of triangles which are not necessarily co-planer [96].

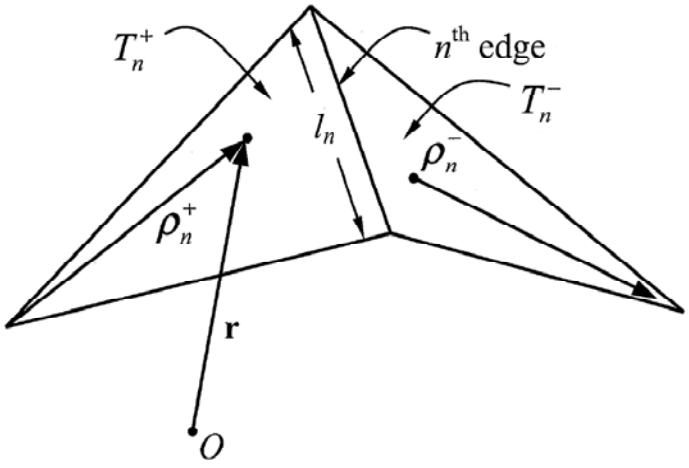

Figure A.1: The geometry of the RWG basis function [96]

The RWG basis functions resembles a small dipole with a positive or negative charge on either triangle T_n^+ or T_n^- which have areas A_n^+ and A_n^-, respectively, and share a common edge l_n. The RWG basis function can be formulated as follow [95]:

$$\vec{S}_n(\vec{r}) = \begin{cases} \dfrac{l_n}{2A_n^+}\rho_n^+(\vec{r}) & \vec{r} \ \ in \ \ T_n^+ \\ \dfrac{l_n}{2A_n^-}\rho_n^-(\vec{r}) & \vec{r} \ \ in \ \ T_n^- \end{cases} \tag{A.8}$$

and

$$\nabla \cdot \vec{S}_n(\vec{r}) = \begin{cases} \dfrac{l_n}{A_n^+} & \vec{r} \ \ in \ \ T_n^+ \\ \dfrac{l_n}{A_n^-} & \vec{r} \ \ in \ \ T_n^- \end{cases} \tag{A.9}$$

where $\rho_n^+(\vec{r}) = \vec{r} - \vec{r}_n^+$ is a vector from the free vertex of the triangle T_n^+ to the observation point $\vec{r}$, and $\rho_n^-(\vec{r}) = \vec{r}_n^- - \vec{r}$ is a vector which starts from the observation point $\vec{r}$ and ends at the free vertex of the triangle T_n^- [96].

Substituting equation (A.8) and (A.9) into equation (A.6), the double integrals in the impedance matrix elements can be written in terms of the RWG basis functions as follow [96, 97]:

$$\int_S\int_S \vec{S}_m(\vec{r})\cdot\vec{S}_n(\vec{r}')\frac{\exp(-jkR)}{R}dS'dS =$$
$$+\frac{l_m l_n}{4A_m^+A_n^+}\int_{T_m^+}\int_{T_n^+}\vec{\rho}_m^+(\vec{r})\cdot\vec{\rho}_n^+(\vec{r}')\frac{\exp(-jkR)}{R}dS'dS+\frac{l_m l_n}{4A_m^+A_n^-}\int_{T_m^+}\int_{T_n^-}\vec{\rho}_m^+(\vec{r})\cdot\vec{\rho}_n^-(\vec{r}')\frac{\exp(-jkR)}{R}dS'dS \quad (A.10)$$
$$+\frac{l_m l_n}{4A_m^-A_n^+}\int_{T_m^-}\int_{T_n^+}\vec{\rho}_m^-(\vec{r})\cdot\vec{\rho}_n^+(\vec{r}')\frac{\exp(-jkR)}{R}dS'dS+\frac{l_m l_n}{4A_m^-A_n^-}\int_{T_m^-}\int_{T_n^-}\vec{\rho}_m^-(\vec{r})\cdot\vec{\rho}_n^-(\vec{r}')\frac{\exp(-jkR)}{R}dS'dS$$

$$\int_S\int_S\left(\nabla\cdot\vec{S}_m(\vec{r})\right)\cdot\left(\nabla'\cdot\vec{S}_n(\vec{r}')\right)\frac{\exp(-jkR)}{R}dS' =$$
$$+\frac{l_m l_n}{A_m^+A_n^+}\int_{T_m^+}\int_{T_n^+}\frac{\exp(-jkR)}{R}dS'dS-\frac{l_m l_n}{A_m^+A_n^-}\int_{T_m^+}\int_{T_n^-}\frac{\exp(-jkR)}{R}dS'dS \quad (A.11)$$
$$-\frac{l_m l_n}{A_m^-A_n^+}\int_{T_m^-}\int_{T_n^+}\frac{\exp(-jkR)}{R}dS'dS+\frac{l_m l_n}{A_m^-A_n^-}\int_{T_m^-}\int_{T_n^-}\frac{\exp(-jkR)}{R}dS'dS$$

The double surface integrals presented in (A.10) and (A.11) have a singularity which creates difficulties in calculating the integrations. There are well-known ways to extract the singularity from the Green's function and calculate the singular integral with the help of analytical calculations [98, 99]. Here, the semi-analytic method presented in [98] and the *Gaussian-Quadrature* method are used to calculate the above integrals. Accordingly, the singularity of integrals can be extracted in the following forms:

$$\int_{T_m}\int_{T_m}\vec{\rho}_m(\vec{r})\cdot\vec{\rho}_n(\vec{r}')\frac{\exp(-jkR)}{R}dS'dS=\int_{T_m}\int_{T_m}\frac{\vec{\rho}_m(\vec{r})\cdot\vec{\rho}_n(\vec{r}')}{R}dS'dS+$$
$$\int_{T_m}\int_{T_m}\vec{\rho}_m(\vec{r})\cdot\vec{\rho}_n(\vec{r}')\frac{(\exp(-jkR)-1)}{R}dS'dS \quad (A.12)$$

$$\int_{T_m}\int_{T_m}\frac{\exp(-jkR)}{R}dS'dS=\int_{T_m}\int_{T_m}\frac{1}{R}dS'dS+\int_{T_m}\int_{T_m}\frac{(\exp(-jkR)-1)}{R}dS'dS \quad (A.13)$$

Two double integrals on the right hand side are not singular anymore since the limit of $(\exp(-jkR)-1)/R$ is $-jk$ when R goes to zero. Therefore, these two integrals can be calculated numerically using the Gaussian-Quadrature method [100]. The analytic results of the inner potential integrals have been presented in [98] which are used to calculate the singular integrals. The outer integrals can be again evaluated numerically by the Gaussian-Quadrature method. The analytic formulas for the inner singular integrals are concisely as follow:

$$\int_T \frac{1}{R} dS' = \sum_{i=1}^{3} \hat{P}_i^0 \cdot \hat{u}_i \left[P_i^0 \, Ln \frac{R_i^+ + l_i^+}{R_i^- + l_i^-} - |d| \times \left(\tan^{-1} \frac{P_i^0 l_i^+}{(R_i^0)^2 + |d| R_i^+} - \tan^{-1} \frac{P_i^0 l_i^-}{(R_i^0)^2 + |d| R_i^-} \right) \right] \quad \text{(A.14)}$$

$$\int_T \frac{\vec{\rho}_n(\vec{r}')}{R} dS' = \int_T \frac{(\vec{r}' - \vec{r})_{\tan}}{R} dS' + (\vec{r} - \vec{r}_n)_{\tan} \int_T \frac{1}{R} dS' \quad \text{(A.15)}$$

where

$$\int_T \frac{(\vec{r}' - \vec{r})_{\tan}}{R} dS' = \frac{1}{2} \sum_{i=1}^{3} \hat{u}_i \left[(R_i^0)^2 \, Ln \frac{R_i^+ + l_i^+}{R_i^- + l_i^-} + R_i^+ l_i^+ - R_i^- l_i^- \right] \quad \text{(A.16)}$$

The geometrical variables used in the analytical formulas have been illustrated in Figure A.2. The detailed calculations and all parameters included in the analytic formulas can be found in [98]. As mentioned before, the outer integration and the second integrations in equations (A.12) and (A.13) can be performed numerically.

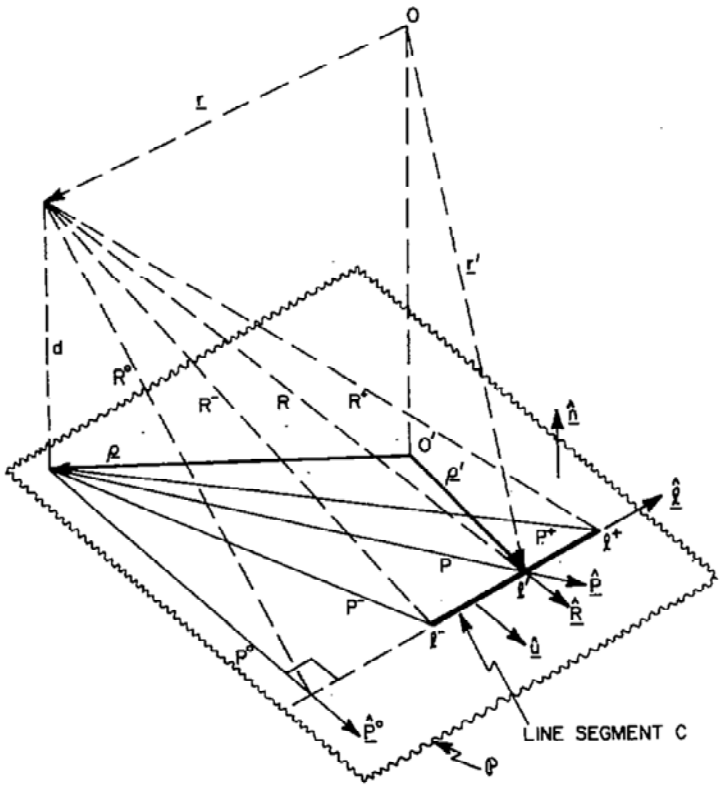

Figure A.2: The variables included in the analytic formulas presented by [98]

Once the impedance matrix elements are calculated, the vector [I] can be obtained using equation (A.7) for any arbitrary source vector [V]. Once the surface current density is known, the scattered electric field can be calculated by substituting (A.3) in (A.2) which gives the following equation:

$$\vec{E}_S = -\frac{j\omega\mu_0}{4\pi}\sum_{n=1}^{N} I_n \int_S \frac{\exp(-jkR)}{R}\vec{S}_n(\vec{r}\,')\,dS' - \frac{j}{4\pi\omega\varepsilon_0}\sum_{n=1}^{N} I_n \int_S \nabla_r \frac{\exp(-jkR)}{R}\nabla'\cdot\vec{S}_n(\vec{r}\,')\,dS' \quad \text{(A.17)}$$
$$R = \left|\vec{r} - \vec{r}\,'\right|$$

A.4 MATLAB functions for MoM

Based on the semi-analytic method formulated in the Section A.3, four MATLAB functions have been written to calculate the four different integrals given by equations (A.10) and (A.11). These MATLAB functions numerically calculates two double integrals over $T_m^+T_n^-$, $T_m^+T_n^-$, $T_m^+T_n^-$, and $T_m^+T_n^-$, respectively. Using equation (A.6), the impedance matrix elements, which show the self and mutual impedances between the RWG basis functions, can be calculated. The integral results of the four MATLAB functions have been verified with two other numerical methods (the fully numerical Gaussian-Quadrature method and the two uniform series approximation of double surface integrals).

The mesh generation on the PEC body is performed using MATLAB, HFSS, or GMesh software [101] which generates triangle and tetrahedral meshes for any surface and volume. Using aforementioned software, it is possible to draw an arbitrary shape and generate the appropriate meshes as a text file including the coordinates of the mesh vertexes.

To calculate the radiation field from the induced surface current $\vec{J}_S$, four major MATLAB codes are developed to implement the following major tasks:

1) Organizing and plotting the generated meshes on the PEC body
2) MoM impedance matrix calculations
3) Calculating the vector [V] in equation (A.5) and obtaining the current distribution $\vec{J}_S$ on the PEC body
4) Calculating the scattered fields and plotting the radiation pattern

The output of each step is saved at the final line of each MATLAB code in order to be used easily for the next step at any time it is needed. The input of the first code can be a text file (*.txt)

containing the coordinates of the mesh vertexes. The first code plots the generated meshes on the PEC body and finds the vertexes of each pair of triangles for the RWG basis function. The second code calculates the Z matrix elements using the semi-analytic method discussed before. In this code, the property of the symmetric impedance matrix has been used to decrease the run time required for the Z matrix elements calculations. The third code calculates the vector [V] for an infinitesimal dipole located far from the PEC cube, and also calculates the current distribution matrix $\vec{J}_S$ by multiplying the Y matrix (Z^{-1}) and vector [V]. The last code calculates the radiated field from $\vec{J}_S$ derived from the previous step, and finally plots the radiation pattern of the scattered fields $\vec{E}_S$.

To verify the accuracy of the MATLAB code, the plane wave excitation of a PEC cube is analyzed using both the commercial software HFSS and the developed MoM in MATLAB, and the results are compared. The incident wave is defined as a plane wave with $\vec{E}_0 = E_0(1/\sqrt{2}\,\hat{x} - 1/\sqrt{2}\,\hat{z})$ and $\hat{k} = -1/\sqrt{2}\,\hat{x} - 1/\sqrt{2}\,\hat{z}$ which is impinging on the PEC cube from $\theta = 45^\circ$ and $\varphi = 0^\circ$ direction. The generated meshes on the PEC cube in MATLAB have been illustrated in Figure A.3.

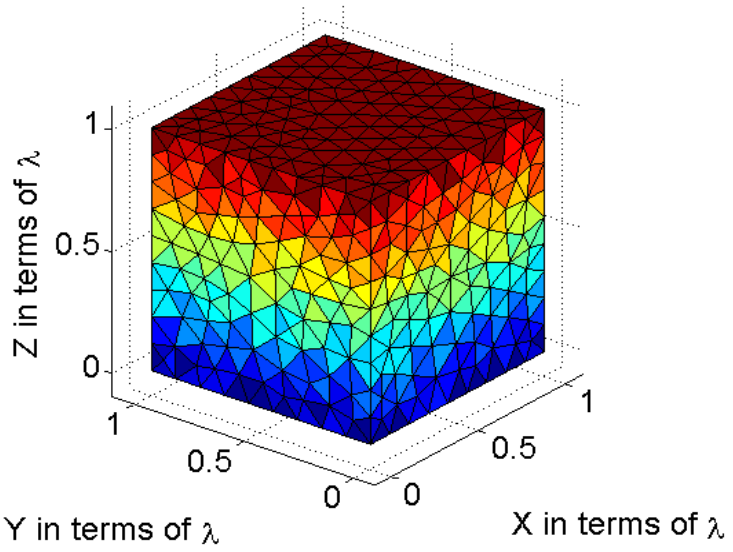

Figure A.3: The generated meshes on the PEC cube for MoM

The far field radiation pattern of the scattered field is calculated in both HFSS and MATLAB MoM code. The scattered field radiation patterns are plotted for $\varphi = 0,\ 45,\ 90,\ 135,\ 180^{\circ}$ and $\theta = 45,\ 90^{\circ}$ planes in Figure A.4 and A.5, respectively. As can be seen, the MoM results agree well with the HFSS results.

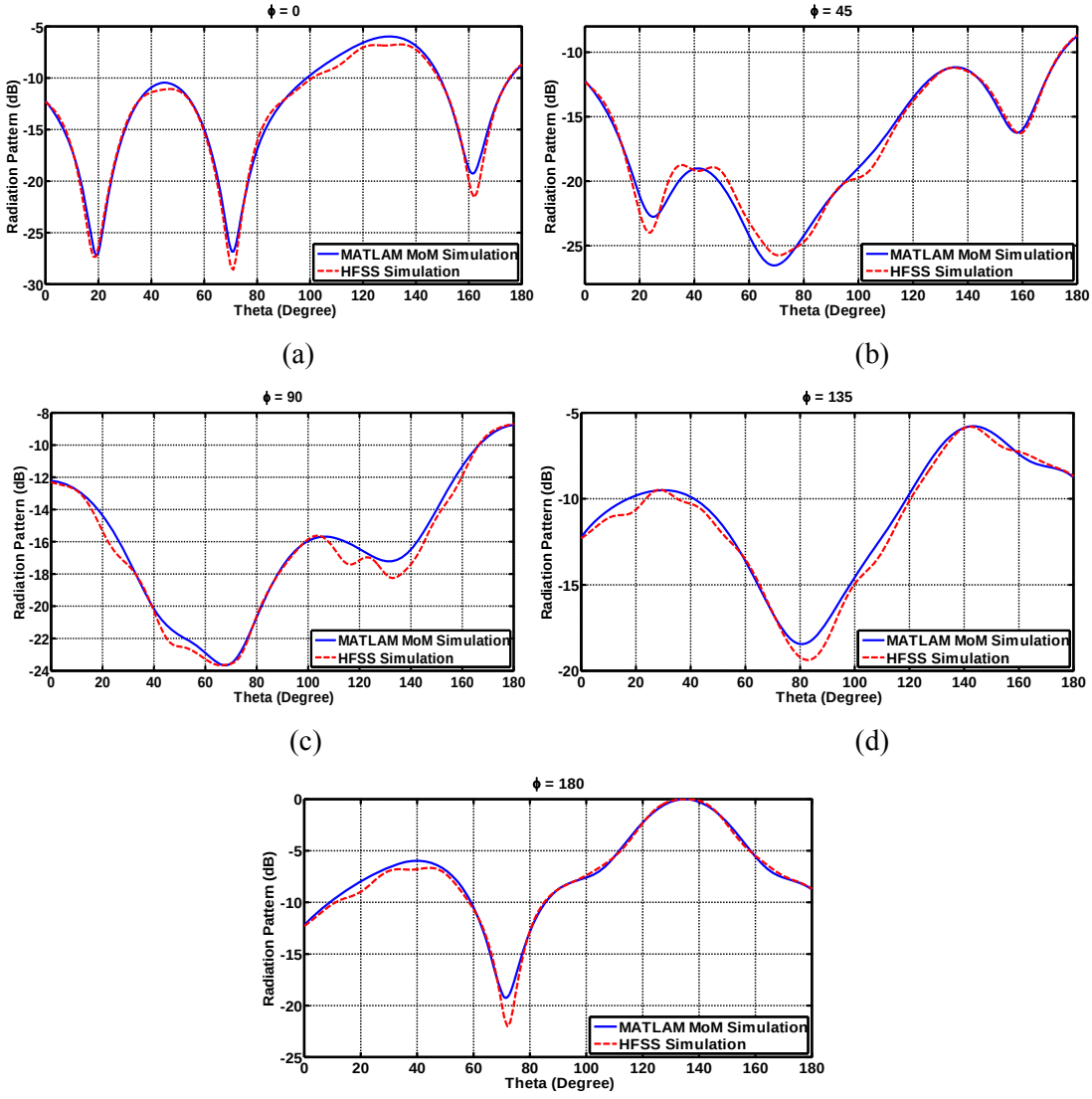

Figure A.4: The scattered field radiation patterns in HFSS and MoM for a) $\varphi = 0^{\circ}$ b) $\varphi = 45^{\circ}$ c) $\varphi = 90^{\circ}$ d) $\varphi = 135^{\circ}$ e) $\varphi = 180^{\circ}$ plane [67, 69]

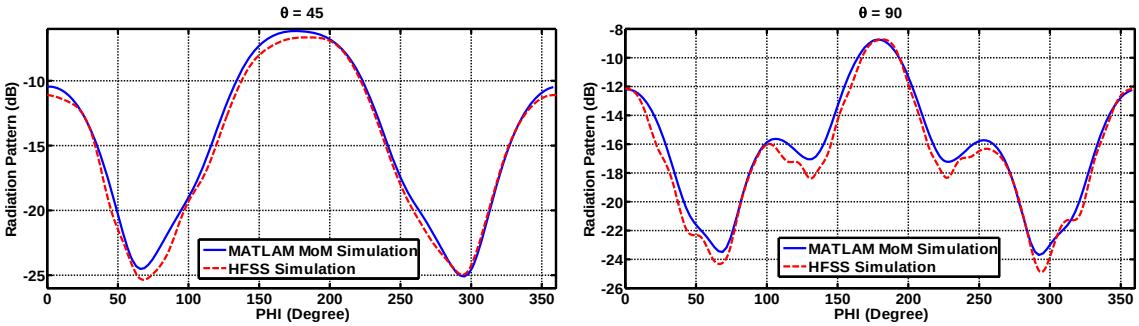

(a) (b)

Figure A.5: The scattered field radiation patterns in HFSS and MoM for a) $\theta = 45^{\circ}$ b) $\theta = 90^{\circ}$ [67, 69]

The slight difference between the results can be attributed to the different mesh arrangement used in HFSS and MoM. However, if very fine meshes are chosen for both simulations, the results would be more closely matched. The results confirm the validity of the developed MoM in MATLAB, and verify that the calculated Z-matrix and the induced current are obtained correctly.

Appendix B
Vector Wave Functions

Considering the general curvilinear coordinates ξ_1, ξ_2, and ξ_3 with the unit vectors $\hat{a}_1$, $\hat{a}_2$, $\hat{a}_3$ and the scale factors h_1, h_2, h_3, the Eigen vector functions of the vector Helmholtz equation can be written in terms of the solution of the scalar Helmholtz equation, ψ, as follow [45-47]:

$$
\begin{aligned}
&\psi(\xi_1,\xi_2,\xi_3) = \psi_1(\xi_1)\psi_2(\xi_2)\psi_3(\xi_3)\\
&\vec{L} = \vec{\nabla}\psi = \frac{\partial}{\partial\xi_1}(\psi_1)\psi_2\psi_3\,\hat{a}_1 + \frac{1}{h_2}\psi_1\frac{\partial}{\partial\xi_2}(\psi_2)\psi_3\,\hat{a}_2 + \frac{1}{h_3}\psi_1\psi_2\frac{\partial}{\partial\xi_3}(\psi_3)\,\hat{a}_3\\
&\vec{M} = \vec{\nabla}\times(\hat{a}_1\chi\psi) = \frac{\chi}{h_3}\psi_1\psi_2\frac{\partial}{\partial\xi_3}(\psi_3)\,\hat{a}_2 - \frac{\chi}{h_2}\psi_1\frac{\partial}{\partial\xi_2}(\psi_2)\psi_3\,\hat{a}_3\\
&\vec{N} = \frac{1}{k}\vec{\nabla}\times\vec{M} = \frac{\chi}{k}\left(k^2\psi_1 + \frac{1}{\chi^2}\frac{\partial}{\partial\xi_1}\left[\chi^2\frac{\partial}{\partial\xi_1}(\psi_1)\right]\right)\psi_2\psi_3\,\hat{a}_1\\
&\qquad + \frac{1}{kh_2}\frac{\partial}{\partial\xi_1}(\chi\psi_1)\frac{\partial}{\partial\xi_2}(\psi_2)\psi_3\,\hat{a}_2 + \frac{1}{kh_3}\frac{\partial}{\partial\xi_1}(\chi\psi_1)\psi_2\frac{\partial}{\partial\xi_3}(\psi_3)\,\hat{a}_3
\end{aligned}
\tag{B.1}
$$

where it is assumed that h_1 is a unit constant, h_2/h_3 is independent of ξ_1, and χ is either 1 or ξ_1. These assumptions are held by six separable coordinate systems including the spherical coordinate system. For the spherical coordinate system, the vector wave functions are given as follows [45-47]:

$$
\begin{aligned}
&\psi^{(i)}_{\substack{e\\o}mn} = \psi_1\psi_2\psi_3 = z_n^{(i)}(kr)\;P_n^m(\cos\theta)\begin{matrix}\cos\\\sin\end{matrix}(m\phi)\\
&\vec{L}^{(i)}_{\substack{e\\o}mn} = \frac{\partial}{\partial r}z_n^{(i)}(kr)P_n^m(\cos\theta)\begin{matrix}\cos\\\sin\end{matrix}m\varphi\,\hat{r} + \frac{1}{r}z_n^{(i)}(kr)\frac{\partial P_n^m(\cos\theta)}{\partial\theta}\begin{matrix}\cos\\\sin\end{matrix}m\varphi\,\hat{\theta}\\
&\qquad \mp\frac{m}{r\sin\theta}z_n^{(i)}(kr)P_n^m(\cos\theta)\begin{matrix}\sin\\\cos\end{matrix}m\varphi\,\hat{\varphi}\\
&\vec{M}^{(i)}_{\substack{e\\o}mn} = \mp\frac{m}{\sin\theta}z_n^{(i)}(kr)P_n^m(\cos\theta)\begin{matrix}\sin\\\cos\end{matrix}m\varphi\,\hat{\theta} - z_n^{(i)}(kr)\frac{\partial P_n^m(\cos\theta)}{\partial\theta}\begin{matrix}\cos\\\sin\end{matrix}m\varphi\,\hat{\varphi}\\
&\vec{N}^{(i)}_{\substack{e\\o}mn} = \frac{n(n+1)}{kr}z_n^{(i)}(kr)P_n^m(\cos\theta)\begin{matrix}\cos\\\sin\end{matrix}m\varphi\,\hat{r} + \frac{1}{kr}\frac{\partial}{\partial r}\left[rz_n^{(i)}(kr)\right]\frac{\partial P_n^m(\cos\theta)}{\partial\theta}\begin{matrix}\cos\\\sin\end{matrix}m\varphi\,\hat{\theta}\\
&\qquad \mp\frac{m}{kr\sin\theta}\frac{\partial}{\partial r}\left[rz_n^{(i)}(kr)\right]P_n^m(\cos\theta)\begin{matrix}\sin\\\cos\end{matrix}m\varphi\,\hat{\varphi}
\end{aligned}
\tag{B.2}
$$

The spherical vector waves with different orders hold the following orthogonality properties on a spherical surface [46, 47]:

$$\begin{aligned}
&\int_0^{2\pi}\int_0^{\pi} \vec{L}^{(i)}_{\substack{e\\o}mn} . \vec{L}^{(i)}_{\substack{e\\o}m'n'} \sin\theta \, d\theta \, d\varphi = 0 \qquad for \;\; n \neq n' \;\; or \;\; m \neq m' \\
&\int_0^{2\pi}\int_0^{\pi} \vec{M}^{(i)}_{\substack{e\\o}mn} . \vec{M}^{(i)}_{\substack{e\\o}m'n'} \sin\theta \, d\theta \, d\varphi = 0 \qquad for \;\; n \neq n' \;\; or \;\; m \neq m' \\
&\int_0^{2\pi}\int_0^{\pi} \vec{N}^{(i)}_{\substack{e\\o}mn} . \vec{N}^{(i)}_{\substack{e\\o}m'n'} \sin\theta \, d\theta \, d\varphi = 0 \qquad for \;\; n \neq n' \;\; or \;\; m \neq m'
\end{aligned} \tag{B.3}$$

Also, the following orthogonality properties are valid for any arbitrary orders [46, 47]:

$$\begin{aligned}
&\int_0^{2\pi}\int_0^{\pi} \vec{M}^{(i)}_{\substack{e\\o}mn} . \vec{N}^{(i)}_{\substack{e\\o}m'n'} \sin\theta \, d\theta \, d\varphi = 0 \\
&\int_0^{2\pi}\int_0^{\pi} \vec{M}^{(i)}_{\substack{e\\o}mn} . \vec{L}^{(i)}_{\substack{e\\o}m'n'} \sin\theta \, d\theta \, d\varphi = 0
\end{aligned} \tag{B.4}$$

The complete orthogonality of the SVWs on a spherical surface is spoiled by a non-vanishing integral of the $\vec{L}$ and $\vec{N}$ vector wave functions with the same orders over the sphere. However, by treating the k and r variables and integrating over them, the orthogonalization can be completed [46].

Bibliography

[1] D. Tse and P. Viswanath, *Fundamentals of Wireless Communication*, Cambridge University Press, 2005.

[2] A. Paulraj, R. Nabar, D. Gore, *Introduction to Space-Time Wireless Communications*, London: Cambridge Univ. Press, 2003.

[3] M. A. Jensen, J. W. Wallace, "A Review of Antennas and Propagation for MIMO Wireless Communications," *IEEE Transactions on Antennas and Propagations*, vol. 52, no. 11, November 2004.

[4] A. J. Paulraj, and et al., "An Overview of MIMO Communications—A Key to Gigabit Wireless," *Proceeding of the IEEE*, vol. 92, no. 2, February 2004.

[5] P. Almers, F. Tufvesson, and A. F. Molisch, "Measurement of keyhole effect in a wireless multiple-input multiple-output (MIMO) channel," *IEEE Communication Letters*, vol. 7, pp. 373–375, August 2003.

[6] P. Almers, F. Tufvesson, and A. F. Molisch, "Keyhole Effect in MIMO Wireless Channels: Measurements and Theory," *IEEE Transactions on Wireless Communications*, vol. 5, no. 12, pp. 3596–3604, December 2006.

[7] S. M. Alamouti, "A simple transmit diversity technique for wireless communications," *IEEE Journal on Selected Areas in Communications*, vol. 16, pp. 1451–1458, October 1998.

[8] V. Tarokh, H. Jafarkhani, and A. Calderbank, "Space–time block codes from orthogonal designs," *IEEE Transactions on Information Theory*, vol. 45, pp. 1456–1467, July 1999.

[9] L. Zheng and D. Tse, "Diversity and multiplexing: A fundamental tradeoff in multiple antenna channels," *IEEE Transactions on Information Theory*, vol. 49, pp. 1073–1096, May 2003.

[10] M. A. Jensen, J. W. Wallace, *Antenna design considerations for MIMO and Diversity Systems*, Chapter 26 in *Modern Antenna Handbook*, Edited by C. A. Balanis, John Wiley & Sons, Inc., 2008.

[11] R. G. Vaughan and J. B. Andersen, "Antenna diversity in mobile communications," *IEEE Transactions on Vehicular Technology*, vol. VT-36, no.4, November 1987.

[12] Forenza, R. W. Heath, "Benefit of Pattern Diversity via Two-Element Array of Circular Patch Antennas in Indoor Clustered MIMO Channels," *IEEE Transactions on Communications*, vol. 54, no. 5, May 2006.

[13] V. Jungnickel, V. Pohl, and C. Helmolt, "Capacity of MIMO Systems with Closely Spaced Antennas," *IEEE Communications Letters*, vol. 7, no. 8, August 2003.

[14] N. Getu and J. B. Andersen, "The MIMO cube—A compact MIMO antenna," *IEEE Transactions on Wireless Communications*, vol. 4, no. 3, May 2005.

[15] C. Waldschmidt, W. Wiesbeck, "Compact Wide-Band Multimode Antennas for MIMO and Diversity," *IEEE Transactions on Antennas and Propagations*, vol. 52, no. 8, August 2004.

[16] M. Stoytchev, H. Safar, A. L. Moustakas, and S. Simon, "Compact antenna arrays for MIMO applications," *Proceeding IEEE Antennas and Propagation Symposium*, vol. 3, July 2001.

[17] Anand S. Konanur, Keyoor Gosalia, Sandeep H. Krishnamurthy, Brian Hughes, and Gianluca Lazzi, "Increasing Wireless Channel Capacity Through MIMO Systems Employing Co-Located Antennas," *IEEE Transactions on Microwave Theory and Techniques*, vol. 53, no. 6, June 2005.

[18] David W. Browne, Majid Manteghi, Michael P. Fitz, and Yahya Rahmat-Samii, "Experiments With Compact Antenna Arrays for MIMO Radio Communications," *IEEE Transactions on Antennas and Propagations*, vol. 54, no. 11, November 2006.

[19] T. I. Lee, S. Kim and Y.E. Wang, "Compact polarisation and spatial multiplexing antenna for MIMO applications," *Electronics Letters*, vol. 42 no. 15, July 2006.

[20] S.B. Yeap, X. Chen, J.A. Dupuy, C.C. Chiau and C.G. Parini, "Integrated diversity antenna for laptop and PDA terminal in a MIMO system," *IEE Proceeding-Microwave, Antennas and Propagations*, vol. 152, no. 6, December 2005.

[21] Y. Gao, C.C. Chiau, X. Chen and C.G. Parini, "Modified PIFA and its array for MIMO terminals," *IEE Proceeding-Microwave, Antennas and Propagations*, vol. 152, no. 4, August 2005.

[22] M. D. Migliore, "On the role of the number of degrees of freedom of the field in MIMO channel," *IEEE Transactions on Antennas and Propagations*, vol. 54, no. 2, Feb. 2006.

[23] M. D. Migliore, "On Electromagnetics and Information Theory," *IEEE Transactions on Antennas and Propagations*, vol. 56, no. 10, October 2006.

[24] A. S. Y. Poon, R. W. Brodersen, and D. N. C. Tse, "Degrees of freedom in multiple-antenna channels: A signal space approach," *IEEE Transactions on Information Theory*, vol. 51, February 2005.

[25] S. Loyka and J. Mosig, *Information theory and electromagnetic: Are they related*, Chapter 3 in *MIMO Systems Technology for Wireless Communication*, Edited by G. Tsoulos, Ed. Boca Raton, FL: CRC & Taylor & Francis, 2006.

[26] B. A. Cetiner, H. Jafarkhani, J.Y. Qian, H. J. Yoo, A. Grau, and F. Flaviis, "Multifunctional reconfigurable MEMS integrated antennas for adaptive MIMO systems," *IEEE Communication Magazine*, vol. 42, no.12, Dec. 2004.

[27] A. Grau, J. Romeu, S. Blanch, L. Jofre, and F. Flaviis, "Optimization of Linear Multielement Antennas for Selection Combining by Means of a Butler Matrix in Different MIMO Environments," *IEEE Transactions on Antennas and Propagation*, vol. 54, no. 11, November 2006.

[28] D. Piazza and K.R. Dandekar, "Reconfigurable antenna solution for MIMO-OFDM systems," *Electronic Letters*, vol. 2, no. 8, April 2006.

[29] B. A. Cetiner, J. Y. Qian, and G. P. Li, "A reconfigurable spiral antenna for adaptive wireless communications," *EURASIP Journal on Wireless Communications and Networking*, vol. 3, September 2005.

[30] Bedri A. Cetiner, Enis Akay, Ersin Sengul, and Ender Ayanoglu, "A MIMO System with Multifunctional Reconfigurable Antennas," *IEEE Antennas and Wireless Propagation Letters*, vol. 5, no.1, December 2006.

[31] E. Erdil, K. Topalli, M. Unlu, O. A. Civi, and T. Akin, "Frequency Tunable Microstrip Patch Antenna Using RF MEMS Technology," *IEEE Transactions on Antennas and Propagation*, vol. 55, no. 4, April 2007.

[32] A. C. K. Mak, C. R. Rowell, R. D. Murch, and C. L. Mak, "Reconfigurable Multiband Antenna Designs for Wireless Communication Devices," *IEEE Transactions on Antennas and Propagation*, vol. 55, no. 7, July 2007.

[33] Y. F. Wu, C. H. Wu, D. Y. Lai, and F. C. Chen, "A Reconfigurable Quadri-Polarization Diversity Aperture-Coupled Patch Antenna," *IEEE Transactions on Antennas and Propagation*, vol. 55, no. 3, March 2007.

[34] R. Vaughan, "Switched parasitic elements for antenna diversity," *IEEE Transactions on Antennas and Propagation*, vol. 47, no. 2, Feb. 1999.

[35] R. J. Garbacz and R. H. Turpin, "A generalized expansion for radiated and scattered fields," *IEEE Transactions on Antennas and Propagation*, vol. 19, no.3, May 1971.

[36] R. F. Harrington and J. R. Mautz, "Theory of characteristic modes for conducting bodies," *IEEE Transactions on Antennas and Propagation*, vol. 19, no.5, September 1971.

[37] Y. Chang and R. Harrington, "A surface formulation for characteristic modes of material bodies," *IEEE Transaction on Antennas and Propagation*, vol. 25, no. 6, pp. 789–795, 1977.

[38] C. Tamgue Famdie, *Small Antennas Radiation Performance Optimization in Mobile Communications*, Ph.D. Thesis, Universitaet Duisburg-Essen, October 30, 2007.

[39] M. Cabedo Fabres, *Systematic design of antennas using the theory of characteristic modes*, Ph.D. Thesis, Universidad Politecnica De Valencia, February 2007.

[40] C. Tamgue Famdie, W. L. Schroeder, and K. Solbach, "Numerical analysis of characteristic modes on the chassis of mobile phones," *Proceeding of 1st European Conference on Antennas and Propagation – EuCAP 2006*, Nice, France, November 2006.

[41] M. Cabedo, E. Antonino, A. Valero, and M. Ferrando, "The theory of characteristic modes revisited: A contribution to the design of antennas for modern applications," *IEEE Antennas Propagation Magazine*, vol. 49, no. 5, pp. 52–68, October 2007.

[42] E. Antonino-Daviu, M. Cabedo-Fabres, M. Gallo, M. FerrandoBataller, and M. Bozzetti, "Design of a multimode MIMO antenna using characteristic modes," *3rd European Conference on Antennas and Propagation, EuCAP 2009*, pp. 1840-1844.

[43] S. K. Chaudhury, W. L. Schroeder, H. J. Chaloupka, "MIMO antenna system based on orthogonality of the characteristic modes of a mobile device," *2nd International ITG Conference on Antennas*, March 2007.

[44] J. Ethier, D. A. McNamara, "The Use of Generalized Characteristic Modes in the Design of MIMO Antennas," *IEEE Transactions on Magnetics*, vol. 45, no.3, pp 1124-1127, March 2009.

[45] P. M. Morse and H. Feshbach, *Methods of Theoretical Physics*, New York: McGraw-Hill, 1953.

[46] J. A. Stratton, *Electromagnetic Theory*, New York: McGraw-Hill, 1941.

[47] C. T. Tai, *Dyadic Green's Functions in Electromagnetic Theory*, San Franscisco: Intext Educational Publishers, 1971.

[48] R. F. Harrington, *Time Harmonic Electromagnetic Fields*, New York, McGraw-Hill, 1961.

[49] O. Klemp, H. Eul, "Analytical approach for MIMO performance and electromagnetic coupling in linear dipole arrays," *2nd international symposium on wireless communication systems*, pp.586-590, 2005.

[50] O. Klemp, G. Armbrecht, H. Eul, "Computation of antenna pattern correlation and MIMO performance by means of surface current distribution and spherical wave theory," *Advances in Radio Science*, Vol. 4, pp.33-39, 2006.

[51] M. Gustafsson, S. Nordebo, "Characterization of MIMO Antennas Using Spherical Vector Waves," *IEEE Transactions on Antennas and Propagation*, vol. 54, no. 9, pp. 2679-2682, Sept. 2006.

[52] A.A. Glazunov, M. Gustafsson, A.F. Molisch, F. Tufvesson, G. Kristensson "Spherical Vector Wave expansion of Gaussian electromagnetic fields for antenna-channel interaction analysis," *IEEE Transactions on Antennas and Propagation*, vol.57, no.7, pp. 2055-2067, July 2009.

[53] A.A. Glazunov, M. Gustafsson, A.F. Molisch, F. Tufvesson, "Physical modeling of multiple-input multiple-output antennas and channels by means of the spherical vector wave expansion," *IET Microwaves, Antennas & Propagation*, vol.4, issue 6, pp. 778-791, June 2010.

[54] M. Mohajer, S. Safavi-Naeini, S. K. Chaudhiri, "Sphercial Vector Wave method for analysis and design of MIMO antenna systems," *IEEE Antennas and Wireless Propagation Letters*, vol. 9, pp. 1267-1270, 2010.

[55] M. Mohajer, S. Safavi-Naeini, S. K. Chaudhuri, "MIMO Antenna Analysis Using Spherical Vector Wave Functions," *European Microwave Week 2010 (EuWiT 2010)*, Paris, France, September 2010.

[56] R. F. Harrington, *Field Computation by Moment Methods*, New York: Macmillan, 1968.

[57] G. J. Foschini and M. J. Gans, "On limits of wireless communications in a fading environment when using multiple antennas," *Wireless Personal Communications*, vol. 6, pp. 311–335, Mar. 1998.

[58] H. Shin and J. H. Lee, "Capacity of multiple-antenna fading channels: Spatial fading correlation, double scattering, and keyhole," *IEEE Transactions on Information Theory*, vol. 49, no. 10, pp. 2636–2647, October, 2003.

[59] P. Almers and et al., "Survey of channel and radio propagation models for wireless MIMO systems," *EURASIP Journal on Wireless Communications and Networking*, volume 2007, Article ID 19070.

[60] Ping Hui, and et al., "Measurements of Correlation Coefficients of Closely Spaced Dipoles," IEEE *International Workshop Antenna Tech.: Small Antennas & Novel Metamaterials (IWAT 2005)*, March 2005.

[61] L. Schumacher, B. Raghothaman, "Closed-Form Expressions for the Correlation Coefficient of Directive Antennas Impinged by a Multimodal Truncated Laplacian PAS," *IEEE Transactions on Wireless Communications*, vol. 4, no. 4, July 2005.

[62] S. Blanch, J. Romeu, and L. Corbella, "Exact representation of antenna system diversity performance from input parameter description," *Electronic Letters*, vol. 39, May 2003.

[63] A.A.M. Saleh and R.A. Valenzuela, "A statistical model for indoor multipath propagation," *IEEE Journal on Selected Areas in Communications*, vol. 5, no. 2, pp. 128-137, 1987.

[64] TGn Channel Models, IEEE 802.11-03/940r4, May 2004.

[65] TGac Channel Model Addendum, IEEE 802.11-09/0308r0, March 2009.

[66] M. Steinbauer, A. F. Molisch, and E. Bonek, "The double-directional radio channel," *IEEE Antennas Propagation Magazine*, vol. 43, no. 4, pp. 51–63, August 2001.

[67] M. Mohajer, S. Safavi-Naeini, "MIMO Antenna Optimization using Method of Moments Analysis," *IEEE International Workshop on Antenna Technology - Small Antennas and Novel Metamterials (iWAT)*, Santa Monica, California, USA, March 2009.

[68] C. A. Balanis, *Antenna Theory*, New York: Wiley, 2005.

[69] M. Mohajer, Gh. Z. Rafi, S. Safavi-Naeini, "MIMO Antenna Design and Optimization for Mobile Applications," *Antennas and Propagation Society International Symposium, 2009. IEEE APSURSI'09*, South Carolina, USA, June 01-05, 2009.

[70] L. J. Chu, "Physical limitations of omni-directional antennas," *Journal of Applied Physics*, vol. 19, 1948.

[71] A. J. Devaney and E. Wolf, "Radiating and nonradiating classical current distributions and the fields they generate," *Physical Review D*, vol. 8, 1973.

[72] A. J. Devaney and E. Wolf, "Multipole expansions and plane wave representations of the electromagnetic field," *Journal of Mathematical Physics*, vol. 15, 1974.

[73] A. J. Devaney and E. A. Marengo, "A method for specifying nonradiating, monochromatic, scalar sources and their fields," *Pure and Applied Optics: Journal of European Optical Society A*, vol. 7, 1998.

[74] A. J. Devaney and G. C. Sherman, "Nonuniqueness in inverse source and scattering problems," *IEEE Transactions on Antennas and Propagation*, vol. 30, no.5, September 1982.

[75] N. Bleistein and J. K. Cohen, "Nonuniqueness in the inverse source problem in acoustics and electromagnetics," *Journal of Mathematical Physics*, vol. 18, 1977.

[76] E. A. Marengo and A. J. Devaney, "The inverse source problem of electromagnetics: linear inversion formulation and minimum energy solution," *IEEE Transactions on Antennas and Propagation*, vol. 47, no.2, February 1999.

[77] E. A. Marengo and R. W. Ziolkowski, "Nonradiating and minimum energy sources and their fields: generalized source inversion theory and applications," *IEEE Transactions on Antennas and Propagation*, vol. 48, no.10, October 2000.

[78] E. A. Marengo, A. J. Devaney, and R. W. Ziolkowski, "New aspects of the inverse source problem with far-field data," *Journal of the Optical Society of America A*, vol. 16, 1999.

[79] E. A. Marengo, A. J. Devaney, and F. K. Gruber, "Inverse source problem with reactive power constraint," *IEEE Transactions on Antennas and Propagation*, vol. 52, no.5, June 2004.

[80] J. C.-E. Sten and E. A. Marengo, "Inverse source problem in the spheroidal geometry," *IEEE Transactions on Antennas and Propagation*, vol. 54, no. 11, November 2006.

[81] J. C.-E. Sten and E. A. Marengo, "Inverse source problem in the spheroidal geometry: vector formulation," *IEEE Transactions on Antennas and Propagation*, vol. 56, no. 4, April 2008.

[82] J. C.-E. Sten and E. A. Marengo, "Transformation formulas for spherical and spheroidal multipole fields," *International Journal of Electronics and Communications (AEÜ)*, vol. 61, 2007.

[83] G. Arfken, *Mathematical Methods for Physicists*, New York: Academic, 1985.

[84] M. Mohajer, S. Safavi-Naeini, S.K. Chaudhuri, "Surface current source reconstruction for given Radiated Electromagnetic Fields," *IEEE Transactions on Antennas and Propagation*, vol. 58, no. 2, pp. 432-439, February 2010.

[85] J. J. Adams, and et al., "Conformal Printing of Electrically Small Antennas on Three-Dimensional Surfaces," *Advanced Materials*, vol. 23, pp. 1335-1340, 2011

[86] J. J. Adams and J. T. Bernhard, "A modal approach to the tuning and bandwidth enhancement of an electrically small antenna," *IEEE Transactions on Antennas and Propagation*, vol. 59, no. 4, pp. 1085-1092, April 2011.

[87] C. Pfeiffer, A. Grbic, X. Xu, S.R. Forrest, "Novel methods to analyze and fabricate electrically small antennas," *Antennas and Propagation Society International Symposium 2011*, Spokane, Washington, USA, July 3-8, 2011.

[88] J. J. Adams, E. B. Duoss, T. F. Malkowski, J. A. Lewis, and J. T. Bernhard, "Design of spherical meanderline antennas," *Antennas and Propagation Society International Symposium 2011*, Spokane, Washington, USA, July 3-8, 2011.

[89] M. Abramowitz, I. Stegun, *Handbook of Mathematical Functions*, Dover Publications, New York, 1972.

[90] M. Mohajer, S. Safavi-Naeini, S.K. Chaudhuri, “Performance limitations of planar antennas,” *Antennas and Propagation Society International Symposium 2010*, Toronto, Ontario, Canada, July 11-17, 2010.

[91] B. T. Quist, M. A. Jensen, “Optimal antenna radiation characteristics for diversity and MIMO systems,” *IEEE Transactions on Antennas and Propagation*, vol. 57, no. 11, pp. 3474 - 3481, November 2009.

[92] D. N. Evans, M. A. Jensen, “Near-optimal radiation patterns for antenna diversity,” *IEEE Transactions on Antennas and Propagation*, vol. 58, no. 11, pp. 3765-3769, November 2010.

[93] R. G. Vaughan, “Two-port higher mode circular microstrip antennas,” *IEEE Transactions on Antennas and Propagation*, vol. 36, no. 3, pp. 309–321, Mar. 1988.

[94] A. Petosa, *Dielectric resonator Antenna Handbook*, Norwood: Artech House Inc., 2007.

[95] A. Bondeson, *Computational Electromagnetics*, Springer, 2005.

[96] S. M. Rao, D. R. Wilton, and A. W. Glisson, “Electromagnetic scattering by surfaces of arbitrary shape,” *IEEE Transactions on Antennas and Propagation*, vol.30, no. 3, May 1982.

[97] Chapter 5, http://ece.wpi.edu/mom/

[98] D. R. Wilton, S. M. Rao, A. W. Glisson, D. H. Schaubert, O. M. Al-Bundak, and C. M. Butler, “Potential integrals for uniform and linear source distribution on polygonal and polyhedral domains,” *IEEE Transactions on Antennas and Propagation*, vol. AP-32, no. 3, March 1984.

[99] T. F. Eibert and V. Hansen, “On the calculation of potential integrals for linear source distributions on triangular domains,” *IEEE Transactions on Antennas and Propagation*, vol. AP-43, no. 12, December 1995.

[100] Z. Wang, J. Volakis, K. Saitou, and K. Kurabayashi, "Comparison of semi-analytical formulations and Gaussian-quadrature rules for quasi-static double-surface potential integrals," *IEEE Antennas and Propagation Magazine*, vol. 45, no. 6, 2003.

[101] http://www.geuz.org/gmsh/